Winter 12-15-2018

A Recombinant Virus and Reporter Mouse System to Study Chronic Chikungunya Virus Pathogenesis

Alissa Roxanne Young
Washington University in St. Louis

WASHINGTON UNIVERSITY IN ST. LOUIS

Division of Biology and Biomedical Sciences
Molecular Microbiology and Microbial Pathogenesis

Dissertation Examination Committee:
Deborah J. Lenschow, Chair
Adrianus C. M. Boon
Michael S. Diamond
Robyn S. Klein
Thaddeus S. Stappenbeck
David Wang

A Recombinant Virus and Reporter Mouse System to Study Chronic Chikungunya Virus Pathogenesis

by
Alissa Roxanne Young

A dissertation presented to
The Graduate School
of Washington University in
partial fulfillment of the
requirements for the degree
of Doctor of Philosophy

December 2018
St. Louis, Missouri

Table of Contents

List of Figures

CHAPTER 1:

CHAPTER 2:

CHAPTER 3:

CHAPTER 4:

List of Abbreviations

Abbreviation	Full Name
3IABkFQ	3' Iowa Black® FQ
A	adipose tissue
ACCP	anti-cyclic citrullinated peptide antibodies
AF	alexa fluor
ANA	antinuclear antibodies
ANOVA	analysis of variance
B	bone
BHK	baby hamster kidney
BSA	bovine serum albumin
BSL	biosafety level
CD	cluster of differentiation
CD	cell debris
CD1	complete DMEM 1% FBS
CD10	complete DMEM 10% FBS
CHIKF	chikungunya fever
CHIKV	chikungunya virus
CP	capsid protein
CPV	cytopathic vacuole
CRP	C-reactive protein
D	dermis
DALY	disability-adjusted life year
DAPI	4′,6-diamidino-2-phenylindole
DMEM	Dulbecco's modified Eagle medium
DNA	deoxyribonuscleic acid
double-stranded DNA	dsDNA
double-stranded RNA	dsRNA
dpi	days post infection
DT	diphtheria toxin
DTR	diphtheria toxin receptor
E	epidermis
ECSA	East/Central/South African
EDTA	ethylenediaminetetraacetic acid
EGF	epidermal growth factor
EtOH	ethanol
FAM	fluorescein amidite
FBS	fetal bovine serum
FW	forward primer
g	gram

Abbreviation	Full Name
GAPDH	glyceraldehyde 3-phosphate dehydrogenase
GFP	green fluorescent protein
Glu	glutamine
H	hypodermis
H&E	hematoxylin and eosin
HBEGF	heparin binding EGF like growth factor
HEPES	4-(2-hydroxyethyl)-1-piperazineethanesulfonic acid
hpi	hours post infection
HPIV	human parainfluenza virus
HSV-1	herpes simplex virus 1
IAV	Influenza A virus
ID	intradermal
IFA	immunofluorescence
IFN	interferon
IHC	immunohistochemistry
IOL	Indian Ocean Lineage
IP	intraperitoneal
IRF	interferon regulatory factor
ISG	interferon stimulated gene
ISH	in-situ hybridization
IV	intravenous
LCM	laser capture microdissection
LR	La Réunion
LUC	luciferase
M	muscle
mAb	monoclonal antibody
MEF	murine embryonic fibroblast
MOI	multiplicity of infection
MV	Measles virus
Mxra8	Matrix Remodeling-Associated Protein 8
NEAA	non-essential amino acids
NK	natural killer
NLS	nuclear localization signal
nsP	non-structural protein
OCT	optimal cutting temperature
ORF	open reading frame
P/S	penicillin-streptomycin
PAMP	pattern-associated molecular pattern
PBMCs	peripheral blood mononuclear cells
PBS	phosphate-buffered saline
PBST	PBS + 0.1% Tween20

Abbreviation	Full Name
PCR	polymerase chain reaction
PFA	paraformaldehyde
PFU	plaque forming unit
PRR	pattern recognition receptor
QOL	quality of life
RdRp	RNA-dependent RNA polymerase
RFP	red fluorescent protein
RM	repeated measures
RMSP	rheumatic musculoskeletal pain
RNA	ribonucleic acid
RNA-seq	RNA sequencing
RO	retro orbital
RRV	Ross River virus
RT	room temperature
RT-qPCR	real-time quantitative PCR
RV	reverse primer
S	synovium
SAA	sarcomeric alpha actinin
SEM	standard error of the mean
SMA	smooth muscle actin
T	tendon
$TCID_{50}$	tissue culture infectious dose which will infect 50% of cells
tdTomato	tandem dimer tomato
TEM	transmission electron microscopy
TF	transframe
UTR	untranslatable region
UV	ultraviolet
VLP	virus-like particle
WHO	World Health Organization
WT	wild-type
WUCCI	Washington University Center for Cellular Imaging

Acknowledgments

Graduate school can feel so paradoxical sometimes. It seems like my PhD has taken an entire lifetime, and yet these past five and a half years have darted from my fingers like a rogue mouse. Sometimes I worry that I have contributed barely anything to science, and yet I can look back on reams of notebooks and files from hundreds of experiments, many from projects that capsized or ran ashore, and rest assured that at least some nuggets are exciting and useful. So many aspects of my life have changed since I started my PhD, and yet I feel like the same person, just with a little more science packed between my ears. What remains clear is that graduate school has far and away been the most difficult thing I have ever done, and I would never have been able to finish without help from so many people.

First off, I am indebted to Debbie Lenschow for being such a remarkable thesis advisor. Her calm mentoring style truly tempered my often frenzied approach to science. I have learned so much from her about experimentation, collaboration, and life. Debbie is an amazing scientist, physician, mentor, and all-around person, and I beyond thankful that she let me join her lab. I am also immeasurably grateful for the free rein she granted me to explore different career paths away from the bench. She may not remember, but it was her voice that actually started me on my grad school sojourn when she called to inform me of my acceptance to WashU; I may or may not have started crying after hanging up, which was made even more awkward by the fact that I was attending an interview weekend at another school.

I am also thankful for my stalwart thesis committee, even though meeting every six months often made it feel like I always preparing for or convalescing from an update meeting. Jacco Boon introduced to me to life as a WashU grad student during my first lab rotation, so I'm grateful he could continue to offer me years of scientific guidance, always with an incorrigible grin. Mike Diamond supplied a terrifyingly encyclopedic knowledge about all things virology, immunology,

and then some; I even got extra helpings of wisdom at our monthly bi-lab CHIKV meetings. Robyn Klein, like Debbie, is an amazing, strong female role model; I am so thankful for her scientific insight, encouragement, and the many kind reminders to stop fidgeting during presentations. To Thad Stappenbeck, I am grateful for all the histological wisdom you offered, even when it meant informing me that my microscopy pictures weren't quite good enough yet. Dave Wang was such an excellent chair for my qualifying exam, I knew that I had to keep him in that chair, sagely probing about experimental techniques and the wider scope of my project.

I am so honored to have belonged to the Lenschow lab. As a small to medium-sized lab, we persevered with bonds of science and friendship, and through bouts and boons of funding. I am grateful to several former lab members for helping me at the very beginning of my grad school career. Jessea Campbell was an amazing rotation mentor, who was patient as I slowly learned how to plan experiments and tried to master new techniques. Anjali Rohatgi's defense was one of the first I attended, giving me hope that I too could one day accomplish such a feat, and the initial groundwork she laid in establishing the CHIKV arthritis mouse model in our lab was invaluable. Dave Morales supplied years of calm and kind support, helping me as I attempted a new *in vitro* system for flu infections. And although I never actually met him, Scott Werneke was always very helpful through email as I tried and then failed to continue his research on CHIKV and IL-6.

To the current Lenschow lab members, I am so grateful to call each one colleague and friend. E.J. Perng has been an amazing bench neighbor, always available to talk about anything, be it science or life-related, and even at times lend a shoulder to cry on; his scientific knowledge is humbling, as is his humility. I am also so happy that I could rely upon Lindsey Cook as we built upon Anjali's work to further entrench the CHIKV arthritis model into our lab; her grasp of immunology and the scientific literature is truly astounding, as is her love-hate relationship with all things politics. Kristen Monte was a phenom of a lab manager, graciously fulfilling my voracious

demands for mice, reagents, and her dissection expertise. As the “baby” of the lab for many years, I was elated when Brad Hiller and Marissa Locke joined our lab. Brad has been an amazing person to talk to about science, experiments, and life; he even laughs at my weird videos that no one else finds funny. Marissa is an amazing scientist and person who tolerates my jokes and often mediocre grasp of immunology. I am so grateful that she is continuing and melding both my and Lindsey’s projects; I feel like I am leaving my science baby in more than capable hands. I am a better person for having been in the Lenschow lab, and I am confident that everyone has bright futures ahead of them.

I am so grateful to belong to the overarching WashU community. Jeanne Silvestrini was an amazingly supportive MMMP coordinator. I am thankful for the many people who have helped and collaborated with me, including many in the Diamond, Miner, and Stappenbeck labs. Thank you to the Musculoskeletal Research Core and the WUCCI, for cutting so many samples and teaching me so much about microscopy, respectively. I would be remise to not note my forms of funding while at WashU, including the internal Cell and Molecular Biology T32 training grant and R21 and R01 NIH grants. I have also beyond happy to have found a second home in the Office of Technology Management. Kathleen Chaffee has been a prodigious mentor in patent law. She has truly nurtured my love of this perhaps esoteric field, and without her I would likely be following a different, and perhaps much less personally fulfilling, career trajectory.

I cannot even begin to innumerate the ways my family and friends have helped me. My parents, Shawn and Linda Becker, endowed in me a great love of learning, encouraged my strange reading fancies (from anatomy to Egyptology), and tolerated my choice of a scientific career, even though for some reason they both thought I should major in English. Zachariah Young got me through college, into grad school, and planted the idea of patent law in my brain; even though our lives have bisected, I know that he will continue to be an ever-astute guiding force in my life. Jared and Kelsey Busby and their family have been a beacon of hope during my

last year of grad school; without their love and their endless supply of hot chocolate, I know that I wouldn't have been able to finish my PhD.

Finally, I would like to thank all of the non-human entities that aided in the completion of my PhD. To the thousands of mice that died at my hands, I am eternally grateful for their sacrifice. My German companion, Smaug the dog, wielded an endless supply of snuggles, kisses, and whiny complaints about everything and nothing in particular. Thank you to all the planks of wood, shards of fabric, and abandoned pieces of furniture for allowing me to funnel my creative rage and stress from grad school into sometimes successful DIY attempts. To everyone and everything that helped me throughout my life and especially during my PhD, if I could I would give all of you honorary doctorates, but I can't so I won't. Thank you!!!

Alissa Roxanne Young

Washington University in St. Louis

December 2018

ABSTRACT OF THE DISSERTATION

A recombinant virus and reporter mouse system for the study of chronic chikungunya virus pathogenesis

by

Alissa Roxanne Young

Doctor of Philosophy in Biology and Biomedical Sciences

Molecular Microbiology and Microbial Pathogenesis

Washington University in St. Louis, 2018

Professor Deborah J. Lenschow, Chair

Chikungunya virus (CHIKV) is an arthritogenic alphavirus that during acute disease causes fever as well as severe joint and muscle pain. Chronic joint and muscle pain persists in a significant subset of patients, yet we still have a poor understanding of what drives this chronic disease. While replicating virus has not been detected in the joints of patients with chronic arthritis or in various animal models at chronic time points, persistent viral RNA can be detected for months after acute infection.

To identify the cells that could be contributing to chronic CHIKV pathogenesis, we developed recombinant viruses that express Cre recombinase (CHIKV-3'-Cre and CHIKV-5'-Cre). These viruses replicated in cell types targeted by CHIKV, including myoblasts and fibroblasts, and they induced acute arthritis in a murine model of CHIKV arthritis. Importantly, they also induced chronic disease, including persistent viral RNA and chronic myositis and synovitis similar to wild-type (WT) virus. CHIKV-3'-Cre infection of tdTomato reporter mice resulted in a population of tdTomato$^+$ cells that persisted for at least 112 days. The majority of these cells localized to the dermis and muscle, and

immunofluorescence profiling revealed that these tdTomato$^+$ cells were dermal and muscle fibroblasts and myofibers. Treatment with an antibody against Mxra8, a host receptor for CHIKV, reduced the levels of viral RNA and the total number of tdTomato$^+$ cells in the chronic phase, with a preferential reduction in fibroblasts. Anti-Mxra8 treatment demonstrated a correlation between chronic viral RNA levels and the number of surviving tdTomato$^+$ cells, thus suggesting that viral RNA can be found within these persistent tdTomato$^+$ cells. This CHIKV-3'-Cre and tdTomato reporter mouse system demonstrates that cells can survive CHIKV infection *in vivo* and represents a powerful tool to study the chronic pathogenesis of CHIKV infection.

In the process of optimizing this reporter system, we observed noticeable effects on pathogenesis depending on viral inoculum. Increasing the dose of CHIKV (WT, 5'-Cre, and 3'-Cre) was associated with an earlier peak of swelling and infectious titers in the ipsilateral ankle, earlier resolution of swelling, and faster clearance of infectious virus in the ipsilateral ankle and distal sites. This accelerated clearance phenotype could explain why levels of persistent viral RNA tended to be lower in the ipsilateral ankle with increasing initial inoculum.

Ultimately, our CHIKV-Cre system could be applied to many aspects of studying chronic CHIKV pathogenesis. For example, single cell or nucleus RNA-seq could help determine whether persistent viral RNA is concentrated in tdTomato$^+$ cells, the nature of this persistent viral RNA, and whether the host transcriptome of tdTomato$^+$ cells is altered. Electron microscopy could help determine the subcellular location of persistent viral RNA within tdTomato$^+$ cells. CHIKV-Cre infection of Diphtheria toxin receptor (DTR) mice could allow for depletion of DTR$^+$ cells and exploration of how these cells contribute to chronic

pathogenesis. Overall, our CHIKV-Cre and tdTomato reporter mouse system marks myofibers and fibroblasts as cells that may harbor viral components and likely contribute to chronic CHIKV pathogenesis. Further characterization of these cells will no doubt aid in our understanding and development of potential treatments for this debilitating infection.

Chapter 1:

Introduction

1.1 Chikungunya Virus

Chikungunya virus (CHIKV) is a re-emerging arthropod-borne virus ("arbovirus") that causes polyarthritis and myalgia. Chronic joint and muscle pain persists in a significant subset of patients for months to years after the initial infection, but chronic pathogenesis of the virus is still poorly understood. CHIKV is endemic throughout tropical regions, including Africa, Asia, islands in the Indian and Pacific Oceans, and Central and South America. The World Health Organization (WHO) classifies CHIKV as a neglected tropical disease, and perhaps as a consequence no vaccines or treatments are currently approved for CHIKV.

1.1.1 Evolution and Epidemiology

CHIKV is a reemerging pathogen originally identified in Tanzania in 1952 [1–3]. The name "chikungunya" derives from the local Makonde tongue and translates into "that which bends up," an apt description for the characteristic joint "pain [that] was frightening in its severity" [1,4]. The prolonged arthritis of Chikungunya fever (CHIKF) was concomitant with rash and leucopenia; despite its significant morbidity, this early CHIKF exhibited no known mortality [1]. Subsequent studies implicated CHIKV as an arbovirus transmitted by *Aedes* genus mosquitos [3]. Ultimately, CHIKF was recognized to be endemic throughout Africa, consisting of the two distinct West African and East/Central/South African (ECSA) lineages [5]; phylogenetic analyses estimate its emergence as a human virus within the last 500 years [6]. A third, Asian lineage likely diverged from the ECSA phylogroup in the middle of the twentieth century [6] and caused its first recognized outbreaks in Thailand in 1958 and India in 1963 [7] (**Figure 1.1A**). Throughout the latter half of the twentieth century, these three lineages caused scattered outbreaks, often with decades spanning cases [6,8]. During this time, CHIKV followed a sylvatic transmission cycle, which comprises cycling between wild animals and vectors, with occasional outbreaks in humans. Known animal reservoirs of CHIKV include monkeys, rodents, bats, and birds [6,9].

Up until the 2000s, CHIKV was considered a self-limiting, tropical virus; however, within the past 15 years CHIKV has reemerged with increased virulence and range, resulting in urban transmission cycles without the need for animal host intermediates. In 2004, an ECSA-derived strain of CHIKV initiated an epidemic in Kenya with over 13,000 cases [10]. By 2005, the virus spread to La Réunion Island, where it infected over 200,000 people [8,11]. The Réunion epidemic included the first reports of increased pathogenicity, including neurological symptoms, intrapartum transmission, and approximately 250 deaths [12–14]. The Réunion strain was surprisingly spread by *Aedes albopictus,* a particularly bloodthirsty mosquito with a much larger spread compared to the previous vector, *A. aegypti* [9,15,16]. Genetic analyses revealed that an A226V mutation in the E1 protein caused this increased *A. albopictus* transmission [17]. Owing in part to this vector shift, CHIKV subsequently spread throughout the Eastern Hemisphere, establishing endemic conditions in tropical regions including India and the South Pacific, infecting millions and killing thousands, and even causing isolated outbreaks in Europe [16,18,19]. This ECSA-derived strain is thus dubbed the Indian Ocean Lineage (IOL) (**Figure 1.1B**).

In 2013, autochthonous (local) CHIKV transmission was reported in the Western Hemisphere, and nearly 2 million suspected CHIKV cases have since been reported in the Caribbean, Central America, and South America [18,20–22]. However, it is likely that the current CHIKV epidemic in the Americas represents a reintroduction of the virus as presumed Dengue epidemics in the American tropics during the 1800s closely resemble CHIKV symptomology [23]. Since 2014, thousands of travel-acquired cases of CHIKV have been reported in the United States [24]. Locally transmitted CHIKV cases have also been reported in Florida (12 cases in 2014) and in Texas (1 case in 2015), but no local cases have been reported within the past three years [25]. The Western Hemisphere CHIKV strains are most closely related to the Asian, not IOL, lineage, which initiated a separate, East Asian epidemic in 2006 [18,26,27]. As such, the Western

Hemisphere CHIKV strains have not been reported to contain the E1 A226V substitution. Overall, CHIKV is a relevant, reemerging virus inciting epidemics around the globe.

1.1.2 Virus Structure and Replication

CHIKV is a positive-sense RNA virus belonging to the *Togaviridae* family and alphavirus genus [5]. While the related New World alphaviruses are associated with encephalitis (e.g. Eastern, Western, and Venezuelan Equine Encephalitis viruses), the Old World alphaviruses, which include CHIKV, often cause musculoskeletal disease and arthralgia (e.g. CHIKV, Ross River virus, Sindbis virus, Semliki Forest virus, O'nyong'nyong virus, Mayaro virus) [28]. CHIKV is currently the most prevalent and widespread of these arthritogenic alphaviruses [29]. As is characteristic of alphaviruses, CHIKV is a relatively small and simple virus. It consists of an 11.8 kilobase, single-stranded RNA genome. The genome is encapsulated within an icosahedral nucleocapsid which is enclosed within a 60-70 nm spherical envelope with proteinaceous spikes [9,28] (**Figure 1.2A**).

The unipartite, positive-sense genome closely resembles host messenger RNA with a 5' cap and 3' polyadenylated tail. The genome sequentially comprises a 5' un-translated region (UTR), a 5' open reading frame (ORF) encoding 4 nonstructural proteins, a subgenomic promoter, a 3' ORF encoding five proteins, and a 3' UTR (**Figure 1.2B**). The 5' and 3' UTRs contain promoters necessary for genome replication and other regulatory elements [9,28,30]. The 3' UTR is highly variable in length amongst alphaviruses and appears to be involved with vector competence [31,32]. Many of the functions of the nine viral proteins and specific replication events have not been directly studied in CHIKV, due to it being a Biosafety Level 3 (BSL3) virus, and are thus extrapolated from studies of related alphaviruses such as Sindbis virus and Semliki Forest virus.

The 5' ORF encodes four non-structural proteins (nsP1-4), which are involved in viral genome replication. The nsP1 protein is involved in 5' capping newly synthesized viral RNA, initiating negative strand synthesis, and anchoring viral replication complexes to the host membrane. The nsP2 protein has helicase, ATPase, and protease activities. The nsP3 protein is an ADP-ribose-1-phosphate phosphatase and has an RNA-binding motif. The nsP4 protein is the virus' RNA-dependent RNA polymerase (RdRp) [28,33,34].

The 3' ORF comprises three structural genes (CP, E1 and E2) and two smaller cleavage products (E3 and 6K). The capsid protein (CP) forms the nucleocapsid around the genomic RNA. CP contains an RNA-binding domain and a protease domain [35]. E1 and E2 are glycosylated, associate in a heterodimer, and form trimeric spikes on the envelope. E1 associates with the viral envelope and capsid, and it functions as a Type II fusion protein during endosomal entry. E2 binds to host cell receptors [28,36,37]. Mxra8 has recently been reported to be a host receptor for CHIKV and other arthritogenic alphaviruses; however, it is likely that CHIKV also uses other host receptors as Mxra8 blockade did not entirely abrogate infection [38]. The E3 and 6K proteins are cleavage products during viral replication. E3 and 6K contain signal peptide sequences and may direct E2 and E1, respectively, to the secretory pathway before being cleaved by host proteases [39]. E3 may help shield the fusion peptide of E1 during viral budding [40]. The 61-amino acid 6K protein may also be involved with viral budding and formation of ion channels [28,37,41].

Replication of CHIKV within target cells appears to be characteristic of alphaviruses (**Figure 1.3A-B**). E2 binds to a host receptor on the cell surface [28,42]. CHIKV infection appears to be dependent on membrane cholesterol, which is suggestive of lipid raft involvement [43,44]. Incidentally, the A229V mutation characteristic of the IOL strain increases dependence on cholesterol [43]; how this enhances replication in *A. albopictus* remains unclear. Receptor binding triggers clathrin-mediated endocytosis [45]. CHIKV infectivity is dependent on endosomal acidification, indicating a pH-dependent activation of the E1 fusion protein. Additionally, CHIKV

replication depends only on early endosomes, indicating that the virus escapes into the cytoplasm prior to endosomal maturation [36,43].

Once released into the cytoplasm, CP associates with the ribosome, which may assist in uncoating of the nucleocapsid [28]. Early during replication, the 5' ORF is directly translated into the P123 polyprotein (**Figure 1.3A**). During approximately 10% of the translation events, suppression of termination occurs at the opal stop codon between nsP3 and nsP4, and readthrough results in production of the P1234 polyprotein [46]. nsP2 proteolytically processes the P123 or P1234 polyproteins into the four non-structural proteins [28,33].

Genome replication cannot occur until after the nsP2 cleavage step as the RdRp (nsP4) is not carried in the capsid and must be translated by host machinery [33]. The P123/nsP4 complex catalyzes replication of the negative strand from the positive genome. The negative-sense RNA strand predominates early in infection, and it serves as a template for a full-length positive-sense genome, which is preferentially catalyzed by the short-lived nsP1/P23/nsP4 complex. Full processing of P23 into nsP2 and nsP3 results in the mature nsP1/nsP2/nsP3/nsP4 complex, which preferentially drives production of the 3' subgenomic 26S RNA [46]. The 26S fragment accumulates later during infection, and it serves as a template for the structural polyprotein driven by the powerful subgenomic promoter [28,33,36]. This subgenomic RNA replication strategy utilized by members of the Togaviridae family thus ensures that structural proteins are produced at a higher amount than non-structural proteins, which are only needed at lower catalytic amounts.

Translation of the subgenomic RNA results in production of the structural polyprotein. As CP emerges from the ribosome, it autocatalyzes its release from the growing polyprotein using its protease domain. The E3-E2-6K-E1 polyprotein is subsequently translated, but 10-18% of the time ribosomal frameshifting in the 6K RNA results in production of the E3-E2-TF (transframe) polyprotein [47]. TF retains the ion-channel properties of 6K, and disrupting TF production

attenuates alphavirus production; however, its exact role is unclear [48]. The structural polyproteins are cleaved into E3-E2, 6K, TF, and E1 by host signal peptidase enzymes.

During viral replication in mammalian cells, the viral RNAs are sequestered into various vesicular bodies derived from host membrane (**Figure 1.3B**). These membranous bodies likely shield double-stranded RNA (dsRNA) intermediates from full detection by host pattern recognition receptors (PRRs). Early in infection, the negative sense genomes are found within spherule extrusions of the cell membrane, with the non-structural proteins associated with the neck of the spherules [49]. Internalization of the spherules and association with lysosomes produces the first iteration of cytopathic vacuoles (CPV-I), where production of full-length genomes and subgenomic RNAs continues [40]. Later during infection, a second type of virally-induced large cytopathic vacuoles is formed, termed CPV-II. CPV-II are derived from the trans-Golgi network and comprise a large vesicle containing helical tubular formations of the envelope glycoproteins; the vesicles are dotted with non-enveloped nucleocapsids. The role of the CPV-II is unclear, but they may facilitate virion assembly [40,50].

Virion assembly occurs in the cytoplasm and commences with the C protein forming a nucleocapsid around genomic RNA; the capsid displays icosahedral symmetry (T=4) and contains 240 CP capsomers [28,51]. Budding occurs through the plasma membrane which has become inundated by the E1 and E2 viral glycoproteins. In order to be infective, E2 must be processed by a host furin protease in order to remove E3. Budding results in an enveloped virion coated by 80 trimers of E1-E2 dimer spikes [28]. The replication cycle begins anew when a virion binds a new cell. Ultimately, CHIKV replication produces cytopathic effects and can be lytic [52].

1.1.3 Tropism and Acute Pathogenesis

As an arbovirus, CHIKV depends on replication within a mosquito vector. The *Aedes* receptor for CHIKV has not yet been identified, but it is known to replicate within the mosquito

midgut and transit into the salivary glands [9,17]. CHIKV can be transmitted to humans in the saliva of an infected, biting mosquito; factors in *Aedes* saliva have been shown to enhance the pathogenesis of other arboviruses such as Dengue virus [53]. The initial infection is followed by a noninfectious, incubation period of 3 to 7 days [11,13,42]. The virus appears to be highly transmissible, especially on geographically constrained islands; for instance 75% of the population of Lamu Island and 30% of La Réunion Island were infected during outbreaks in 2004 and 2006, respectively [10,28]. An estimated 75-95% of people who are infected with CHIKV become symptomatic [11,54].

It is thought that CHIKV can propagate within stromal cells, including fibroblasts, surrounding the site of injection [55,56]. *In vitro*, mouse embryonic fibroblasts (MEFs) and other primary fibroblasts can be thus used as a model cell for CHIKV infection [54,57]. Within hours, CHIKV spreads from the connective tissue around the bite site into the microvasculature and lymph vessels [29,57]. From there, the virus spreads into the liver, lymph nodes, and spleen (**Figure 1.4**); viral replication in these sites ultimately leads to viremia and initiation of symptoms such as fever [29]. High levels of viremia last for several days, with titers in infected humans reported to be as high as 10^8 to 10^9 viral RNA copies per milliliter [42,58]. The transmission cycle begins anew when an uninfected *Aedes* mosquito takes a blood meal from a viremic individual. It has not been demonstrated whether the blood titers result from free virus, blood cells infected with virus, or a combination of both. Nonetheless, there are some indications that infected hematopoietic cells can be found in the blood.

For instance, one study assayed viral growth in a barrage of cell lines and reported that CHIKV can replicate in macrophages but not monocytes or dendritic cells [42]. However, another study reported that in human blood samples from acute CHIKV patients up to 7% of $CD14^+$ monocytes and 3% of $CD303^+$ plasmacytoid dendritic cells harbored CHIKV antigen [59]. The overall viral load in the blood also correlated with the percentage of infected monocytes,

suggesting that infected monocytes could serve to shuttle virus through the blood during viremia. The study also demonstrated that live CHIKV but not heat-inactivated CHIKV could infect monocytes isolated from peripheral blood mononuclear cells (PBMCs) [59]. Growth in hematopoietic cells such as macrophages and monocytes could prove to be a critical step in CHIKV pathogenesis. Infected monocytes could spread CHIKV to sequestered organs such as the brain and muscle; infected macrophages may also contribute to chronic infection and potentially inflammasome activation [56,59]. *In vitro*, CHIKV can infect RAW 264.7 cells (an immortalized mouse macrophage cell line), which results in secretion of TNF-α, IL-6 and GM-CSF [60]. No studies have reported substantive CHIKV growth in lymphocytes.

During this short-lived viremia, CHIKV spreads to many regions of the body, including the joints, muscles, and brain. Like other alphaviruses, CHIKV displays a propensity to infect multiple tissue types. CHIKV can productively replicate in epithelial cells, endothelial cells, fibroblasts, and osteoblasts [29,42]. In addition to epithelial and connective tissues, CHIKV also grows to high titers in neurons and muscle satellite cells [52,55,61]. Specific strains can grow in additional tissue types. For instance, one study demonstrated that a virulent IOL CHIKV strain isolated in 2006 from the La Réunion Island outbreak (LR2006-OPY1) can infiltrate and grow within skeletal muscle fibers while a pre-epidemic strain cannot [57]. It is unclear how CHIKV can transit the insulating barriers surrounding muscle and other targets such as the brain.

Infection of these target tissues triggers a vigorous inflammatory response. Within the joints, infection of synoviocytes leads to expression of chemokines and inflammatory cytokines, including IL-6, MCP-1, and IL-1β [29,54,62]. This is followed by a massive influx of immune cells, including macrophages, monocytes, natural killer (NK) cells, and T cells into the synovial cavity [54,63,64]. This substantial immune infiltrate results in painful distention of the joint capsule, leading to CHIKF's characteristic arthralgia and arthritis [29]. The infiltrating immune cells may also become overactive and cause tissue damage through secretion of metalloproteinases

[29,54]. In addition to inflamed joints, CHIKV can also cause muscle, tendon, and brain damage [64,65]. The exact mechanism of this pathology is unclear but likely involves a combination of host and virus factors. Not only is CHIKV infection itself lytic, but it can also induce apoptosis [52,60] and results in the secretion of many potentially toxic pro-inflammatory cytokines [9,63,65]. Acute CHIKV symptoms can in large part be attributed to a hyper-responsive innate immune system.

1.1.4 Prophylactics and Therapeutics

No licensed anti-virals or vaccines are currently available for acute or chronic CHIKV disease. Current therapeutics include supportive measures such as maintaining patient water and electrolyte levels, as well as non-specific drugs including analgesics, antipyretics, and non-steroidal anti-inflammatory drugs [16,56,64]. Public health efforts also aim to decrease transmission with vector elimination and mosquito netting [22].

A variety of studies have identified compounds with antiviral activity against CHIKV *in vitro* or *in vivo*. For instance, drugs against other microorganisms have demonstrated *in vitro* efficacy against CHIKV infection [11,66,67]. Examples of repurposed antivirals include Favipiravir, arbidol, ribavirin, and interferon-α, but their actual *in vivo* or clinical effectiveness remains untested [68–70]. A recent *in vitro* loss-of-function screen identified several pro-viral host factors with pre-existing small-molecule inhibitors available, some of which showed *in vivo* efficacy alone or in combination [71]. Additional *in vivo* studies have demonstrated the efficacy of monoclonal antibodies against CHIKV, alone or in combination with immunomodulatory agents such as CTLA4-Ig [72–75].

Multiple vaccine candidates have been produced, but none are currently approved for human use [76]. Three vaccine candidates have completed Phase I and II clinical trials with varying results. The first CHIKV vaccine candidate tested involved a lab-attenuated CHIKV strain

derived from the Asian lineage [77] (**Figure 1.1A**); this vaccine proved to be immunogenic in Phase I and II clinical trial. However, a small percentage of participants developed transient arthritis, so this candidate has not been pursued further [76,77]. A second candidate involves a recombinant live-attenuated measles virus (MV) that expresses virus-like particles (VLPs) containing CP, E3, E2, 6K, and E1 proteins from the La Réunion ECSA CHIKV strain [78]. A recent Phase II trial of the MV-CHIKV vaccine reported good safety, tolerability, and immunogenicity, with CHIKV-neutralizing antibodies detectable in all MV-CHIK treatment groups [79]. A third CHIKV vaccine candidate (VRC-CHKVLP059-00-VP) also involves VLPs, but in this case the vaccine itself comprises VLPs containing CP, E1, and C2 proteins from the 37997 West African CHIKV strain; Phase I results using this vaccine were promising [80]. The Phase II trial was scheduled to end in October 2018, but the results of this trial have not yet been reported.

Additional vaccine candidates are in the pre-clinical pipeline having showed efficacy in animal models of CHIKV infection. One CHIKV vaccine candidate involves a chimeric virus combining the non-structural proteins of Eilat virus (an insect-specific alphavirus) with CP, E1, and E2 structural proteins from CHIKV-99659, a human isolate from the British Virgin Islands. This vaccine demonstrated immunogenicity in mice and non-human primate models [81]. Another potential vaccine involves a La Réunion CHIKV strain attenuated with site-directed mutations in the nuclear localization sequence (NLS) of CP. This vaccine demonstrated efficacy against both CHIKV and Ross River virus (RRV) in mice [82].

The majority of the clinical testing for these antivirals and vaccines rely on readouts from acute disease, such as early viral titers, or later titers of neutralizing antibodies. It is unclear how these therapeutics and prophylactics would impact chronic CHIKV disease; presumably, a reduction in acute disease would also result in a reduction of chronic disease. A better understanding of the intricacies of both acute and chronic CHIKV pathogenesis could ultimately lead to better treatments for this debilitating disease.

1.2 Chronic CHIKV Pathogenesis

Following acute CHIKV infection, an estimated 10-60% of patients report symptoms that can persist for 6 weeks to 6 years after the initial infection. The most common symptoms include arthritis, arthralgia, alopecia, and depression. Risk factors for these persistent symptoms include female sex, old age, and prolonged or more severe acute disease. A handful of studies of human or animal samples have reported detection of CHIKV antigen or RNA within joint and muscle tissues, often associated with macrophages and endothelial cells; however, detection of viral components in tissues at chronic time points is rare, especially in human samples. Hypotheses to explain the chronic manifestations of CHIKV infection include persistent viral RNA causing inflammation, a low level of actively replicating virus, or viral induction of autoimmunity. The chronic pathogenesis of CHIKV infection remains poorly understood, thus necessitating the development of better tools and model systems.

1.2.1 Chronic Clinical Manifestations

As discussed previously, acute CHIKV is associated with one to two weeks of musculoskeletal symptoms, including fever, rash, headache, asthenia, and joint and muscle pain often so severe that upright gait is too painful; neurological symptoms are also sometimes reported during acute infection [83]. Following acute CHIKV infection, the fever and rash resolve, and virus is no longer detectable by RT-PCR in the serum [84]. However, a significant subset of patients continues to report persistent symptoms.

The most common chronic symptoms reported by patients are persistent arthralgia (joint pain or stiffness), arthritis (joint swelling), or more general rheumatic musculoskeletal pain (RMSP) in distal joints such as the ankles and wrists, typically with a bilateral and symmetrical manifestation. The prevalence of these symptoms depends on the study, with ~50-60% on the high end and ~10-20% on the low end. For example, one study of 250 CHIKV patients following

the 2007 Italian outbreak reported that 72.3% of patients described persistent arthralgia 4 to 5 months post infection and 60.8% at 12 to 13 months; the prevalence of persistent arthralgia at 12 to 13 months was as high as 73.8% in patients who had pre-existing joint pain prior to CHIKV infection [85]. In another study of 437 CHIKV patients in South India 15 months following a 2007 epidemic, 57% reported post-viral polyarthralgia [86]. A similar study identified 1195 CHIKV patients 18 months following a 2009 outbreak in rural India and found that 48.6% had persistent RSMP [87].

Other studies report lower prevalence of chronic arthralgia symptoms, such as 12.5% (2 out of 16) of German patients 6 months after travel to endemic Asian areas in 2006 [88], or 10% (3 out of 30) of patients 3 months after acute infection in a 2008 Singapore outbreak [89]. A study of 403 adult CHIKV patients in South India in 2006 reported persistent arthralgia in 16% of patients 3 to 6 months following infection, 12.7% between 6 and 12 months, and 7% beyond 1 year [90]. The majority of other studies report percentages falling somewhere in the middle of these extremes [91–93]. For example, the TELECHIK survey, which was a 2-year follow-up of the acute SEROCHIK survey for the 2006 La Réunion Island outbreak, found that 42.8% of 515 $CHIKV^+$ patients still reported chronic RMSP [94]; however, a reanalysis of the TELECHIK survey reported that 81.9% of 422 $CHIKV^+$ patients experienced chronic RMSP [95]. Meta-analyses of chronic CHIKV studies have reported an average of approximately 40% of CHIKV patients developing chronic symptoms [96,97]. Including studies with only 1 year or more follow-ups, the overall CHIKV chronic symptom rate was 21% [97].

Many factors likely influenced the wide range of reported prevalence in these studies, including the specific epidemic and CHIKV strain, as well as specific study design and inclusion criteria. For example, studies associated with the 2006 La Réunion Island epidemic [94,95,98] or outbreaks in India [86,87] tended to be associated with a higher prevalence of chronic CHIKV symptoms. A meta-analysis of 38 chronic CHIKV studies found a similar trend, with ECSA-

diverged CHIKV strains (e.g., La Réunion Island, India, France) inciting a higher average prevalence of chronic symptoms than recent Caribbean strains or South African ECSA strains from the 1980s [96]. Of note, retrospective studies tended to have a higher percentage of patients reporting persistent arthralgia compared to prospective studies [97], which suggests at least some degree of memory and reporting bias.

Not only did patients report joint-associated pain or swelling, but joint damage could sometimes be detected through radiographic changes. For example, one study examined 21 CHIKV patients two years following the 2006 La Réunion Island outbreak and identified 5 patients with bone erosions and 12 patients with joint space narrowing in the hands and or feet [99]. Another study also from La Réunion Island identified bone lesions by radiography in 50% of the patients diagnosed with chronic inflammatory rheumatism following CHIKV infection [100]. However, a third study found no evidence of structural damage by radiography in the 437 $CHIKV^{+}$ patients examined [86].

1.2.2 Non-Rheumatic Chronic Symptoms

In addition to joint-associated symptoms, other commonly reported chronic CHIKV symptoms include alopecia, depression, sleep disorders, and overall loss in the quality of life (QOL) [96,97]. Two studies reported alopecia prevalence of 10-30% [85,101], while one study reported no change in the prevalence of hair loss [94]. Rates of depression following CHIKV infection ranged from 13 to 54% [92,98,101–103]; however, one case reported a low depression prevalence of 6.3% (3 of 47) [104]. Overall, the quality of life for CHIKV patients was reduced, often for several years. For example, a study of French gendarmes (military police) following the 2006 La Réunion Island epidemic found a significant negative impact on completing daily activities (such as showering, making bed) and a higher consumption of healthcare 30 months after infection [98]. In a 6-year follow-up of these gendarmes, the QOL scores had not

significantly improved from the 30-month survey [103]. Another study in rural India reported that a fifth to a quarter of patients reported moderate or severe difficulty in completing simple physical tasks such as arising and walking [87]. Additional studies using the standardized Short Form questionnaires (SF-36 and SF-12) described a significant QOL reduction in the physical and or mental health domains [101,105].

1.2.3 Chronic Biomarkers

Multiple studies have attempted to identify predictive markers for CHIKV-induced chronic arthralgia. Older age (>35-45 year old) individuals, females, and people who experienced prolonged or severe acute disease appear to be most at risk for development of chronic symptoms [54,85,90,91,102,106]. One group found an increased likelihood of chronic CHIKV in patients with high acute serum concentration of C-reactive protein (CRP) [54]. Another group indicated elevated acute IL-6 and GM-CSF as predictors, but found no association with acute disease severity, viremia, or CRP levels [89]. One study reported an association of chronic arthralgia with CHIKV-RNA detection beyond 7 days of symptom onset [107]. A study in rural Southern India identified vegetarianism as the strongest determinant of chronic CHIKV development [87]. While these studies agree that chronic CHIKV pathogenesis is characterized by a chronic inflammatory state, they do not arrive at consistent markers, and the biomarkers themselves are not indicative of an exact disease mechanism.

1.2.4 Congenital CHIKV

In addition to symptoms in infected adults, long-term complications can also arise from congenital CHIKV, acquired by neonates through vertical transmission from infected mothers, likely via intrapartum transmission (during childbirth). In the infants who survived the acute CHIKV infection during the La Réunion Island epidemic, many neurological manifestations occurred, included encephalopathy, intracranial hemorrhage, cerebral palsy, ataxia, and

blindness [108]. Further follow-up of these congenital CHIKV cases at 2 years of age revealed continued neurodevelopmental deficits [109]. One study of pregnant CHIKV-infected women in Thailand found no vertical transmission of CHIKV to neonates [110], which could indicate that perinatal transmission is strain-specific. These studies highlight that neurological symptoms dominant during neonatal infection, likely due to increased accessibility to the infant brain, compared to adults where rheumatic symptoms predominate with neurological manifestations only rarely reported.

1.2.5 Hypotheses for Chronic Pathogenesis

Hypotheses to explain chronic CHIKV pathogenesis abound, including the induction of autoimmunity, the persistence of ultralow levels of replicating virus, and the activation of inflammatory responses against residual viral RNA. The role of autoimmunity in chronic CHIKV pathogenesis is unclear. A small subset of chronic CHIKV patients test positive for antinuclear antibodies (ANA); however, their pre-CHIKV status is unknown [24,102,111]. Viral infections are also known to transiently induce ANA, so the relevance of this observation to the development of chronic arthritis is unclear. Furthermore, these same studies have not detected other known autoantibodies, including anti-dsDNA, anti-endomysium, anti-Sm, anti-Jo-1, or anti-cyclic citrullinated peptide antibodies (ACCP), or rheumatoid factor [24,102,111]. It has been proposed that CHIKV patients could harbor unknown autoantibodies through molecular mimicry [112]. As it stands, proving or disproving the involvement of autoimmunity in chronic CHIKV pathogenesis remains challenging.

There is evidence that CHIKV antigen may persist in tissues chronically. CHIKV antigen was detected in the synovial macrophages of one patient 18 months after infection [54], as well as in a human muscle specimen at least three months after acute infection [61]. Cells positive for CHIKV antigen can also be detected in persistently-infected macaques [56] or wild-type mice

[113]. Recombinant CHIKV expressing firefly luciferase also produce detectable luminescence during the chronic stage of disease, suggesting that the virus could be undergoing low levels of replication [114–116]. However, these and other studies have not demonstrated that the virus itself is replication proficient. One study reported the detection of infectious CHIKV by $TCID_{50}$ assay at 44 dpi in the spleen, liver, and muscle tissue of IV-inoculated macaques, but not the joint tissue [56]. To our knowledge, infectious virus has not been isolated from the joint tissue of chronic patient or wild-type animal samples [117,118]. Therefore, while it is impossible to completely dismiss autoimmunity and low-level viral replication as the driving force behind chronic disease, the data supporting these hypotheses has not been definitively seen in various human or animal studies.

A prevailing hypothesis for chronic CHIKV pathogenesis is that non-infectious CHIKV RNA remains in infected tissues, and its dsRNA intermediates act as a proinflammatory pattern-associated molecular patterns (PAMPs) [119]. Chronic CHIKV RNA can consistently be detected through qPCR in animal models, including the joints and spleen of mice and the spleen, lymph nodes, and liver of macaques, despite the fact that infectious virus is cleared much sooner [56,120]. Detection of chronic CHIKV RNA in human samples has been less consistent. One study reported the presence of CHIKV E1 and nsP2 RNAs in a human synovial fluid sample, but others have failed to detect chronic CHIKV RNA in patient serum or synovial fluid [54,118]. Such negative results could reflect the difficulty in obtaining more invasive patient samples such as joint, muscle, or spleen biopsies, as can be readily obtained in animal models.

Of note, administering viral or synthetic dsRNA or IFN-α by itself can even induce arthritis in mice through activation of IL-1R signaling, and IFNAR-/- mice are protected from these effects [121,122]. Therefore, administration of a viral PAMP alone or the downstream effector (type I IFN) can be sufficient to cause arthritic disease, even in the absence of an actively replicating virus.

1.3 Tools to Study Chikungunya Virus Infection

While clinical data provides some insight into the acute and chronic pathogenesis of CHIKV, the exact mechanisms of disease can only truly be dissected with *in vivo* models of infection. Fortunately, the past 10 to 15 years has seen vast advancements in CHIKV animal models. Furthermore, the cloning of CHIKV has allowed for the production of recombinant viruses that can be manipulated with the insertion of reporter genes or mutations, rather than relying on immutable and heterogenous clinical isolates.

1.3.1 Animal Models

Mice and nonhuman primates have both been used as models of CHIKV infection [123]. Mouse models include neonatal mice, immunocompromised mice, and WT mice that develop arthritis and myositis. Infection of neonatal mice results in lethality, often with neurological symptoms, which parallels neonatal human infection; decreasing the age of infection from 12 to 9 to 6-day-old pups subsequently increases mortality [124]. Knockout neonatal mice have been used to explore the involvement of specific interferon-stimulated genes (ISGs) during CHIKV infection [125]. Immunocompromised adult mice also develop severe CHIKV disease that can result in lethality. For example, mice that lack the type I IFN receptor ($IFNAR^{-/-}$) or type I IFN regulatory factors ($IRF3/7^{-/-}$) exhibit 100% mortality 3 to 8 days after infection [124,126,127]. As such, these mice are useful in the testing of neutralizing CHIKV antibodies [75]. However, due to the high levels of lethality, neither neonatal nor immunocompromised mice are useful for the study of chronic CHIKV pathogenesis.

The arthritis mouse model allows for study of both acute and chronic CHIKV pathogenesis. This model comprises inoculating immunocompetent adolescent (3-4 weeks old) mice with CHIKV subcutaneously into the rear footpad, mimicking a mosquito bite. This model recapitulates many acute aspects of human disease including viral replication in the joint and muscle tissues,

tenosynovitis and myositis, viremia, and dissemination to distal joint and lymphoid tissues [64,66,128]. Inoculation of mice into the footpad results in a biphasic swelling pattern in the ipsilateral foot, with the first swelling peak corresponding to cell lysis, local proinflammatory cytokine production, edema, and monocyte infiltration. The second peak is associated with an influx of inflammatory infiltrates, including B and T lymphocytes [64,66,128]. This model also recapitulates aspects of chronic CHIKV disease. CHIKV RNA persists in the joints for several months after infection, and there are signs of chronic myositis and synovitis [117,120]. However, the arthritis model is not without its limitations, including lack of bilateral symmetrical joint involvement [129].

Nonhuman primate models have also been used to study aspects of CHIKV pathogenesis. Rhesus macaques have been used since the 1960s for CHIKV virulence studies [130], and in more recent years studies of CHIKV pathogenesis and transmission or testing of vaccines and antivirals have also utilized Rhesus macaques [131–134]. Cynomolgus macaques have also been used to study CHIKV pathogenesis. For instance, one study used cynomolgus macaques to identify cell types that harbor CHIKV antigen at chronic time points [56]. While nonhuman primate models more closely recapitulate human disease and are typically required prior to clinical testing in humans, they do not offer the flexibility and specificity of mouse models, as non-WT animals are typically not used.

1.3.2 Recombinant Viruses

While clinical isolates were used for much of the early research on CHIKV, recombinant CHIKV constructs allow for increased manipulation of the virus. Reporter genes can be inserted into the CHIKV genome through introduction of a second subgenomic promoter, either in between the structural and non-structural genes (5') or at the end of the genome (3'). Previous studies have introduced fluorescent proteins such as GFP or mCherry into these locations, resulting in

viruses with tissue fluorescence only during active viral replication. These reports demonstrate that 5' clones (e.g. CHIKV-5'-GFP) have lower recombinant protein expression but higher stability than the 3' variants (e.g. CHIKV-3'-GFP); these viruses are also somewhat attenuated compared to WT CHIKV [135,136]. Firefly luciferase has also been successfully introduced into CHIKV clones [114–116]. Other groups have also reported success with introducing reporter genes into the nsP3 gene [137].

While fluorescent or luminescent viruses are useful for the study of acute CHIKV pathogenesis, fluorescent protein expression is typically transient, and luminescent output is often only resolvable on the tissue level; thus, such strategies are less helpful for the detailed study of chronic CHIKV pathogenesis. In order to study the chronic pathogenesis of other viruses, some groups have utilized recombinant viruses expressing Cre recombinase, which can indelibly mark infected cells in reporter cells or mice. This Cre-virus approach has been previously used to explore the chronic pathogenesis of influenza virus [138,139] and HSV-1 [140,141], but it has not yet been attempted with any alphaviruses, to our knowledge. As such, this dissertation concerns optimization and characterization of two CHIKV-Cre viruses, which we use to investigate the chronic pathogenesis of CHIKV.

1.4 Figures

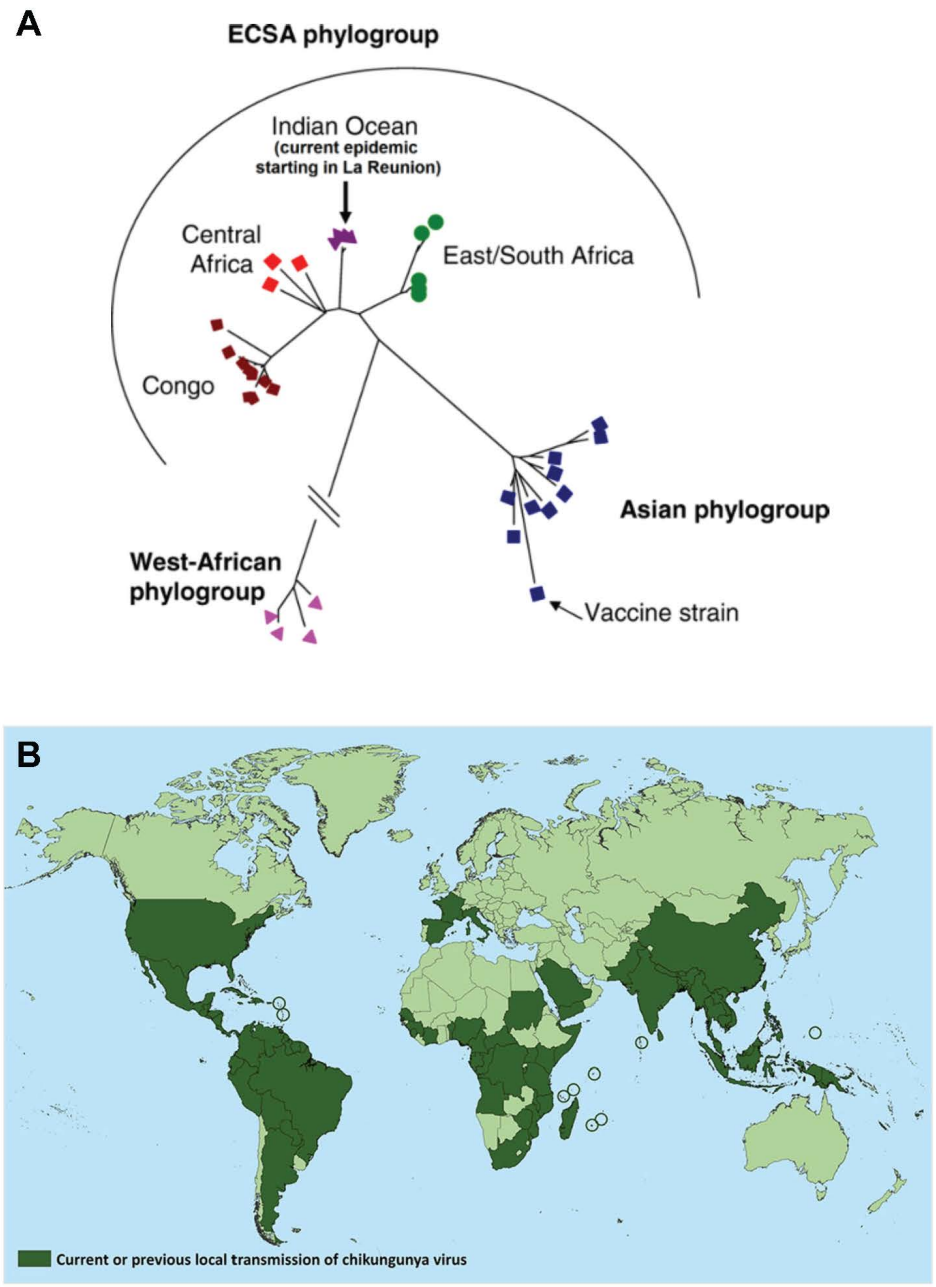

Figure 1.1: Evolution and epidemiology of CHIKV

(A) Phylogenetic map displaying the three CHIKV phylogroups: ECSA, Asian, and African; adapted from [142]. **(B)** World map showing the countries and territories where CHIKV cases have been reported as of May 29, 2018. The map does not include countries or territories where only travel-acquired cases have been reported; figure was adapted from [143].

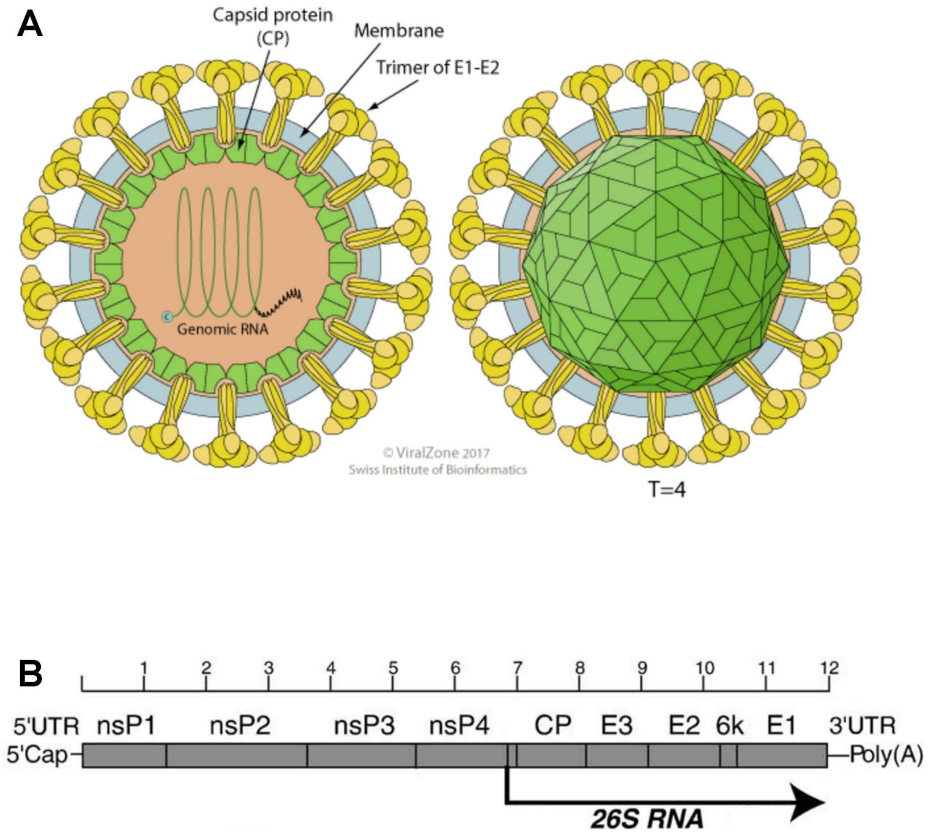

Figure 2.2: CHIKV virion and genome structure

(A) CHIKV virion structure; adapted from [144]. **(B)** CHIKV genome; adapted from [28].

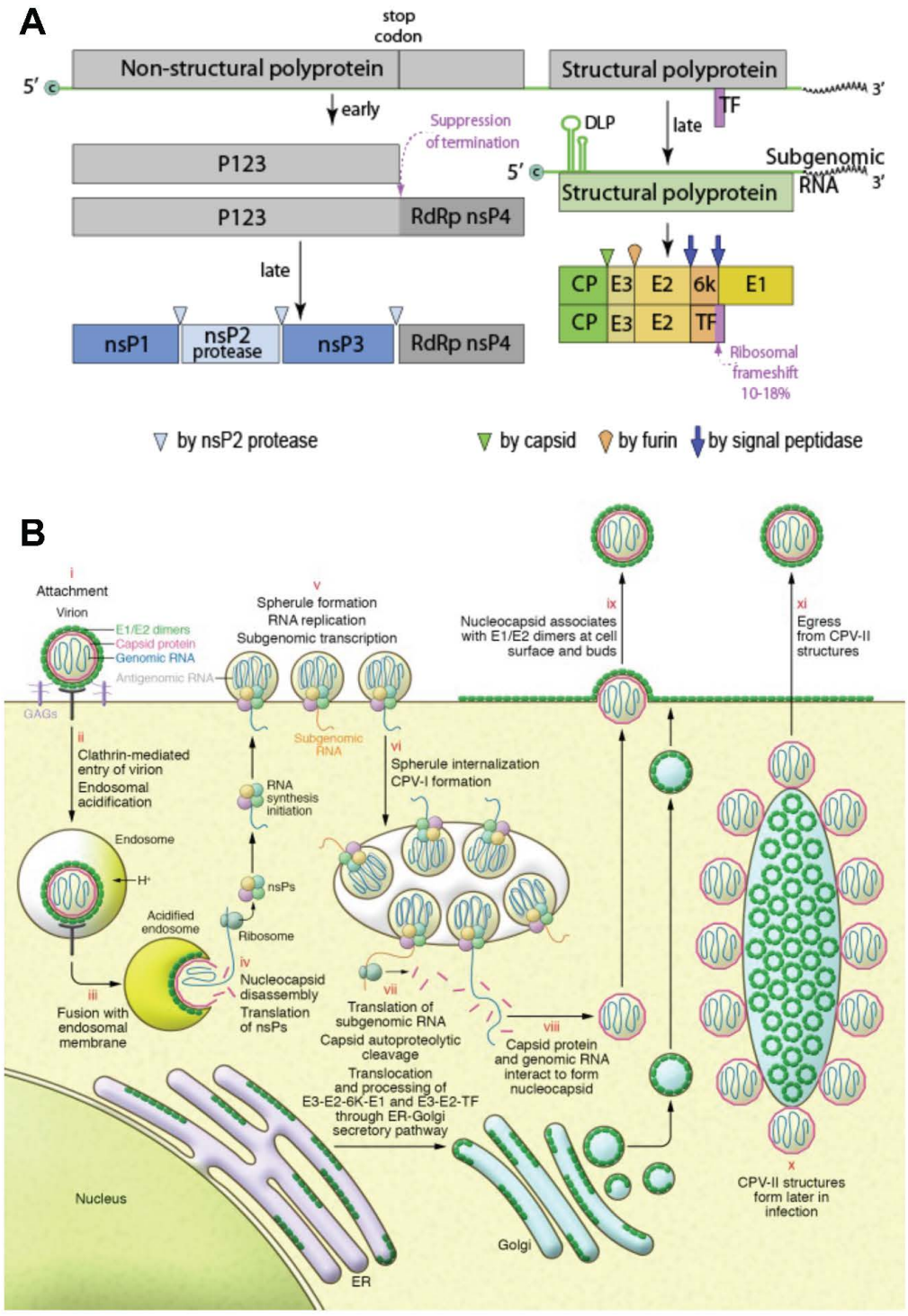

Figure 3.3: Replication cycle of CHIKV in mammalian cells

(A) CHIKV genome replication and transcription; adapted from [144]. **(B)** CHIKV replication in mammalian cells; adapted from [40].

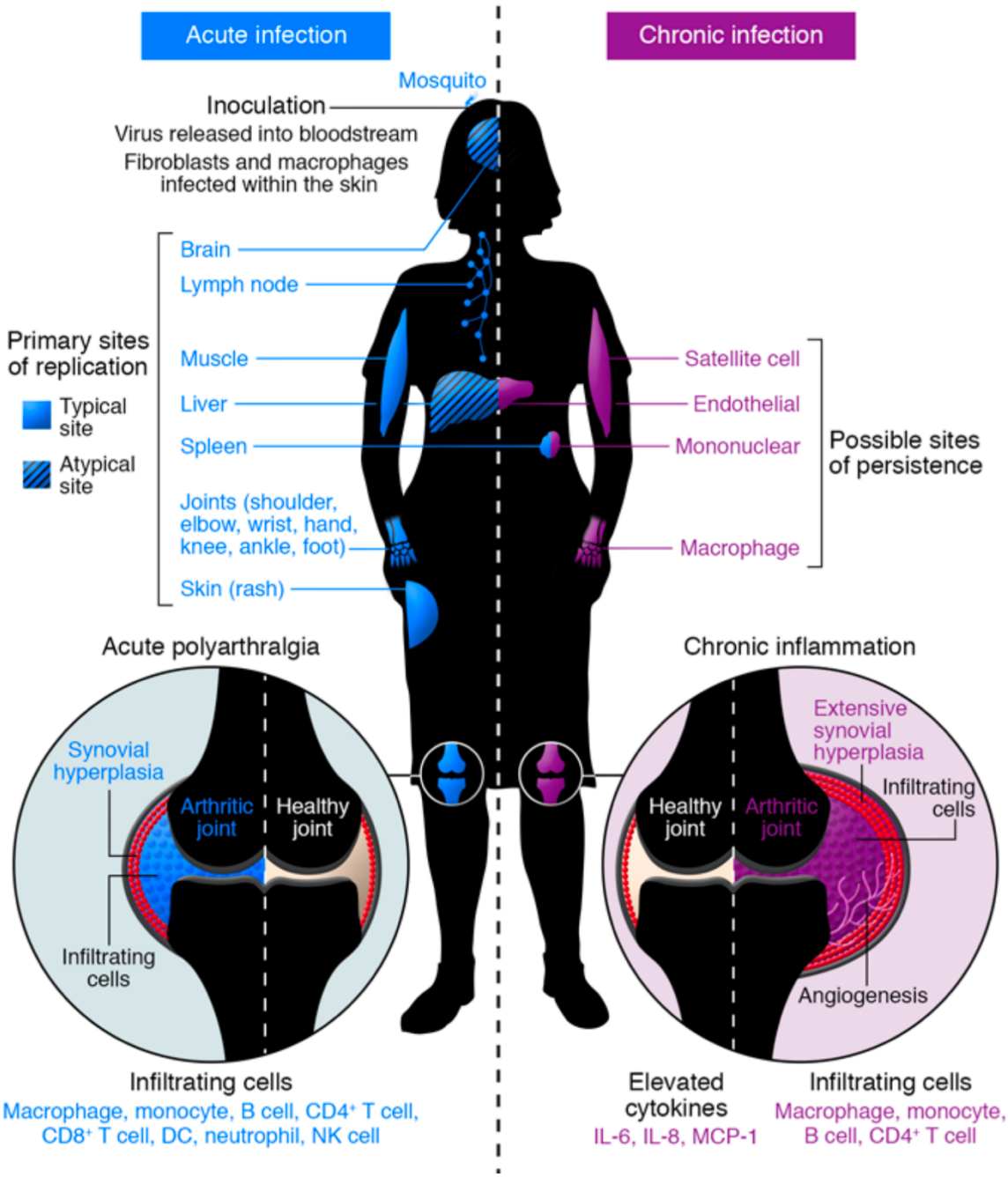

Figure 4.4: Acute and chronic pathogenesis of CHIKV

Acute CHIKV symptoms are associated with disseminated viral replication in a variety of tissues. It is hypothesized that chronic CHIKV disease is due to persistence of virus, inflammatory cytokines, and joint damage; adapted from [40].

Chapter 2:

A Recombinant Chikungunya Virus Reporter System

This chapter contains data from a manuscript in preparation for submission:

Alissa R. Young, Marissa C. Locke, Lindsey E. Cook, Bradley E. Hiller, Rong Zhang, Matthew L. Hedberg, Kristen J. Monte, Deborah J. Veis, Michael S. Diamond, and Deborah J. Lenschow. A recombinant chikungunya virus reporter system defines dermal and muscle fibroblasts and skeletal myofibers as targets during the chronic phase of infection. In preparation to submit to PLoS Pathogens (2019).

2.1 Abstract

Chikungunya virus (CHIKV) is an arthritogenic alphavirus that during acute disease causes fever as well as severe joint and muscle pain. Chronic joint and muscle pain persists in a significant subset of patients for months to years after the initial infection, yet we still have a poor understanding of what drives this chronic disease. While replicating virus has not been detected in the joints of patients with chronic arthritis or in various animal models at chronic time points, persistent viral RNA can be detected for months after acute infection. To identify the cells that might contribute to chronic CHIKV pathogenesis, we developed a recombinant virus that expresses Cre recombinase (CHIKV-3'-Cre). This virus replicated in cell types targeted by CHIKV, including myoblasts and fibroblasts, and it induced acute arthritis in a murine model of CHIKV arthritis. Importantly, it also induced chronic disease, including persistent viral RNA and chronic myositis and synovitis similar to wild-type (WT) virus. CHIKV-3'-Cre infection of tdTomato reporter mice resulted in a population of tdTomato$^+$ cells that persisted for at least 112 days. The majority of these cells localized to the dermis and muscle, and immunofluorescence profiling revealed that these tdTomato$^+$ cells were dermal and muscle fibroblasts and myofibers. Treatment with an antibody against Mxra8, a host receptor for CHIKV, reduced the levels of viral RNA and the total number of tdTomato$^+$ cells in the chronic phase, with a preferential reduction in fibroblasts. Anti-Mxra8 treatment demonstrated a correlation between chronic viral RNA levels and the number of tdTomato$^+$ cells, thus suggesting that viral RNA can be found within these persistent tdTomato$^+$ cells. This CHIKV-3'-Cre and tdTomato reporter mouse system demonstrates that cells can survive CHIKV infection *in vivo* and represents a powerful tool to study the chronic pathogenesis of CHIKV infection.

2.2 Introduction

Chikungunya virus (CHIKV) is a globally re-emerging arbovirus originally identified in Tanzania in 1952 [1–3]; phylogenetic analyses estimate its original emergence as a human virus within the last 500 years [6]. Up until the 2000s, CHIKV was considered a self-limiting, tropical virus of minimal concern; however, within the last 15 years, CHIKV has reemerged with increased virulence and range. In 2004, an East/Central/South African (ECSA) lineage [5] of CHIKV initiated an epidemic in Kenya with over 13,000 cases, the first large epidemic in decades [10]. By 2005, the virus spread to La Réunion Island off the east coast of Madagascar, where it infected over 200,000 people [8,11]. The La Réunion epidemic included the first reports of increased pathogenicity, including neurological symptoms, intrapartum transmission, and approximately 250 deaths [12–14]. The virus subsequently spread throughout the Eastern Hemisphere, establishing endemic conditions in tropical regions including India and the South Pacific, and even causing isolated outbreaks in Europe [18]. In 2013, an Asian lineage strain of CHIKV spread to the Americas and has caused nearly 2 million suspected cases in the Caribbean, Central, and South America [18,20–22].

An estimated 75-95% of people who acquire CHIKV by a mosquito bite [9,15,16] experience an acute disease characterized by fever, rash, arthralgias, and myalgias that last for approximately one to two weeks [11,29,54]. Follow-up studies have reported that between 30% to 60% of CHIKV infected patients develop chronic joint and muscle pain that lasts for months to years after the acute infection [96,118,145]. Whereas CHIKV disease is rarely fatal, the acute and chronic viral arthritis has a high morbidity. For instance the 2005 outbreak on La Réunion Island resulted in an estimated loss of 55,000 DALYs (disability-adjusted life years) or healthy years lost to illness [145], and the CHIKV epidemic in the Americas is predicted to cause an estimated one million cases of chronic CHIKV symptoms [146]. Furthermore, there are no approved vaccines or therapeutics for CHIKV, and over-the-counter medications provide little relief [67]. Despite its high

prevalence in patients and significant morbidity, the mechanism of chronic CHIKV pathogenesis is poorly understood.

Overall, chronic CHIKV disease is characterized by elevated inflammatory markers and immune activation. A number of pro-inflammatory cytokines are elevated in the serum during chronic CHIKV disease, including IL-1β, IL-6, and G-CSF [62,147–149]. Chronic CHIKV patients also have higher levels of activated $CD8^+$ T cells and NK cells, resembling seronegative Rheumatoid arthritis [24]. Mouse models of CHIKV infection have highlighted the importance of adaptive immunity in determining CHIKV clearance or persistence; mature B cells and a productive antibody response appear to be especially critical, as $RAG1^{-/-}$ and μMT mice (both of which lack mature B cells) fail to clear infectious CHIKV [115,117,120,150,151]. Multiple studies have attempted to identify predictive markers for CHIKV-induced chronic arthralgia [54,89,97,107,152]. While these studies agree that chronic CHIKV pathogenesis is characterized by a chronic inflammatory state, they do not define consistent biomarkers or disease mechanisms.

Hypotheses to explain chronic CHIKV pathogenesis abound, including the induction of autoimmunity, the persistence of ultralow levels of replicating virus, and activation of inflammatory responses against residual viral RNA. There is evidence that CHIKV antigen may persist in tissues chronically. CHIKV antigen was detected in the synovial macrophages of one patient 18 months after infection [54], as well as in a human muscle specimen at least three months after acute infection [61]. Cells positive for CHIKV antigen can also be detected in persistently-infected macaques [56] or wild-type mice [113]. Recombinant CHIKV expressing firefly luciferase also produce detectable luminescence during the chronic stage of disease [114–116]. However, these and other studies have not demonstrated that the virus itself is replication proficient, and to our knowledge, infectious virus has not been isolated from the joint tissue of chronic patient or wild-type animal samples [117,118]. Therefore, while it is impossible to completely dismiss

autoimmunity and low-level viral replication as the driving force behind chronic disease, the data supporting these hypotheses has not been consistently seen in various human or animal studies.

A prevailing hypothesis for chronic CHIKV pathogenesis is that non-infectious CHIKV RNA remains in infected tissues, and its dsRNA intermediates act as a proinflammatory pattern-associated molecular patterns (PAMPs) [119]. Chronic CHIKV RNA can consistently be detected through qPCR in animal models, including the joints and spleen of mice and the spleen, lymph nodes, and liver of macaques, despite the fact that infectious virus appears to be cleared much sooner [56,120]. Detection of chronic CHIKV RNA in human samples has been less consistent. One study reported the presence of CHIKV E1 and nsP2 RNAs in a human synovial fluid sample, but others have failed to detect chronic CHIKV RNA in patient serum or synovial fluid [54,118]. Such negative results could reflect the difficulty in obtaining more invasive patient samples such as joint, muscle, or spleen biopsies, as can be readily obtained in animal models.

Despite the presence of chronic RNA is these various models, the cells that potentially harbor the viral RNA are unknown. Histological detection tools such as immunohistochemistry (IHC) are only rarely able to detect CHIKV antigen-positive cells in wild-type mice, likely owing to the insensitivity of these techniques [113]. Moreover, studies using RNA *in situ* hybridization (ISH) for detection of CHIKV RNA have not been published beyond acute time points in mice. Much remains to be explored surrounding chronic CHIKV pathogenesis, including the identification of cells that survive infection and potentially harbor viral RNA, the state of the viral RNA that persists, and why the immune response cannot clear this persistent RNA.

To begin to address these questions, we have established a model that allows for the permanent marking of cells that are infected by CHIKV. We engineered a recombinant CHIKV clone that expresses Cre recombinase, as has been done previously for influenza virus [138,139] and HSV-1 [140,141]. We demonstrate that this CHIKV-Cre virus infects and replicates in cell types targeted by CHIKV including myoblasts and fibroblasts and induces acute arthritis in mice.

Importantly, this virus was also able to establish chronic disease including the persistence of viral RNA for weeks after acute infection. Combining this Cre expressing virus with reporter mice we were able to visualize and identify the surviving marked cells in the chronic phase that were likely infected in the acute phase. This system represents a powerful tool to study how cells that survive infection by CHIKV contribute to chronic disease pathogenesis of this debilitating virus.

2.3 Results

2.3.1 Generation and *in vitro* characterization of CHIKV-3'-Cre

To identify cells that survive CHIKV infection, we generated a recombinant chikungunya virus using the La Réunion clone, LR2006 OPY1, (denoted CHIKV-WT) and engineered it to express the bacteriophage Cre recombinase gene under control of a second subgenomic promoter. Two versions of the Cre recombinase virus were generated: in one version the second subgenomic promoter and Cre recombinase was introduced between the non-structural and structural genes (denoted CHIKV-5'-Cre), and in the other version the subgenomic promoter and Cre recombinase were inserted downstream of the structural genes (denoted CHIKV-3'-Cre) (**Figure S2.1A**).

For these studies, we used reporter mice harboring a fluorescent protein (tdTomato) driven by a constitutive Rosa promoter interrupted with a stop cassette. Infection of these mice with our recombinant viruses should result in the expression of Cre recombinase, which can bind to the LoxP sites, excise the stop cassette, and promote constitutive expression of the fluorescent protein. Thus, the fluorescent reporter will be expressed in all cells where Cre recombinase was expressed, even when viral replication is abrogated (**Figure 2.1A**). This system can help determine whether individual cells can survive the initial CHIKV infection.

To characterize the system, we tested the ability of CHIKV-3'-Cre to function in reporter cells in culture. Murine embryonic fibroblasts (MEFs) from tdTomato reporter mice were isolated

and infected with either CHIKV-WT or CHIKV-3'-Cre. Two days post infection (dpi), a population of tdTomato$^+$ cells was detected following CHIKV-3'-Cre infection, whereas no tdTomato$^+$ cells were identified during infection with media (mock) or CHIKV-WT (**Figure 2.1B-C**). Infection with CHIKV-5'-Cre also induced reporter expression, although in a lower number of cells than CHIKV-3'-Cre, and this difference was seen across several multiplicities of infection (MOIs) (**Figure S2.1B**).

To determine if viral replication was required to activate the reporter, we pretreated cells with IFN-β and then infected them with CHIVK-3'-Cre. Pretreatment with IFN-β prevented expression of the tdTomato reporter by CHIKV-3'-Cre, demonstrating that viral replication and protein expression are required (**Figure 2.1C**). As another control, cell debris from BHK-21 cells infected with CHIKV-3'-Cre was tested for its ability to activate reporter cells; non-virion components in the cell debris from lysed cells, such as Cre protein, could be taken up by uninfected cells and lead to aberrant reporter expression. Cell debris itself resulted in many tdTomato$^+$ cells; however, UV-inactivation of infectious virus in this cell debris inhibited activation of the tdTomato reporter (**Figure 2.1C**). Similar results were also seen with CHIKV-5'-Cre (**Figure S2.1C**). Taken together, these results suggest that active viral replication and expression of Cre recombinase in the infected cell is necessary for activation of tdTomato expression.

We next assessed the ability of CHIKV-3'-Cre to replicate in fibroblasts and muscle cells, two cell types that are targeted during acute CHIKV infection [29,42,54,55,57,58,66]. C2C12 myoblasts or MEFs from C57BL/6 mice were inoculated with CHIKV-WT or CHIKV-3'-Cre at an MOI of 1, and viral replication was assessed at various time points post infection. In C2C12 myoblasts, CHIKV-3'-Cre replicated to similar levels and with similar kinetics as CHIKV-WT (**Figure 2.1D**). CHIKV-3'-Cre also replicated in MEFs, although it was attenuated compared to CHIKV-WT (**Figure 2.1E**). Similar results were seen when C2C12 cells or MEFs were infected at an MOI of 0.05 or with CHIKV-5'-Cre (**Figure S2.1D-E**). Therefore, the CHIKV-3'-Cre virus retains

its ability to replicate in key target cells during infection, though with some attenuation in fibroblasts.

2.3.2 CHIKV-3'-Cre induces acute arthritis

A mouse model of CHIKV infection has been shown to recapitulate several aspects of human infection [64,66,129]. Acute infection is characterized by footpad swelling that resolves within 10-14 dpi and by replication of the virus within the infected footpad and ankle as well as dissemination to other tissue sites including the contralateral ankle, wrists, quadriceps muscle, spleen, and serum. In addition, during acute disease, edema and immune cell infiltration into the joint and muscle is observed. We therefore next evaluated the ability of CHIKV-3'-Cre to induce acute clinical disease.

C57BL/6 mice were inoculated with either CHIKV-WT or CHIKV-3'-Cre into the footpad and analyzed for swelling, viral replication, and histopathology. Injection of each virus into the hind paw resulted in a biphasic pattern of acute ipsilateral footpad swelling with peaks seen at 3 and 6 dpi and with resolution of the swelling by 10-14 dpi (**Figure 2.2A**). Although the initial swelling peak at 2-3 dpi, thought to be driven by edema and monocyte infiltration [128], was reduced in CHIKV-3'-Cre infection, the latter and more pronounced swelling peak at 6 dpi, thought to be driven by the infiltration of monocytes and $CD4^+$ T cells [115,128], was equivalent between the two viruses (**Figure 2.2A**). Similar results were also seen with CHIKV-5'-Cre (**Figure S2.2A Fig**). The resolution of swelling was similar between both viruses.

We next measured viral titers in the ipsilateral ankle of the infected mice. High viral loads were detected in both the CHIKV-WT and CHIKV-3'-Cre infected mice at 1, 3, and 5 dpi, although CHIKV-3'-Cre was mildly attenuated with ~10-fold lower viral loads compared to CHIKV-WT. Infectious virus from either CHIKV-WT and CHIKV-3'-Cre was undetectable by 10-14 dpi (**Figure 2.2B**). Again, similar results were seen with CHIKV-5'-Cre (**Figure S2.2B Fig**). Infection with

CHIKV-WT also resulted in viremia and dissemination to and replication in distal tissues such as the ipsilateral quadriceps muscle, contralateral ankle, and spleen. Whereas viral replication of both CHIKV-3'-Cre and CHIKV-5'-Cre was detected at these distal sites, they were attenuated compared to CHIKV-WT (**Figure S2.2C-F**).

We also utilized RNA in-situ hybridization (ISH) to detect viral RNA in various tissue compartments. RNA ISH was performed on the ipsilateral foot and ankle two days after mock infection or infection with CHIKV-WT or CHIKV-3'-Cre. CHIKV E1 RNA could be detected for both viruses in several tissue compartments, including skeletal muscle, skin, and synovium (**Figure S2.3A**). However, the ISH staining for CHIKV-3'-Cre was often less intense than CHIKV-WT, likely a reflection of its attenuation. Notwithstanding these differences, CHIKV-3'-Cre had a similar tissue tropism to CHIKV-WT.

CHIKV infection results in moderate to severe arthritis that can be detected at acute and subacute time points in animal models [117,120]. This is characterized by edema and swelling within the skin and subcutaneous tissue and cellular infiltrates into the joint space, muscle, and tenosynovial tissues. Specimens comprising the ipsilateral foot and ankle were harvested seven days after mock-infection or infection with either CHIKV-WT or CHIKV-3'-Cre, and H&E sections were scored for overall inflammation (**Figure 2.2C-D**).

Histopathologic examination and analysis revealed significant edema, especially in the dermis and hypodermis, and inflammation with tissue damage in the footpad, skeletal muscle, and tenosynovial joint tissues was evident in mice infected by either virus compared to mock-infected animals (**Figure 2.2D**). Based on histological analysis, the overall severity of the inflammatory response in the joint space, muscle, and tenosynovial soft tissues was indistinguishable between CHIKV-WT and CHIKV-3'-Cre at 7 dpi (**Figure 2.2C**). Similar results were seen with CHIKV-5'-Cre at 7 dpi (**Figure S2.3B-C**). Thus, CHIKV-3'-Cre retains the pathogenic potential to induce acute musculoskeletal disease.

2.3.3 CHIKV-3'-Cre induces chronic disease

Chronic CHIKV arthritis is characterized by persistent myositis and chronic synovial inflammation and proliferation with mild histological features. In addition, persistent viral RNA can be detected in these tissues in mice long after acute disease, despite the absence of detectable replicating virus [117,120]. Therefore, we next evaluated if the CHIKV-3'-Cre virus could establish chronic disease.

Ipsilateral foot and ankle joints were harvested twenty-eight days after inoculation with media (mock-infection), CHIKV-WT, or CHIKV-3'-Cre. Histopathological examination and analysis showed patchy areas of chronic inflammatory infiltrates within the muscle, with some evidence of synovial proliferation within the joints, consistent with a remote/resolving arthritis, in both the CHIKV-WT and CHIVK-3'-Cre infected but not mock-infected mice (**Figure 2.3A**). However, compared to the specimens harvested at 7 dpi (**Figure 2.2C-D**), there was markedly less histologic evidence of inflammation and tissue damage in the specimens harvested at 28 dpi.

Mild inflammation was not identified in any of the mock-infected joints, and it was only histologically identified in a subset of CHIKV-WT or CHIKV-3'-Cre chronically infected specimens; however, the difference did not achieve statistical significance at the cohort level (**Figure 2.3B**). Similar results were observed for CHIKV-5'-Cre (**Figure S2.4A-B**). These results are consistent with the comparatively mild histologic findings previously described in CHIKV-associated chronic arthritis and highlight the importance of diagnostic techniques with greater sensitivity than histopathology.

We next evaluated if viral RNA persisted in tissues after infection with the CHIKV-3'-Cre virus. Samples harvested at 28 dpi were analyzed for the presence of CHIKV viral E1 RNA by real-time quantitative PCR (RT-qPCR). CHIKV RNA was detected in the ipsilateral ankles of mice infected with either CHIKV-WT or CHIKV-3'-Cre, although at this time point the level of viral RNA were slightly decreased (~3.5-fold) in the CHIKV-3'-Cre infected mice compared to CHIKV-WT

(**Figure 2.3C**). As expected, mock infection or infection with UV-inactivated CHIKV-3'-Cre did not result in a positive signal for viral RNA (**Figure 2.3C**).

An analysis of the kinetics of CHIKV viral RNA in the ankles of infected mice revealed that both CHIKV-WT and CHIKV-3'-Cre established peak levels of viral RNA during acute disease, 1-7 dpi (**Figure 2.3D**). Persistent levels of chronic viral RNA were detected through 112 dpi (16 weeks), and both viruses established similar levels of persistent viral RNA at these late time points (**Figure 2.3D**). Again, similar results were observed for CHIKV-5'-Cre (**Figure S2.4C**). While RNA ISH could identify cells during acute infection (**Figure S2.3A**), it was not sensitive enough to identify RNA positive cells in the chronic phase (data not shown).

At peak productive infection, engagement of the subgenomic promoter produces a subgenomic RNA segment containing the structural genes [28,33,36]. As such, this results in more copies of structural genes, such as E1, being produced than copies of non-structural genes, such as nsP1, during active replication. Consistent with this description and as seen previously [120], during the first 7 days of infection the ratio of E1 to nsP1 RNA copies was greater than 1 for both CHIKV-WT and CHIKV-3'-Cre indicating viral replication was occurring (**Figure 2.3E**). However, after 7 dpi the ratio of E1 to nsP1 was approximately 1, and the viral RNA levels decreased with a similar time course for both viruses. Similar results were observed for CHIKV-5'-Cre (**Figure S2.4D**). These results indicate that the subgenomic promoter is only active during the first week of acute infection, as supported by infectious virus only being detected during the same time course (**Figure 2.2B**). Thus, persistent RNA detected after 7 dpi is likely non-replicative and non-infectious.

These results indicate that CHIKV-3'-Cre retains its pathogenic potential and can induce both acute and chronic disease. Despite displaying slight attenuation during acute infection, CHIKV-3'-Cre can establish chronic disease including persistent viral RNA and histological

damage. Such data justifies its utilization as a tool to identify the cells that can survive CHIKV infection and may contribute to chronic arthritis pathogenesis.

2.3.4 CHIKV-3'-Cre marks dermal and muscle fibroblasts and myofibers

Previous reports have indicated that CHIKV is highly cytopathic and induces cell death in the majority of cells that it infects [52,60]. Yet, persistent viral RNA can be detected long past acute infection. To test whether cells could survive CHIKV infection, tdTomato reporter mice were inoculated with media (mock), CHIKV-WT, or CHIKV-3'-Cre and analyzed for the presence of tdTomato$^+$ cells at time points in the chronic phase. Notably, tdTomato$^+$ cells were observed in the ipsilateral foot 28 dpi with CHIKV-3'-Cre, but not in C57BL/6 or reporter mice that were mock-infected or infected with CHIKV-WT or UV-inactivated CHIKV-3'-Cre (**Figure 2.4A-B**, **Figure S2.5A**). Infection with CHIKV-5'-Cre infection also resulted in tdTomato$^+$ cells in the ipsilateral foot, but to a much lower level than CHIKV-3'-Cre (**Figure S2.5B-D**). tdTomato$^+$ cells were detected up to at least 112 days (16 weeks) after infection with CHIKV-3'-Cre (**Figure 2.4C**).

Closer examination of ipsilateral feet infected with CHIKV-3'-Cre revealed that the majority of tdTomato$^+$ cells appeared to be concentrated in the skeletal muscle and in the dermal layer of the skin (**Figure 2.4A**). In the muscle, the tdTomato$^+$ cells appeared to be a mixture of long, multi-nucleated myofibers and small, uni-nucleated non-myofiber cells (**Figure 2.4A**). A high amount of tdTomato$^+$ cells were also observed in the dermis of the skin. Other connective tissues such as bone, synovium, and tendons contained rarer populations of tdTomato$^+$ cells (**Figure S2.5E**).

To define the identity of the tdTomato$^+$ cells, we performed co-staining with a variety of cell specific markers. Since the majority of the tdTomato$^+$ cells were localized to the muscle and the dermis we focused our analysis on these two areas. In the muscle, the long multi-nucleated, striated cells that histologically were consistent with striated muscle fibers co-stained with sarcomeric alpha actinin (SAA), a microfilament protein that attaches actin filaments to the Z-

discs in myofibers and exhibits a striated pattern (**Figure 2.5A**), confirming that these tdTomato$^+$ cells are skeletal muscle cells.

Within the muscle we also observed a subset of tdTomato$^+$ cells that were small, uni-nucleated, and negative for SAA staining. CHIKV is known to infected fibroblasts and the morphology of these cells was consistent with fibroblasts. Although there is no specific marker for fibroblasts, these tdTomato$^+$ cells co-stained for vimentin, an intermediate filament that is highly expressed in fibroblasts. In the dermis of the skin, many of the tdTomato$^+$ cells also co-stained strongly with vimentin (**Figure 2.5A**). Some of the tdTomato$^+$ cells in the skin or muscle also co-stained with CD44, CD29, or CD105, additional fibroblast markers (**Figure 2.5A**, **Figure S2.6**).

As these mesenchymal markers can be expressed in other cell types, sections also were stained with CD31 (endothelial cell marker), CD45 (hematopoietic cell marker), or smooth muscle actin (SMA, myofibroblast and smooth muscle marker). tdTomato$^+$ cells in the skin and muscle did not strongly co-stain with these markers, suggesting that these tdTomato$^+$ fibroblast-like cells are not immune cells, endothelial cells, or smooth muscle cells (**Figure 2.5B)**. A small subset of tdTomato$^+$ cells in the skin also co-stained with beta III tubulin (**Figure S2.6**). These cells could be part of nerve fibers [153] or fibroblasts with stem cell characteristics that can become neuroectodermal cells [154,155]. Co-staining demonstrates that many of the tdTomato$^+$ cells appear to be myofibers and dermal and muscle fibroblasts.

2.3.5 Anti-Mxra8 treatment preferentially reduces fibroblasts

Mxra8 is a cell adhesion molecule that was described as an entry receptor for multiple arthritogenic alphaviruses. Treatment with anti-Mxra8 monoclonal antibodies (mAbs) reduced CHIKV infection and foot swelling at 3 dpi during acute disease [38]. We assessed the impact of Mxra8 blockade on the establishment of chronic disease and the persistence of infected cells

after acute infection. tdTomato reporter mice were treated with either isotype control antibody or with anti-Mxra8 mAbs 12 hours prior to infection and then at 4, 8, 12, 16, 20, and 24 dpi. Mice treated with anti-Mxra8 mAbs showed a significant reduction (73% decrease) in persistent viral RNA detected in the ipsilateral ankle 28 dpi compared to the isotype control mAb treated mice as judged by RT-qPCR (**Figure 2.6A**).

Consistent with this data, the anti-Mxra8 treated mice had significantly reduced numbers (75% decrease) of tdTomato$^+$ cells in the ipsilateral ankle 28 days after infection as compared to the isotype control (**Figure 2.6B-C**). Quantification of cell co-staining demonstrated that the most significant reductions with anti-Mxra8 treatment were observed in CD29$^+$ fibroblasts in the muscle and skin (**Figure 2.6D**), with an 89% and 78% decrease, respectively. Anti-Mxra8 treatment also reduced the number of tdTomato$^+$ SAA$^+$ myofibers by 57%, thus to a lesser extent than fibroblasts (**Figure 2.6E**). As such, anti-Mxra8 treatment perturbed the distribution of tdTomato$^+$ cell types in the muscle, with a higher percentage of remaining tdTomato$^+$ cells staining for SAA than for CD29 in the muscle (**Figure 2.6F**). Anti-Mxra8 treatment thus reduced the amount of persistent viral RNA and overall numbers and distribution of tdTomato$^+$ cells in musculoskeletal tissues during the chronic phase.

2.4 Discussion

CHIKV causes a debilitating acute disease that results in chronic arthralgias and myalgias in a significant subset of patients. The mechanism of this chronic CHIKV pathogenesis is unclear but may be related to persistent viral RNA in musculoskeletal tissues. To begin to identify the cells that contribute to chronic pathogenesis, we created a recombinant CHIKV that expresses Cre recombinase and permanently marks infected cells in reporter mice. Using this tool, we provide evidence that a subset of cells infected with CHIKV can survive infection.

Previous reports have used immunofluorescence microscopy, immunohistochemistry, or RNA quantification tools to detect CHIKV antigen or RNA in animal and patient cells at time points in the chronic phase of disease [54,56,61,113]. However, CHIKV antigen-positive cells are reported to be rare in these samples from the subacute or convalescent phase, likely owing to the insensitivity of these techniques. Our reporter virus system constitutively marks cells that were once productively infected as opposed to those which acquired antigen by passive engulfment.

We constructed two variants of the CHIKV-Cre construct, inserting the Cre recombinase gene into the CHIKV genome through introduction of a second subgenomic promoter, either in between the structural and non-structural genes (CHIKV-5'-Cre) or at the 3' end of the genome (CHIKV-3'-Cre). As has been reported previously with CHIKV-GFP clones [135,136], the introduction of Cre recombinase resulted in mild attenuation of both viruses. However, the CHIKV-Cre viruses retained sufficient virulence to infect targets of CHIKV replication (fibroblasts and myoblasts) and induce acute swelling and histopathology that was comparable to CHIKV-WT. The CHIKV-Cre viruses also established chronic disease resulting in persistence of viral RNA, chronic myositis, and synovial inflammation. From our more detailed studies, we used the CHIKV-3'-Cre rather than CHIKV-5'-Cre, as certain aspects of CHIKV-3'-Cre infection more closely resembled CHIKV-WT infection. For example, the ratio of E1:nsP1 in the first seven days of infection was more similar between CHIKV-3'-Cre and CHIKV-WT than with CHIKV-5'-Cre. This difference is likely because the E1 gene is under the replicative direction of the subgenomic promoters; the internal genomic structure of CHIKV-3'-Cre is identical to CHIKV-WT in contrast to CHIKV-5'-Cre.

Using CHIKV-Cre viruses and tdTomato reporter mice, we also show that, like viral RNA, tdTomato$^+$ cells can be detected in the ankle for at least 112 days (16 weeks) after infection. One limitation of our CHIKV-Cre reporter mouse system is that it cannot distinguish when during infection a cell is marked. We favor the hypothesis that cells are infected during the first week of

infection, survive acute infection without lysing, and persist for the lifetime of the cell. The infectious viral titers and E1:nsP1 ratios support this idea that CHIKV is only actively replicating during the acute phase of infection. Another scenario is that some tdTomato$^+$ cells may arise as daughter cells from mitotic replication of directly infected tdTomato$^+$ cells; while these daughter cells were not themselves infected, they may still retain viral RNA or an altered transcriptome. A third hypothesis is that tdTomato$^+$ cells arise throughout acute and chronic time points via undetectable levels of replicating virus. It is also a possibility that all three scenarios occur in our reporter mice, perhaps at different levels in various cell types.

Using our CHIKV-3'-Cre and tdTomato reporter mouse system, we sought to identify the cell types targeted by CHIKV that persist into the chronic phase. In the acute phase, CHIKV has been shown to acutely infect a vast array of cell types, including fibroblasts, synoviocytes, macrophages, skeletal muscle fibers, satellite cells, osteoblasts, endothelium, keratinocytes, and neurons [29,42,55,61]. *In vitro* infections with many of these cell types exhibit high levels of cytopathic effects and cell death [52,60]. Immunofluorescence analysis using our reporter mice shows that the persistent tdTomato$^+$ cells are predominantly a mixture of SAA$^+$ skeletal myofibers and vimentin$^+$ CD44$^+$ CD29$^+$ CD105$^+$ cells that are likely mesenchymal cells such as fibroblasts, both of which are cell types reported be permissive to CHIKV infection [57,156].

Not all cells known to be infected by CHIKV in the acute phase were apparent in our analysis in the chronic phase. Few cells in the synovial membrane were tdTomato$^+$, even though mild synovial inflammation was present at chronic time points as has been previously reported [117,120]. During the acute stage of infection, we could detect staining for viral RNA in the synovium; however, the synovial staining was much less pronounced than in the muscle or skin for both CHIKV-WT and CHIKV-3'-Cre. These results may indicate that synovial cells are not infected in large numbers *in vivo*, or more likely, given synovial fibroblasts' permissiveness to CHIKV infection *in vitro*, many synovial cells are infected but do not survive acute, lytic infection.

These results could explain why previous efforts to detect viral components in patient samples at chronic time points have generally been unsuccessful as they have focused on synovial fluid analysis and occasionally synovial tissue, but rarely skin or muscle samples.

In addition to a paucity of tdTomato$^+$ synovial cells, few tdTomato$^+$ cells were associated with the bone or other connective tissues like tendons and ligaments. A small number of tdTomato$^+$ cells were sometimes found associated with the periosteum, which could represent a population of fibroblasts or osteoblasts. Previous reports have suggested that acute infection of osteoblasts can perturb osteoclast function and can lead to chronic histological damage [157,158], which is not precluded by our results as the osteoblasts may accomplish such outcomes while still succumbing to lytic infection.

Additional cell types that have been linked to chronic pathogenesis were not detected in our mice with CHIKV-3'-Cre. Endothelial cells or macrophages reportedly contain CHIKV antigens during chronic infection in humans, macaques, or mice [54,56,113]. Some reports have also suggested that hematopoietic cells such as monocytes or macrophages can be directly infected by CHIKV [42,59]. However, the vast majority of tdTomato$^+$ cells were CD31$^-$ and CD45$^-$, which is consistent with previous reports examining acute CHIKV staining in skin samples [58]. Although further study is warranted, these cell types may not survive CHIKV infection, they may be poorly infected by CHIKV (not enough to induce sufficient Cre recombinase), or they may not be productively infected and instead phagocytose viral antigen from adjacent infected cells.

We also explored how Mxra8 blockade affected the tropism of CHIKV in the chronic stage of pathogenesis. Mxra8 was recently discovered as a host entry receptor for several arthritogenic alphaviruses including CHIKV, and its blockade reduced acute viral load both *in vitro* and *in vivo* [38]. In our reporter mice, anti-Mxra8 treatment reduced the viral RNA burden in musculoskeletal tissue in the chronic phase. Other CHIKV treatments, such as mAbs against viral envelope proteins, have been successful at reducing acute viral loads but have not significantly affected

persistence of viral RNA levels [159]. Such results suggest that targeting viral entry early in infection could be key to alleviating both acute and chronic symptoms of disease.

In addition to decreasing chronic RNA levels by 73%, anti-Mxra8 treatment also reduced the total number of tdTomato$^+$ by 75%, thus correlating the level of chronic viral RNA and the number of persistent tdTomato$^+$ cells in the chronic phase. Such correlative results suggest that persistent viral RNA might be contained within the tdTomato$^+$ cells. However, current RNA ISH techniques are not sensitive enough to directly visualize CHIKV RNA within tdTomato$^+$ cells at this stage. Immunofluorescence analysis revealed that anti-Mxra8 treatment resulted in a significant reduction of CD29$^+$ tdTomato$^+$ fibroblast-like cells in the dermis and skeletal muscle. Anti-Mxra8 treatment also impacted the abundance of tdTomato$^+$ SAA$^+$ myofibers, although to a lesser extent than fibroblasts, suggesting that another host receptor may exist on myofibers for CHIKV-LR, the strain used for the present studies. Such results underline the fact that CHIKV likely utilizes multiple host entry receptors in addition to Mxra8, making potential treatments even more difficult to target.

Indeed, Mxra8 was shown to be a stronger determinant of CHIKV infection of Asian than ECSA strains [38], such as the La Réunion strain used for this study. Thus, it could be informative to repeat these studies with other CHIKV lineage strains that express Cre recombinase. Other strains or viruses may persist in distinct populations of tdTomato$^+$ cells and or demonstrate differential susceptibility to treatments such as anti-Mxra8 treatment. The CHIKV-3'-Cre and tdTomato model thus also represents a method of testing anti-viral treatments for their efficacy at chronic timepoints, supplemented with viral RNA analysis.

A significant unanswered question in CHIKV disease pathogenesis is the mechanistic driving force of symptoms during the chronic phase. Replicating virus has not been detected at chronic time points, yet chronic inflammation is clearly present in tissue, serum, and synovial samples, both histologically and transcriptionally [37,160,161]. While chronic viral RNA can be

detected, to date it has been difficult to identify the cells harboring this RNA. Our model provides insight into these questions by identifying the cell types that have been productively infected by CHIKV and are present in the chronic phase. A limitation of the model is that we cannot be certain at what stage a given tdTomato$^+$ cell became infected with CHIKV. Ultimately, by combining reporter gene expression with flow cytometric cell sorting and single cell RNA sequencing analysis, we may be able to determine the transcriptional programs and inflammatory states of these marked cells in the acute and chronic phase of CHIKV disease.

In conclusion, our CHIKV-3'-Cre and tdTomato system provides further evidence for key musculoskeletal cells as targets of CHIKV infection in the acute and chronic stages of disease. How exactly these cells contribute to pathogenesis remains to be elucidated. Uncovering the mechanisms for long-term pathogenesis could aid in the development of treatments and preventative measures for this incapacitating virally-induced chronic arthritis.

2.5 Materials and Methods

2.5.1 Viruses

The wild-type strain of chikungunya virus (denoted CHIKV-WT) used for these studies is LR2006 OPY1, an ECSA strain of CHIKV isolated from the La Réunion Island outbreak [135]. This strain has been characterized by many groups and used extensively by our lab [17,56,57,64,66]. Plasmids for CHIKV-5'-GFP and CHIKV-3'-GFP were obtained from Stephen Higgs (Kansas State University), and the Cre recombinase gene, with a nuclear localization signal (NLS) sequence, was substituted for GFP in both viruses [135,136]. To produce the CHIKV-5'-Cre plasmid, Cre was PCR amplified from a Cre-containing plasmid with a forward primer (FW, containing an AscI restriction enzyme recognition site and homology to the 5' end of the Cre gene) and a reverse primer (RV, containing a PmeI site and homology to the 3' end of the Cre gene). This amplicon was inserted into a CHIKV-5'-GFP plasmid linearized with AscI and PmeI. To

produce the CHIKV-3'-Cre plasmid, Cre was PCR amplified from the CHIKV-5'-Cre plasmid using AscI-Cre FW and BsmBI-Cre RV primers. The 3' UTR was also PCR amplified from the CHIKV-3'-GFP virus using BsmBI-3'UTR FW and NotI-3'UTR RV primers. Both PCR fragments were simultaneously inserted into a CHIKV-3'-GFP plasmid linearized with AscI and NotI. The infectious clone plasmids for CHIKV-WT, CHIKV-3'-Cre, and CHIKV-5'-Cre were sequenced, and they exhibited 100% identity with reference and predicted sequences.

To produce recombinant viral stocks, the infectious clone plasmids were linearized with NotI, and RNA was produced using a SP6 *in vitro* RNA transcription kit (Agilent, Promega, BioLabs). The RNA was transfected into baby hamster kidney 21 cells (BHK-21 cells) using Lipofectamine 2000 (Invitrogen) and CD1 media without antibiotics. After 48 hours, the supernatant was collected, centrifuged at 150-300 g to clear cell debris, aliquoted, and stored at -80°C. Titers of the viral stocks were regularly assessed by plaque assay as previously described [125]. All cell and animal work with live CHIKV was performed in a BSL3 facility and followed strict guidelines established by the Environmental Health and Safety committee at Washington University School of Medicine.

2.5.2 Mice

The following strains of mice were obtained from the Jackson Laboratory: C57BL/6 (JAX Stock No: 000664; C57BL/6J) and tdTomato reporter mice (JAX Stock No: 007914; B6.Cg-*Gt(ROSA)*$^{26Sortm14(CAG-tdTomato)Hze}$/J). Mice were bred and maintained as congenic colonies at Washington University School of Medicine animal facilities in accordance with all federal and University guidelines. C57BL/6 mice were primarily used for viral titer and viral RNA analysis, whereas the tdTomato reporter mice were used for histological analysis. For all experiments, mice were weight- and sex-matched prior to infection; both sexes were used. For mouse studies, the principles of good laboratory animal care were adhered to in strict accordance with NIH

recommendations [162]. All animal protocols were approved by the Animal Studies Committee at Washington University. Every effort was made to minimize animal suffering.

2.5.3 Cells and Media

Murine embryonic fibroblasts (MEFs) were generated from C57BL/6 and tdTomato reporter mice, and they were grown at 37°C and 5% CO_2 in CD10 media: Dulbecco's modified Eagle medium (DMEM) (Corning) supplemented with 10% fetal bovine serum (FBS) (Biowest), 1% penicillin-streptomycin (P/S; Corning), 1% L-glutamine (Glu; Corning), 1% non-essential amino acids (NEAA; Corning), and 1% HEPES (Corning). For some experiments CD1 media (CD10 media with only 1% FBS) was used. MEFs were used prior to passage number 5 for these studies. The C2C12 myoblast cell line was obtained from ATCC (ATCC CRL1772) and cultured using the same conditions as the MEFs.

2.5.4 Viral Growth Curves

MEFs and C2C12 myoblasts were grown as described above. For viral growth curves, MEFs were plated at 2 x 10^4 cells/well and C2C12s at 1 x 10^4 cells/well in 96-well tissue culture-treated plates and allowed to adhere overnight. Cells were rinsed with CD1 media: DMEM containing 1% FBS, 1% P/S, 1% Glu, 1% NEAA, and 1% HEPES. Diluted virus was then added at the indicated multiplicity of infection (MOI) and allowed to adhere for 1 hour. The input virus was then removed, the cells were washed once with CD1, and fresh CD1 media was added. At each time point, a plate was frozen at -80°C and underwent three freeze-thaw cycles before titers were determined on BHK-21 cells by plaque assay.

2.5.5 *In Vitro* Coverslip Studies

tdTomato reporter MEFs were plated onto collagen type I-treated 22mm glass coverslips (Corning) at 4 x 10^5 cells/well in 6-well tissue culture-treated plates in CD10. If indicated, cells

were also concurrently pre-treated with ~100 U IFN-β, and all cells were allowed to adhere to the coverslips overnight. Cells were infected with virus at the indicated MOI, as described above. After 48 hours, the supernatant was removed, and the cells were fixed to the coverslips with 4% paraformaldehyde (PFA) for at least 10 minutes. Coverslips were stored in the wells with phosphate-buffered solution (PBS) at 4°C until further processing.

Alternatively, the MEFs were treated with lysed cell debris (CD). Briefly, BHK-21 cells were plated at 5 x 10^5 in tissue culture-treated plates in CD10 and allowed to adhere overnight. The cells were infected with CHIKV-3'-Cre at an MOI of 10, and the supernatant was removed at 24 hours p.i. Large cellular debris was cleared from these supernatants by centrifugation at 150-300 g, leaving behind virus and cellular lysate (including virus-produced Cre protein). Aliquots of this CD were stored at -80°C. In some instances, virus in these samples was UV-inactivated using a Stratagene Stratalinker 1800 with two sessions at 500 mJ.

Coverslips were prepared for microscopy as follows. Coverslips were permeabilized for 10 min at room temperature (RT, ~23°C) with 0.2% Triton-X in PBST (PBS + 0.1% Tween20), washed with PBST, stained with DAPI (100 μg/mL in PBST) for 10 min at RT, washed with PBST, mounted onto a glass slide using ProLong Gold (Invitrogen), and allowed to cure protected from light at RT overnight. Coverslips were imaged using a Nikon Spinning Disk Confocal Microscope, maintained at the Washington University Center for Cellular Imaging (WUCCI). For illustration purposes, cells were imaged at 4x or 10x with a single capture using the DAPI and RFP channels. For quantification purposes, four random locations were selected on each coverslip, and a 4x4 stitched image of 16 adjacent 4x images (15% overlap) was produced from each location. Image files were processed and automatically quantified for cell number and tdTomato$^+$ cell count using ImageJ. The nuclei or cells were automatically quantified using the Quantify Particles function, with the size being a minimum of 500 pixels^2. The DAPI$^+$ nucleus count represents the total number of cells per field, and the RFP$^+$ cell count

represents the total number of tdTomato$^+$ cells per field. The % of tdTomato$^+$ cells was calculated by dividing the total number of tdTomato$^+$ cells per field by the total number of cells per field for each image.

2.5.6 Viral Burden Studies in Animals

Four-week old C57BL/6 mice sedated with ketamine were injected subcutaneously with 10^6 plaque-forming units (PFU) of virus diluted in 10-30 μL of CD1 without P/S into the left (ipsilateral) footpad, between the second and third digits. Swelling of the infected foot was monitored daily using digital calipers, by measuring both height and width. For infectious virus and viral RNA samples, mice were sedated and sacrificed with ketamine at the indicated time point, blood samples were taken by cutting of the inferior vena cava or abdominal aorta, and 5-10 mL PBS was perfused into heart. Various tissues (spleen, ipsilateral and contralateral ankles with toes removed and skin included, and ipsilateral quadriceps muscles) were harvested into homogenization bead tubes and stored at -80°C. For infectious virus samples, the bead tubes contained 600 μL PBS, were weighed prior to and after addition of tissue sample, and were stored on ice until transferred to -80°C; infectious virus titer was determined by plaque assay. For viral RNA samples, the bead tubes contained no PBS and were snap frozen in liquid nitrogen before being transferred to -80°C; viral RNA levels were determined using RT-qPCR, as described below. Alternatively, viral RNA levels could be measured from infectious virus samples by isolating RNA from tissue homogenates after 25 μL was removed for a plaque assay. Blood samples were allowed to coagulate at RT, samples were spun down at 9,000 g for 5-10 minutes, and serum was removed into a fresh tube and stored at -80°C.

For Mxra8 mAb studies, tdTomato reporter mice were infected with CHIKV-3'-Cre as described above. The mice were injected intraperitoneally with 250 ug of Armenian hamster isotype control (Bio X Cell # BE0260) or Armenian hamster anti-Mxra-8 mAbs diluted in PBS

[38] (125 ug each of 1G11.E6 and 7F1.D8) at 12 hours prior to infection and at 4, 8, 12, 16, 20, and 24 dpi. Samples were harvested for RNA or histology as described above. RT-qPCR analysis, frozen section slides and quantification, and immunofluorescence was performed as described herein.

2.5.7 Quantitative Real-Time PCR

RNA was isolated from Trizol-tissue homogenates using the standard Trziol-chloroform extraction protocol and or an RNAeasy mini-prep kit (Qiagen). Isolated RNA was resuspended in UltraPure H_2O (Ambion) and stored at 4°C overnight or -80°C for long-term storage. Viral standards were produced by producing RNA from the infectious clone plasmids as described above. The copy number of the standard was determined by quantifying the sample and calculating the copy number using the known ssRNA genome length. A 1:10 dilution series of the standard was prepared ranging from ~10^1 copies to ~10^9 copies. RT-qPCR was performed on a Bio-Rad CFX machine using the TaqMan™ RNA-to-CT™ 1-Step Kit (Applied Biosystems™) with a 25 μL total reaction volume per well, 2 uL of RNA sample, and the indicated amount of Taqman primers and probe from Integrated DNA Technologies: E1 FW (5'- TCG ACG CGC CCT CTT TAA -3'), E1 probe (5'- /56-FAM/ ACC AGC CTG/ ZEN/ CAC CCA TTC CTC AGA C/ 3IABkFQ/ -3'), E1 RV (5'- ATC GAA TGC ACC GCA CAC T -3'), nsP1 FW (5'- AAA GGG CAA ACT CAG CTT CAC -3'), nsP1 probe (5'-/ 56-FAM/ CGC TGT GAT/ ZEN/ ACA GTG GTT TCG TGT G/ 3IABkFQ/ -3'), and nsP1 RV (5'- GCC TGG GCT CAT CGT TAT TC -3'). To quantify the Cre copy number, pre-made Enterobacteria phage P1 cyclization recombinase FAM Taqman copy number primers/probe were used (ThermoFischer Mr00635245_cn), and 1.25 μL of the 20x working stock was used per 25 μL reaction. The following PCR cycling protocol was used: 30 minutes at 48°, 10 min at 95°, and 40 cycles of 15 sec at 95° and 1 min at 60°C. RNA copy number was determined for each sample using the

matching RNA standard, and the copy number was normalized to the total μg of RNA for each sample (determined by NanoDrop).

2.5.8 Histology Studies

Four-week old tdTomato mice were infected as described above. For histology samples, mice were sedated with ketamine and sacrificed at the indicated time point, and 5-10 mL 4% PFA was perfused into heart. Various tissues (spleen, ipsilateral and contralateral feet/ankles) were harvested and fixed in 4% PFA. After 48 h of immersion fixation, tissues were washed with PBS and transferred to BSL2 facilities for further processing. Tissues containing bone (*e.g.*, whole foot/ankle samples) were decalcified in 14% acid-free EDTA (VWR) for 14 days. For frozen section processing, decalcified tissues and soft tissues (e.g., spleen) were equilibrated overnight in 30% sucrose in PBS and then frozen in optimal cutting temperature (OCT) compound (Tissue Tek). Samples were then cut with a cryostat at 10 μm for spleens or 30 μm for foot/ankle samples onto SuperFrost Plus slides (Fisher). Slides were stored at -20°C until further processing.

Frozen section slides were prepared for microscopy by fixing with cold acetone, permeabilizing with 0.2% Triton-X in PBST, washing with PBST, and mounting with a No. 1-1/2 glass coverslip (VWR) using Vectashield containing DAPI (Vector Laboratories H-1200). Slides were imaged using a Nikon Spinning Disk Confocal Microscope, maintained at the WUCCI. Whole tiled images of the foot and ankle were prepared using the 4x objective and the DAPI, GFP, and RFP channels using large-image capture and 15% overlap. Alternatively, frozen section slides were processed and imaged using immunofluorescence, as described below.

Image files were processed using ImageJ. The total number or tissue-specific number of tdTomato$^+$ cells was quantified by eye using manual cell counters in ImageJ or Photoshop; counters were blinded to sample identity. The total area of each foot/ankle or tissue was measured using ImageJ, and each count of total tdTomato$^+$ cells was normalized to respective area.

Tissues were prepared as described above. For paraffin section processing, decalcified tissues were dehydrated using washes of 30% ethanol (EtOH), 50% EtOH, and 70% EtOH. Samples were submitted to the Musculoskeletal Research Center for paraffin embedding, sectioning, and H&E staining. Histopathologic examination and analysis was performed by a pathologist blinded to intervention groups. The presence of acute and/or chronic inflammation within the skeletal muscle, synovial tissues, and joint space was noted. The overall severity of inflammation was scored as follows: 0 for none, 1 for mild, 2 for moderate, and 3 for severe. Representative images were taken using the Zeiss Axio Imager Z2 Fluorescence Microscope with ApoTome 2, managed at the WUCCI.

2.5.9 Immunofluorescence

To process for immunofluorescence, frozen section slides were first fixed with cold acetone. If indicated for the specific antibody, the samples underwent antigen retrieval using antigen unmasking solution (H3300; Vector Laboratories), which was incubated overnight in a 60°C water bath, protected from light. Samples were then permeabilized with 0.2% Triton-X in PBST (PBS + 0.1% Tween 20) and then washed with PBST. Samples were blocked for 1-2 h with TSA blocking reagent (Perkin Elmer FP1012). Samples were then incubated overnight at 4°C in primary antibody diluted 1:100 in 3% normal goat serum (NGS, Equitech-Bio, Inc.) and 3% bovine serum albumin (BSA, Sigma) in PBST. After two washes with PBST, samples were incubated for 1-2 h at RT in secondary antibody diluted 1:500 in 1% BSA PBST. Samples were washed once with PBST, stained with DAPI (100 μg/mL in PBST) for 10 min at RT, washed once with PBST, and a glass coverslip was mounted with ProLong Gold and slides were allowed to cure protected from light at RT overnight. Slides were imaged using a Nikon Spinning Disk Confocal Microscope or a Nikon A1Rsi Confocal Microscope, both maintained at the WUCCI. For illustration purposes,

cells were imaged at 20x or 100x with a single capture using the DAPI, GFP, RFP, and or AF647 channels.

The following primary antibodies were used for these studies with antigen retrieval: anti-vimentin (Abcam, clone EPR3776); anti-beta III tubulin (Abcam, clone EP1569Y); anti-CD45 (Abcam, polyclonal ab10558); anti-CD44 (Abcam, clone EPR18668); anti-CD29 (eBioscience, clone KMI6). The following antibodies did not require antigen retrieval: anti-CD31 (BD Biosciences, clone MEC 13.3); anti-SAA (Abcam, clone EA-53); anti-105 (eBioscience, clone MJ7/18).

2.5.10 RNA In-Situ Hybridization

Paraffin sections were processed using the provided RNAscope reagents and protocols from Advanced Cell Diagnostics. Slides were first prepared as directed for indicated in formalin-fixed paraffin-embedded (FFPE) sample (ACD Document Number 322452). The prepared samples were then exposed to RNAscope® Probe- V-CHIKV-sp (ACD) or negative control probe (ACD). The probed samples were then detected following the RNAscope® 2.5 HD Detection Reagent – BROWN protocol (ACD Document Number 322310), with the only modification being that slides were washed via pipetting the wash buffer onto the slides instead of submerging the slides into wash buffer. Representative images were taken using the Zeiss Axio Imager Z2 Fluorescence Microscope with ApoTome 2, managed at the WUCCI.

2.5.11 Statistical Analysis

All data were analyzed using the Prism software, version 7 (GraphPad), as detailed in the figure captions. The following statistical tests were used: unpaired t test, Mann-Whitney test, ordinary one-way analysis of variance (ANOVA), ordinary two-way ANOVA, and two-way repeated-measures ANOVA. The following post-tests for multiple comparisons were also used: Bonferroni's post-test, Dunnett's post-test, Tukey's post-test, and Sidak's post-test. All error bars

indicate standard error of the mean (SEM); if error bars are not visible, then they are shorter than the height of the symbol. Asterisks indicate statistical significance, with only relevant comparisons shown (*, $P < 0.05$; **, $P < 0.01$; ***, $P < 0.001$; ****, $P < 0.0001$).

2.6 Figures

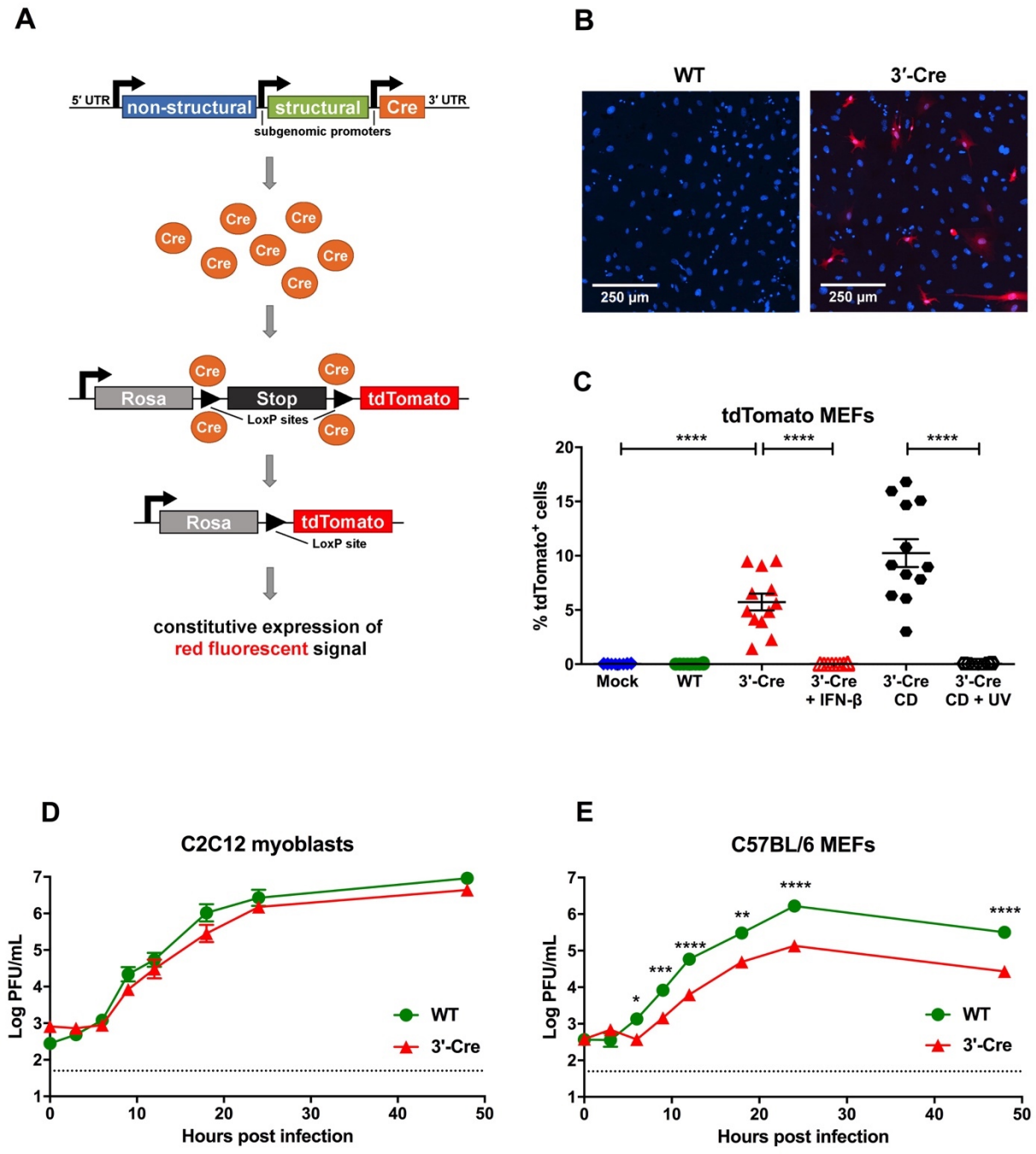

Figure 2.1: CHIKV-3'-Cre marks reporter cells in vitro and productively infects muscle cells and fibroblasts

(A) Schematic of CHIKV-3'-Cre and tdTomato reporter mouse system. **(B-C)** tdTomato MEFs were analyzed 2 days after mock infection or infection at an MOI of 10 with CHIKV-WT or CHIKV-3'-Cre. **(B)** Representative images of CHIKV-WT or CHIKV-3'-Cre. Blue shows DAPI staining, and

red is tdTomato; scale bar represents 250 μm. **(C)** The percentage of total $DAPI^+$ cells that were $tdTomato^+$ was quantified by confocal microscopy for tdTomato MEFs that were mock-infected (mock) or infected at an MOI of 10 with CHIKV-WT (WT), CHIKV-3'-Cre (3'-Cre), CHIKV-3'-Cre pretreated with ~100 U IFN-β (3'-Cre + IFN-B), CHIKV-3'-Cre cell debris (3'-Cre CD), or CHIKV-3'-Cre cell debris that was UV-inactivated (3'-Cre CD + UV) as described in the Methods Section 2.5.5. **(D)** Growth curves of C2C12 myoblasts or **(E)** BL/6 MEFs infected with CHIKV-WT (green circles) or CHIKV-3'-Cre (red triangles) at an MOI of 1. Data for each condition in **C** were pooled from 2-3 independent experiments; data in **C** were statistically analyzed with an ordinary one-way ANOVA with Tukey's post-test. Each curve in **D** and **E** represents 8 total replicates pooled from 2 independent experiments at each time point; data were then log-transformed and statistically analyzed with a two-way ANOVA using Sidak's post-test. All error bars indicate mean with standard error of the mean (SEM); if error bars are not visible, then they are shorter than the height of the symbol. Asterisks indicate statistical significance, with only relevant comparisons shown (*, $P < 0.05$; **, $P < 0.01$; ***, $P < 0.001$; ****, $P < 0.0001$).

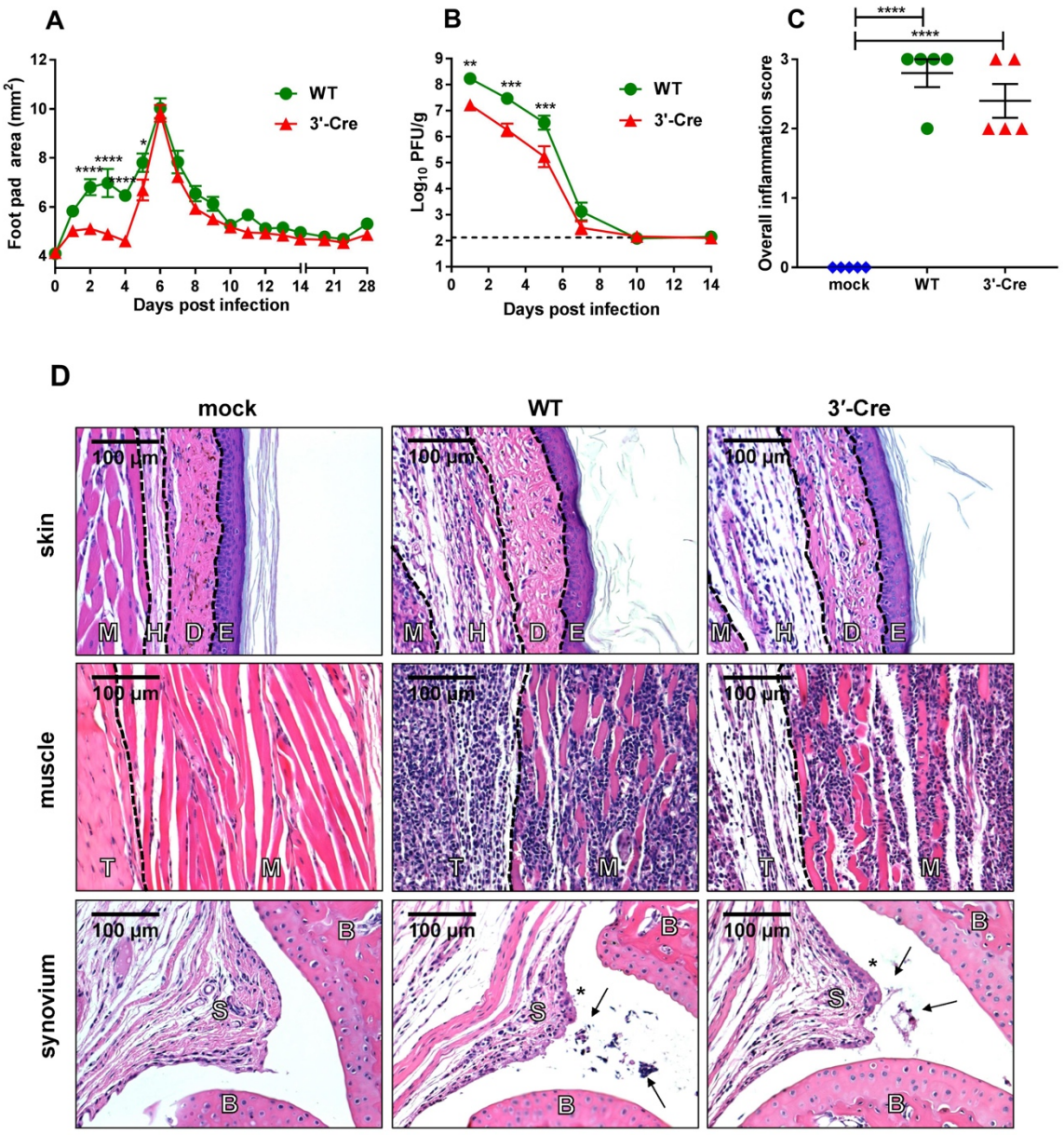

Figure 2.2: CHIKV-3'-Cre retains its pathogenic properties to induce acute arthritis

(A) Swelling curves from the ipsilateral feet of mice infected with 10^6 PFU of CHIKV-WT (green circles) or 10^6 PFU of CHIKV-3'-Cre (red triangles). Data were pooled from two independent experiments with n=10 for each virus. **(B)** Levels of infectious virus in the ipsilateral ankle during acute infection as measured by plaque assay, normalized to gram of tissue. Each time point for each virus represents 5-7 mice and were pooled from at least 2 independent experiments. **(C-D)** Mice were mock-infected (mock, blue diamonds) or infected with 10^6 PFU CHIKV-WT (WT, green circles) or 10^6 PFU CHIKV-3'-Cre (3'-Cre, red triangles), and ipsilateral ankles were taken for H&E

histology at 7 dpi. **(C)** Ankles were scored for overall histological damage. **(D)** Representative images of the skin, muscle, and synovium. The skin and associated tissue is divided (from left to right) into muscle (M), hypodermis (H), dermis (D), and epidermis (E). The muscle sections are divided into tendon (T) and muscle (M). The synovium sections show synovium (S) and bone (B), with asterisks indicating synovial inflammation and arrows indicating immune infiltrates into the synovial cavity. Samples were pooled from two independent experiments with five mice for each condition. The dashed line for **B** represents limit of detection, and data in **B** were log-transformed prior to analysis. Data in **A** were statistically analyzed with a two-way repeated measures (RM) ANOVA with Bonferroni's post-test. Data in **B** were statistically analyzed with an ordinary two-way ANOVA with Bonferroni's post-test. Data in **C** were statistically analyzed with an ordinary one-way ANOVA with Tukey's post-test. Scale bars in **D** represent 100 μm. All error bars indicate SEM. Asterisks indicate statistical significance, with only relevant comparisons shown (*, $P < 0.05$; **, $P < 0.01$; ***, $P < 0.001$; ****, $P < 0.0001$).

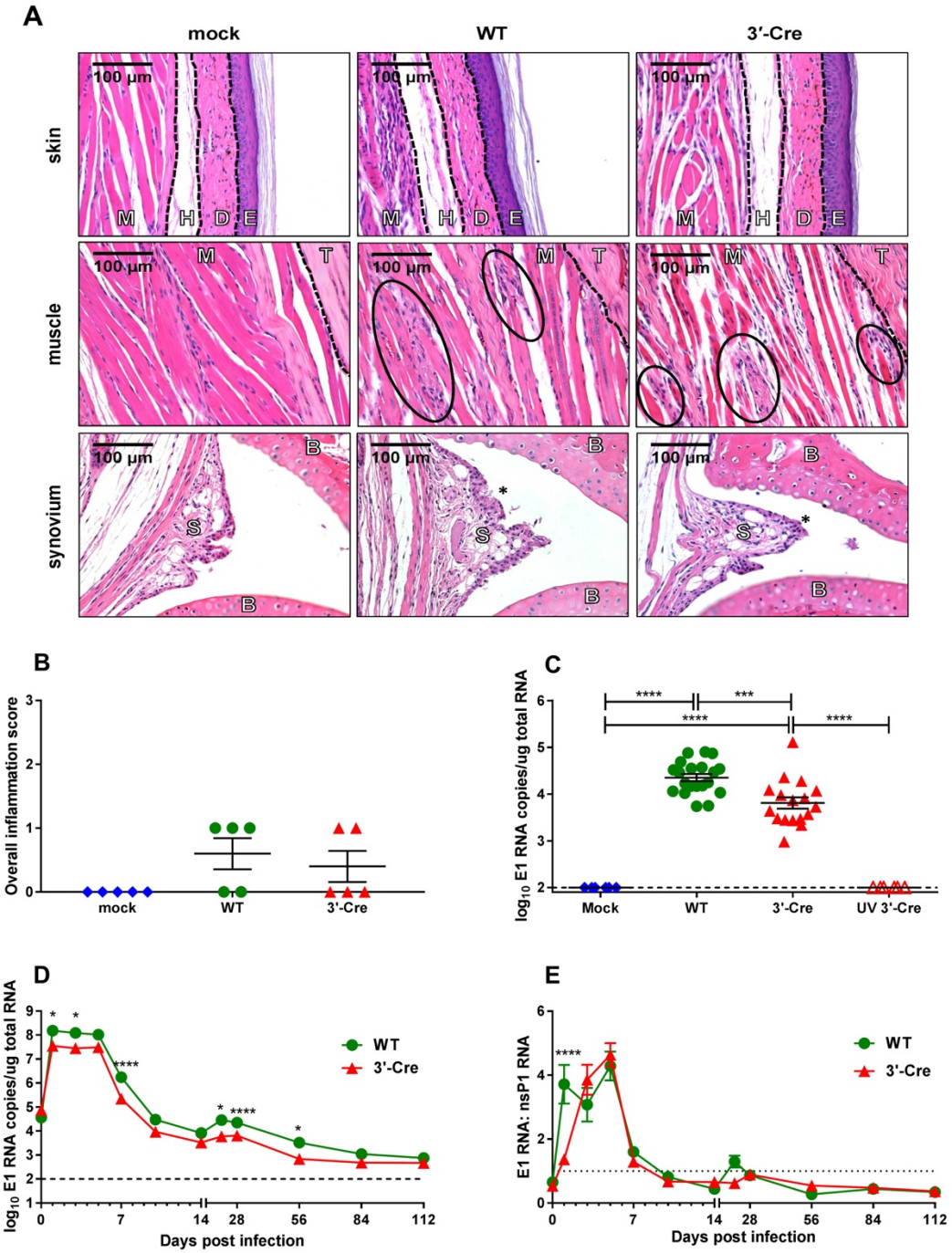

Figure 2.3: CHIKV-3'-Cre retains its pathogenic properties to induce chronic disease

(A-B) Mice were mock-infected (mock, blue diamonds) or inoculated with 10^6 PFU CHIKV-WT (WT, green circles) or 10^6 PFU CHIKV-3'-Cre (3'-Cre, red triangles), and ipsilateral ankles were taken for H&E histology at 28 dpi. **(A)** Representative images of the skin, muscle, and synovium. The skin and associated tissue is divided (from left to right) into muscle (M), hypodermis (H), dermis (D), and epidermis (E). The muscle sections are divided into muscle (M)

and tendon (T), with black ovals around focal patches of cellular filtrates. The synovium sections show synovium (S) and bone (B), with asterisks indicating synovial inflammation and proliferation. **(B)** Ankles were scored for overall histological damage. Samples were pooled from two independent experiments with five mice for each condition. **(C-D)** The ipsilateral ankles of mice were subjected to RT-qPCR to measure viral E1 RNA copy number, normalized to total μg of RNA isolated for each sample. **(C)** Mice were mock-infected (mock) or inoculated with 10^6 CHIKV-WT (WT), 10^6 CHIKV-3'-Cre (3' Cre) or UV-inactivated dose of 10^6 CHIKV-3'-Cre (UV 3'-Cre), and viral E1 RNA levels in the ipsilateral ankles were assayed at 28 dpi. Data were pooled from at least 2 independent experiments. **(D)** Viral E1 RNA levels were measured in the ipsilateral ankles of mice infected with 10^6 PFU of CHIKV-WT (green circles) or 10^6 PFU of CHIKV-3'-Cre (red triangles) at time points ranging from 0 to 112 dpi. **(E)** The ratio of viral E1 RNA to viral nsP1 RNA in the same samples as **D**. For **D-E**, each time point for each virus represents 5-20 mice and was pooled from at least 2 independent experiments. The dashed line for **C** and **D** represents limit of detection; for **E**, the dotted line represents an E1: nsP1 ratio of 1. Data in **C** and **D** were log-transformed prior to analysis. Data in **B** and **C** were each statistically analyzed with an ordinary one-way ANOVA using Tukey's post-test, with only relevant comparisons shown. Data in **D** and **E** were statistically analyzed with an ordinary two-way ANOVA using Bonferroni's post-test. All error bars indicate SEM. Asterisks indicate statistical significance, with only relevant comparisons shown (*, $P < 0.05$; **, $P < 0.01$; ***, $P < 0.001$; ****, $P < 0.0001$).

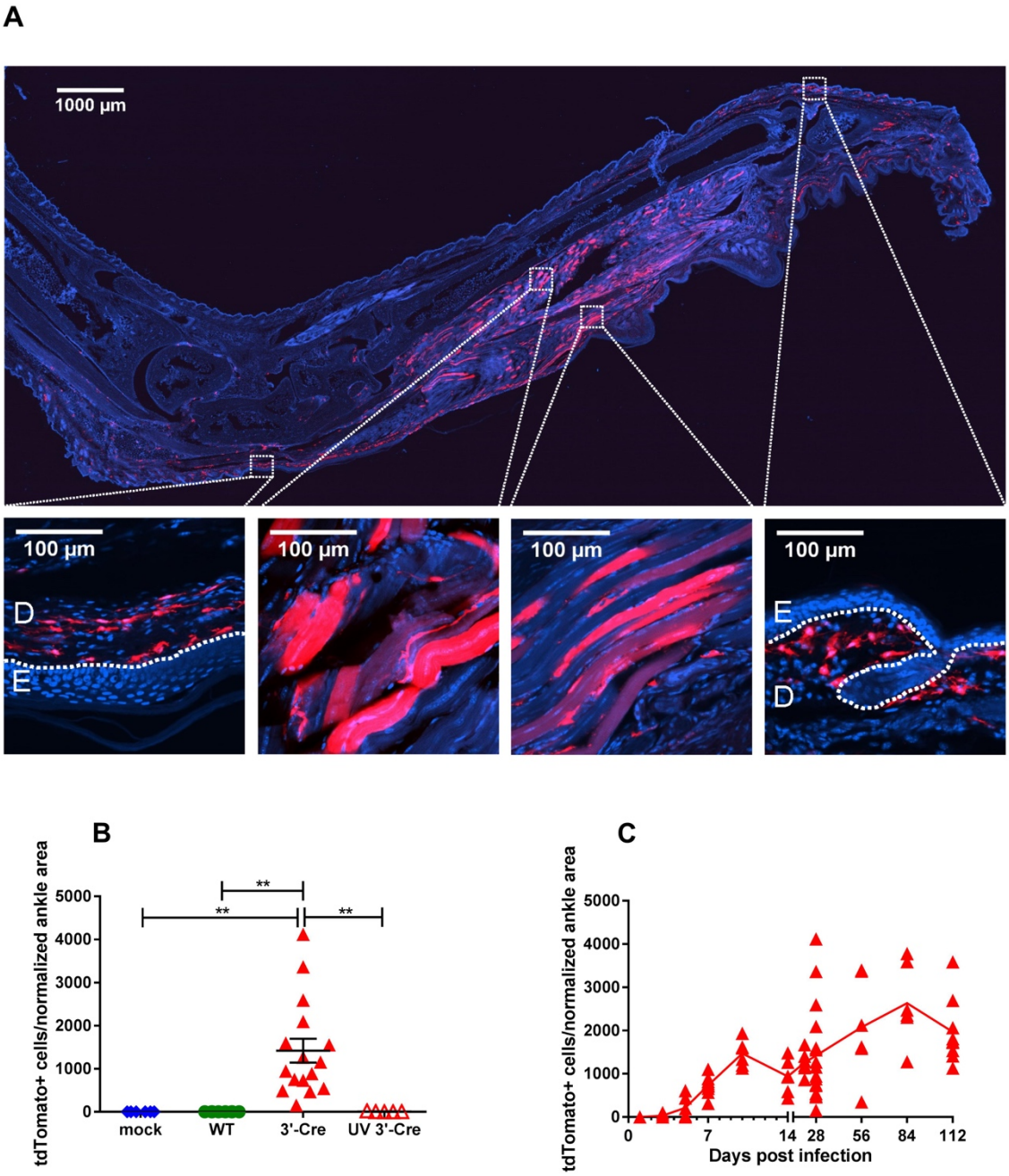

Figure 2.4: Cells are marked by CHIKV-3'-Cre at chronic time points

tdTomato mice were mock-infected (mock, blue circles) or inoculated with 10^6 PFU CHIKV-WT (WT, green circles), 10^6 PFU CHIKV-3'-Cre (3'-Cre, red triangles), or UV-inactivated 10^6 PFU CHIKV-3'-Cre (UV 3'-Cre, open red triangles), and ipsilateral ankles were taken for frozen sections at 28 dpi. **(A)** A representative image of a whole ankle and foot 28 dpi with CHIKV-3'-Cre. Blue shows DAPI staining, and red is tdTomato; scale bar represents 1000 µm. Higher

magnification inset images of skin and muscle from mice infected with CHIKV-3'-Cre. Scale bars represent 100 μm; the skin is divided into dermis (D) and epidermis (E). **(B)** The total number of tdTomato$^+$ cells from was quantified at 28 dpi and normalized to ankle area as described in the Methods Section 2.5.8. **(C)** Time course of tdTomato mice infected with 3'-Cre from 1 to 112 dpi. Data from **B** and **C** were pooled from at least two independent experiments. **B** was statistically analyzed with an ordinary one-way ANOVA using Sidak's post-test. All error bars indicate SEM. Asterisks indicate statistical significance, with only relevant comparisons shown (*, $P < 0.05$; **, $P < 0.01$; ***, $P < 0.001$; ****, $P < 0.0001$).

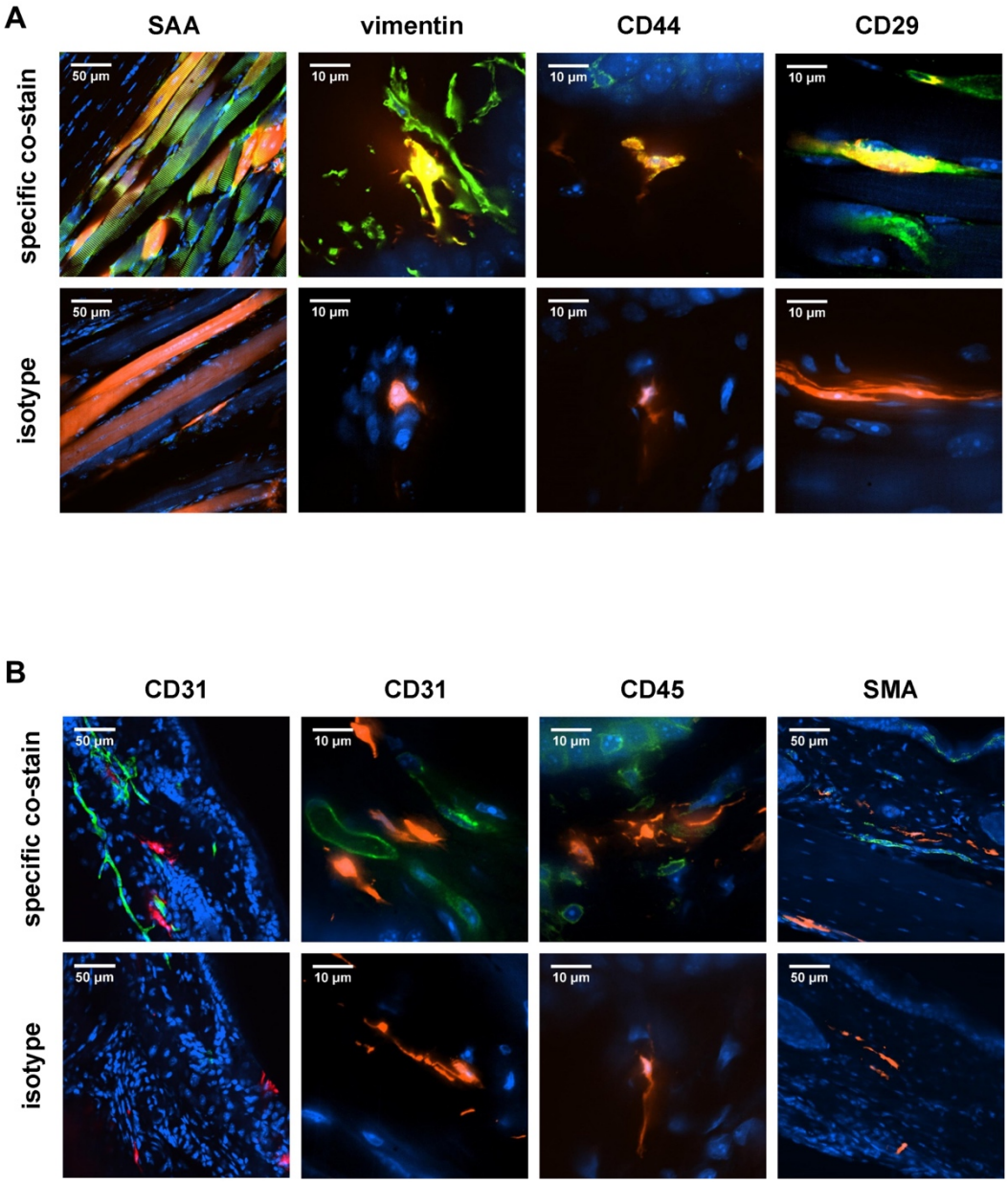

Figure 2.5: Immunofluorescence profiling of tdTomato$^+$ cells in the skin and muscle

tdTomato mice were infected with 10^6 PFU CHIKV-3'-Cre (3'-Cre), and ipsilateral ankles/feet were taken for frozen sections at 28 dpi. **(A)** Frozen sections were stained for SAA$^+$ myofibers, vimentin$^+$ fibroblasts, CD44$^+$ fibroblasts, or CD29$^+$ fibroblasts, with the corresponding isotype control shown below each co-stain. **(B)** Frozen sections were stained for CD31$^+$ endothelium, CD45$^+$ hematopoietic cells, or SMA$^+$ smooth muscle cells, with the corresponding isotype control

shown below each co-stain. Blue shows DAPI staining, red is tdTomato, and green is the indicated co-staining marker; scale bars represent 10 or 50 μm. Images are representative of 2-3 experiments with 3-5 mice reviewed for each co-stain.

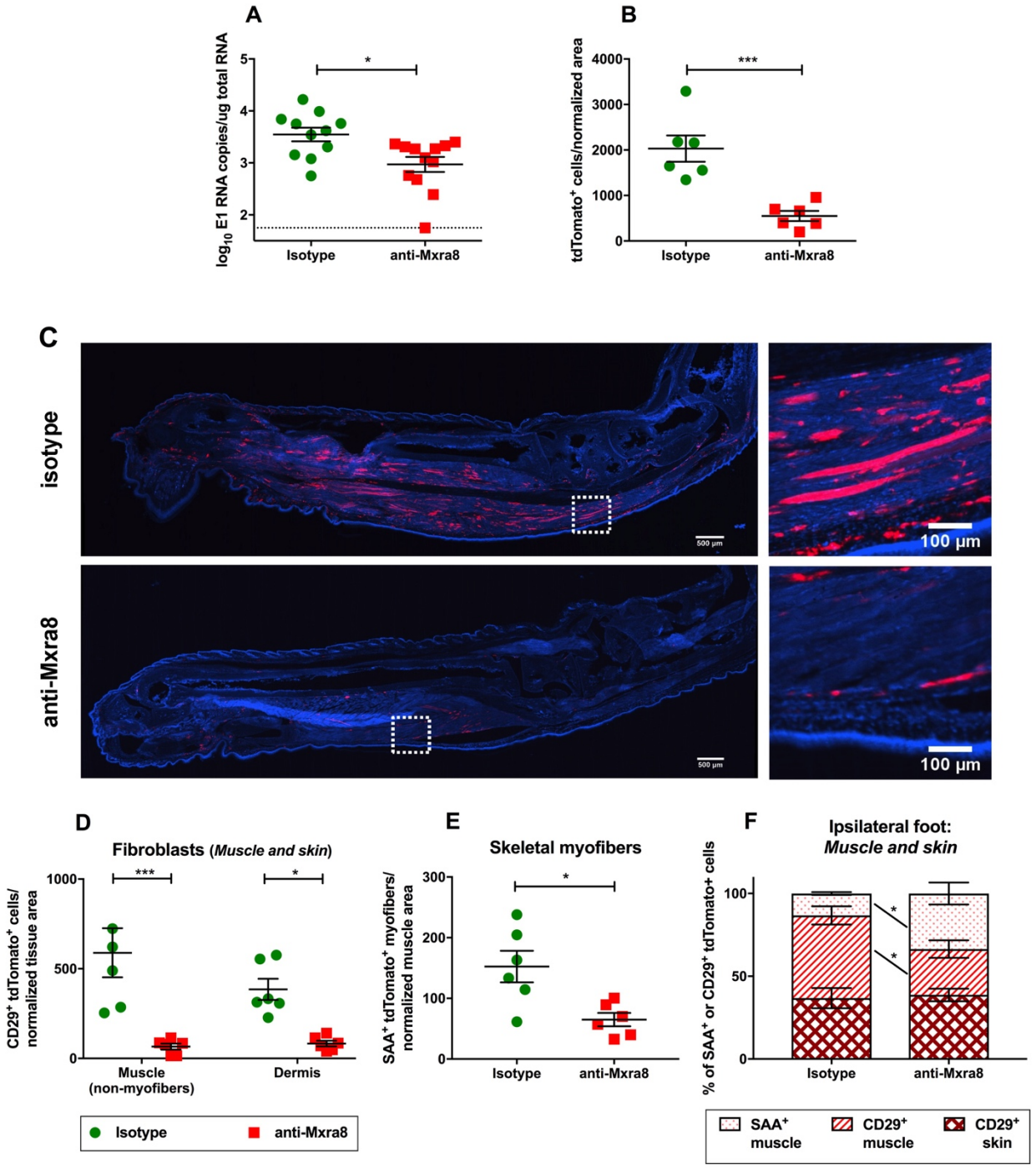

Figure 2.6: Mice treated with anti-Mxra8 antibodies exhibit reduced levels of chronic viral RNA and a reduced number of persistent tdTomato$^+$ cells

tdTomato mice were infected with 10^6 PFU CHIKV-3'-Cre and treated with anti-Mxra8 mAbs (anti-Mxra8; red squares) or an isotype control (isotype; green circles). **(A)** At 28 dpi, mice were harvested for quantification of CHIKV E1 RNA in the ipsilateral ankle; data represent three

independent experiments. **(B-F)** Ipsilateral ankles/feet were harvested for histological analysis at 28 dpi; data represent two independent experiments. **(B)** Total number of tdTomato$^+$ cells in ipsilateral ankles/feet. **(C)** Representative images of ipsilateral feet/ankles, with higher magnifications of dotted squares inset to the right. Blue shows DAPI staining, and red is tdTomato; scale bars represent 100 or 500 μm as indicated. **(D-F)** tdTomato$^+$ cells were quantified by morphology and co-staining as described in the Methods Section 2.5.9: **(D)** CD29$^+$ muscle and skin cells, and **(E)** SAA$^+$ myofibers. **(F)** Percentage distribution of cell types for each treatment. Data in **A** were normalized to total μg of RNA isolated for each sample and then log-transformed. Data in **A** were analyzed with a Mann-Whitney test. Data in **B** and **E** were statistically analyzed with an un-paired t test. Data in **D** and **F** were statistically analyzed with a two-way ANOVA using Sidak's post-test. All error bars indicate SEM. Asterisks indicate statistical significance, with only relevant comparisons shown (*, $P < 0.05$; **, $P < 0.01$; ***, $P < 0.001$; ****, $P < 0.0001$).

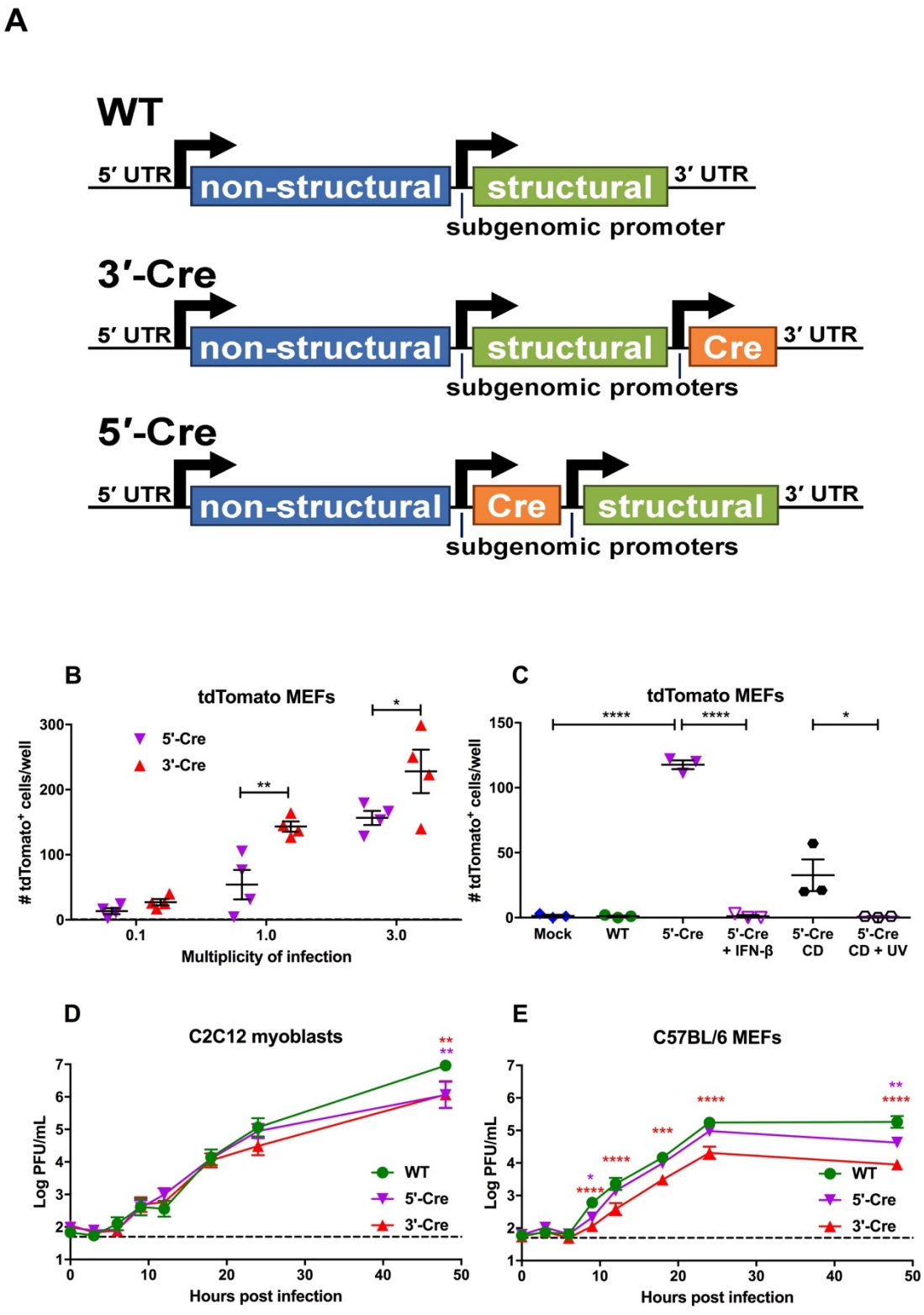

Figure S2.1: CHIKV-5'-Cre and CHIKV-3'-Cre mark reporter cells *in vitro* and grow productively in muscle cells and fibroblasts

(A) Genome maps of the three CHIKV clones were used in these studies: CHIKV-WT, CHIKV-3'-Cre, and CHIKV-5'-Cre. **(B)** tdTomato MEFs plated in 96-well plates ($2.5*10^4$ cells/well) were infected with CHIKV-5'-Cre (purple inverted triangles) or CHIKV-3'-Cre (red triangles) at an MOI of 0.1, 1.0, or 3.0. **(C)** tdTomato MEFs plated in 96-well plates ($2.5*10^4$ cells/well) and were mock-infected (mock) or infected at an MOI of 3.0 with CHIKV-WT (WT), CHIKV-5'-Cre (5' Cre), CHIKV-5'-Cre pretreated with ~100 U IFN-β (5' Cre + IFN-B), CHIKV-5'-Cre cell debris (5' Cre CD), or CHIKV-5'-Cre cell debris that was UV-inactivated (5'-Cre CD + UV). **(D)** Growth curves of C2C12 myoblasts or **(E)** C57BL/6 MEFs infected with CHIKV-WT (green circles), CHIKV-5'-Cre (purple inverted triangles), or CHIKV-3'-Cre (red triangles) at an MOI of 0.05. The number of $tdTomato^+$ cells per well in **B** and **C** were quantified at 2 dpi by eye using a fluorescent microscope. Data in **B** were analyzed with a two-way ANOVA using Sidak's post-test. Data in **C** were statistically analyzed with an ordinary one-way ANOVA using Sidak's post-test. Data in **D** and **E** were log-transformed and statistically analyzed with a two-way ANOVA using Dunnett's post-test. All error bars indicate SEM. Asterisks indicate statistical significance, with only relevant comparisons shown (*, $P < 0.05$; **, $P < 0.01$; ***, $P < 0.001$; ****, $P < 0.0001$).

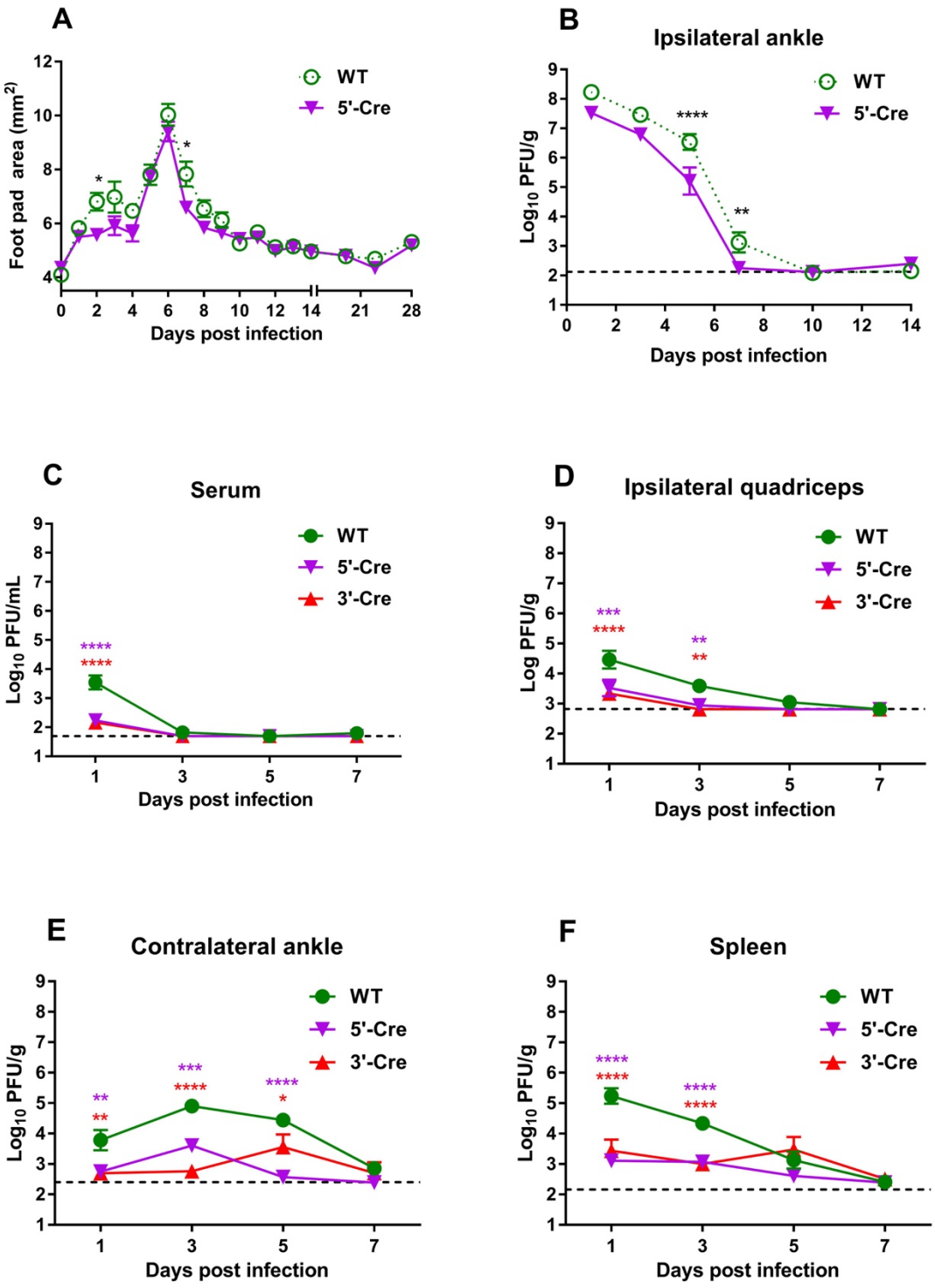

Figure S2.2: CHIKV-5'-Cre and CHIKV-3'-Cre replicate similarly to CHIKV-WT in a mouse model, with attenuation in sites of dissemination

(A) Swelling curves from the ipsilateral footpads of mice infected with 10^6 PFU of CHIKV-WT (open green circles; also shown in Figure 2.2A) or 10^6 PFU of CHIKV-5'-Cre (purple). Data were pooled from two independent experiments with n=10 for each virus. **(B-F)** Levels of infectious virus in mice infected with 10^6 PFU of CHIKV-WT (solid green circles; or open green circles in S2B also shown in Figure 2.2B), 10^6 PFU of CHIKV-5'-Cre (purple inverted triangles), or 10^6 PFU of CHIKV-3'-Cre (red triangles) in **(B)** ipsilateral ankle, **(C)** serum, **(D)** ipsilateral quadriceps muscle, **(E)** the contralateral ankle, or **(F)** spleen. For **B-F**, each time point for each virus and organ represents 5-7 mice and were pooled from at least 2 independent experiments. Infectious levels during acute infection was measured by plaque assay, normalized to gram of tissue, and then log-transformed. The dashed line for **B-F** represents limit of detection for the plaque assay. Data in **B**-**F** were log-transformed prior to analysis. Data in **A** were statistically analyzed with a two-way repeated measures (RM) ANOVA with Bonferroni's post-test, and data in **B**-**F** were statistically analyzed with an ordinary two-way ANOVA. Sidak's post-test was used for **A**, and **B**; Dunnett's post-test comparing WT as the control column was used for **C-F**. All error bars indicate SEM. Asterisks indicate statistical significance, with only relevant comparisons shown (*, $P < 0.05$; **, $P < 0.01$; ***, $P < 0.001$; ****, $P < 0.0001$).

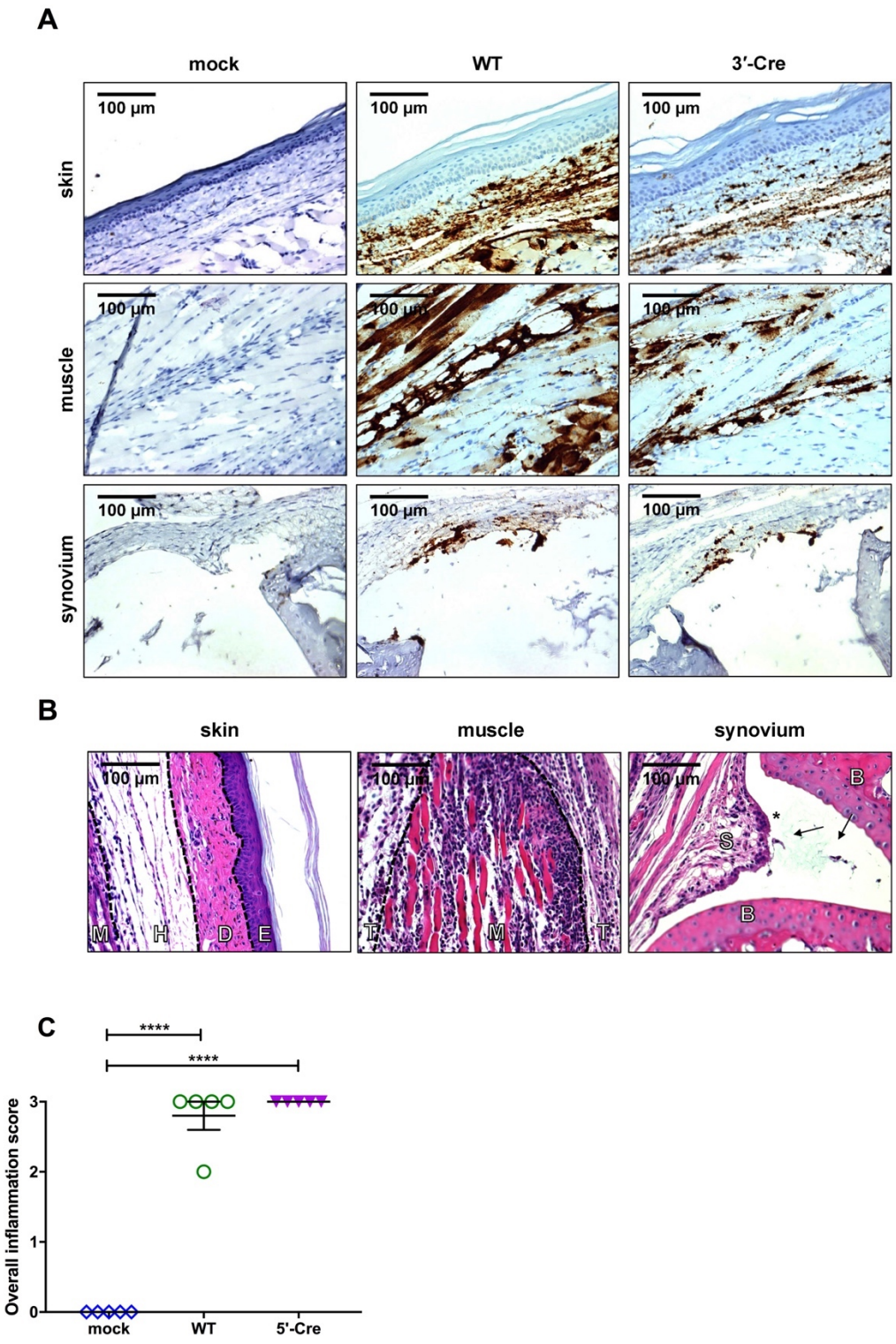

Figure S2.3: CHIKV-5'-Cre and CHIKV-3'-Cre retain their pathogenic properties to induce acute arthritis

(A) Mice were mock infected or infected with 10^6 PFU CHIKV-WT (WT) or 10^6 PFU CHIKV-3'-Cre (3'-Cre), and ipsilateral ankles were taken for CHIKV ISH at 2 dpi. Paraffin sections were stained with a probe for E1 CHIKV-LR RNA. Representative images are shown of the skin, muscle, and synovium. Scale bars represent 100 μm. Represents two independent experiments with 6 mice per virus and 2 mock-infected mice. **(B-C)** Mice were mock-infected (mock, blue diamonds) or infected with 10^6 PFU CHIKV-WT (WT, green circles) or 10^6 PFU CHIKV-5'-Cre (5'-Cre, purple inverted triangles), and ipsilateral ankles were taken for H&E histology at 7 dpi. **(B)** Representative images are shown of the skin, muscle, and synovium from CHIKV-5'-Cre samples; scale bar represents 100 μm. The skin and associated tissue is divided (from left to right) into muscle (M), hypodermis (H), dermis (D), and epidermis (E). The muscle section is divided into tendon (T) and muscle (M). The synovium section shows synovium (S) and bone (B), with asterisks indicating synovial inflammation and arrows indicating immune infiltrates into the synovial cavity. **(C)** Ankles from **B** were scored for overall histological damage, compared to mock-infected and CHIKV-WT-infected samples. Open symbols for mock and WT indicate that these data are also shown in the corresponding Figure 2.2C graph. Samples were pooled from two independent experiments. Data in **C** were statistically analyzed with a one-way ANOVA with Tukey's post-test. All error bars indicate SEM. Asterisks indicate statistical significance, with only relevant comparisons shown (*, $P < 0.05$; **, $P < 0.01$; ***, $P < 0.001$; ****, $P < 0.0001$).

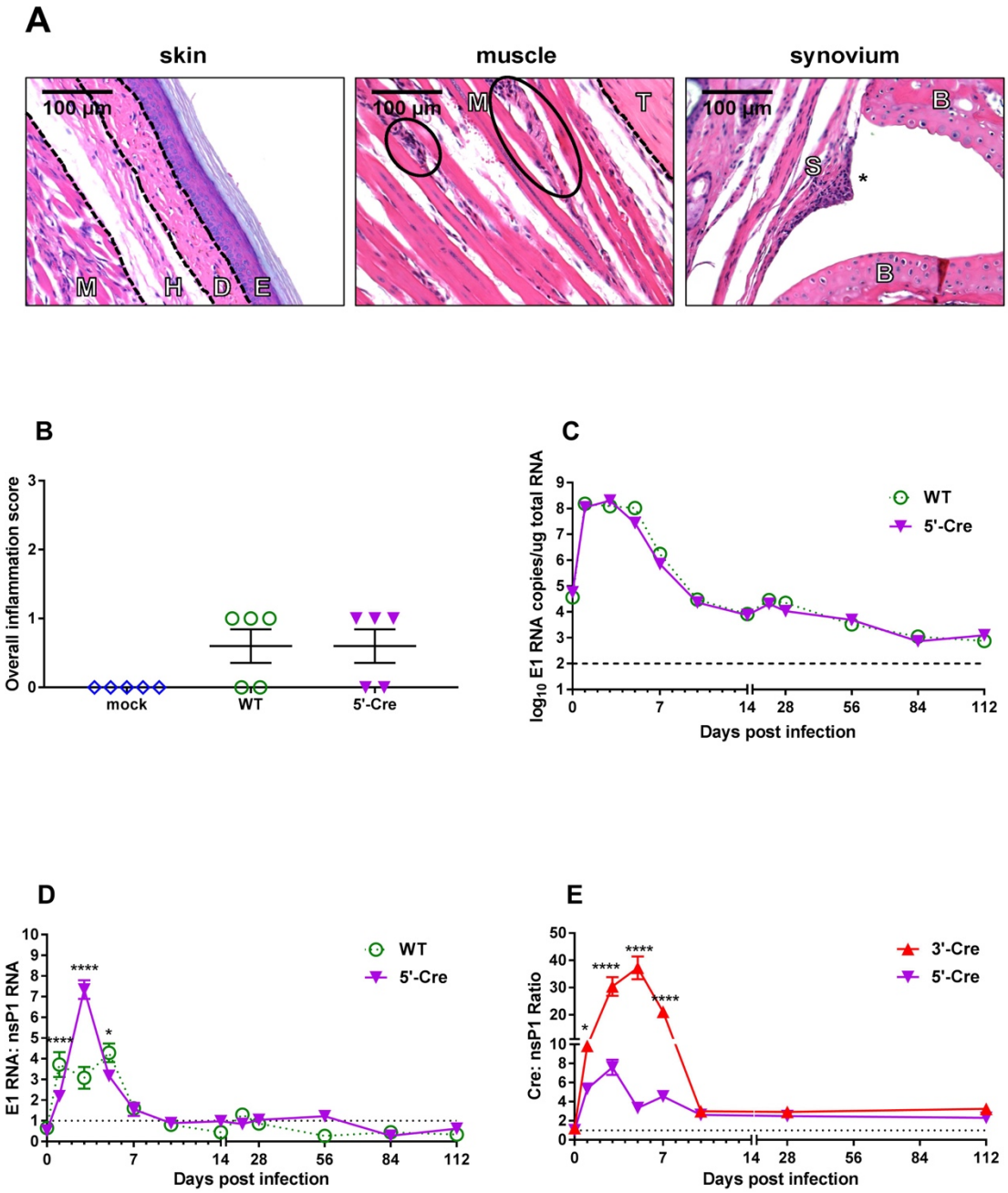

Figure S2.4: CHIKV-5'-Cre and CHIKV-3'-Cre retain their pathogenic properties to induce chronic disease

(A-B) Mice were mock-infected (mock, blue diamonds) or infected with 10^6 PFU CHIKV-WT (WT, green circles) or 10^6 PFU CHIKV-5'-Cre (5'-Cre, purple inverted triangles), and ipsilateral ankles were taken for H&E histology at 28 dpi. **(A)** Representative images are shown of the skin, muscle, and synovium from CHIKV-5'-Cre samples; scale bar represents 100 µm. The skin and associated tissue is divided (from left to right) into muscle (M), hypodermis (H), dermis (D), and epidermis

(E). The muscle section is divided into muscle (M) and tendon (T), with black ovals around focal patches of cellular filtrates. The synovium section shows synovium (S) and bone (B), with asterisks indicating synovial inflammation and proliferation. **(B)** Ankles from **A** were scored for overall histological damage, compared to mock-infected and CHIKV-WT-infected samples. Open symbols for mock and WT indicate that these data are also shown in the corresponding Figure 2.3B graph. **(C-E)** The ipsilateral ankles of mice were subjected to RT-qPCR to measure viral E1, nsp1, or Cre RNA copy number, normalized to total μg of RNA isolated for each sample and then log-transformed. **(C)** Viral E1 RNA levels were measured in the ipsilateral ankles of mice infected with 10^6 PFU of CHIKV-WT (open green circles, also shown in Figure 2.3D) or 10^6 PFU of CHIKV-5'-Cre (purple inverted triangles) at time points ranging from 0 to 112 dpi. **(D)** The ratio of viral E1 RNA to viral nsP1 RNA in the same samples as **C** (open green circles, also shown in Figure 2.3E). **(E)** The ratio of viral Cre RNA to viral nsP1 RNA in mice infected with 10^6 PFU of CHIKV-5'-Cre (purple inverted triangles) or 10^6 PFU of CHIKV-3'-Cre (red triangles). Data in **B** were statistically analyzed with a one-way ANOVA with Tukey's post-test. For **C**-**E**, each time point for each virus represents 4-20 mice and was pooled from at least 2 independent experiments. The dashed line in **C** represents the limit of detection for the RT-qPCR assay; for **D** and **E**, the dotted line represents a ratio of 1. Data in **C** were normalized to total μg of RNA isolated for each sample and then log-transformed. Data in **C**-**E** were statistically analyzed with a two-way ANOVA with Sidak's post-test. All error bars indicate SEM. Asterisks indicate statistical significance, with only relevant comparisons shown (*, $P < 0.05$; **, $P < 0.01$; ***, $P < 0.001$; ****, $P < 0.0001$).

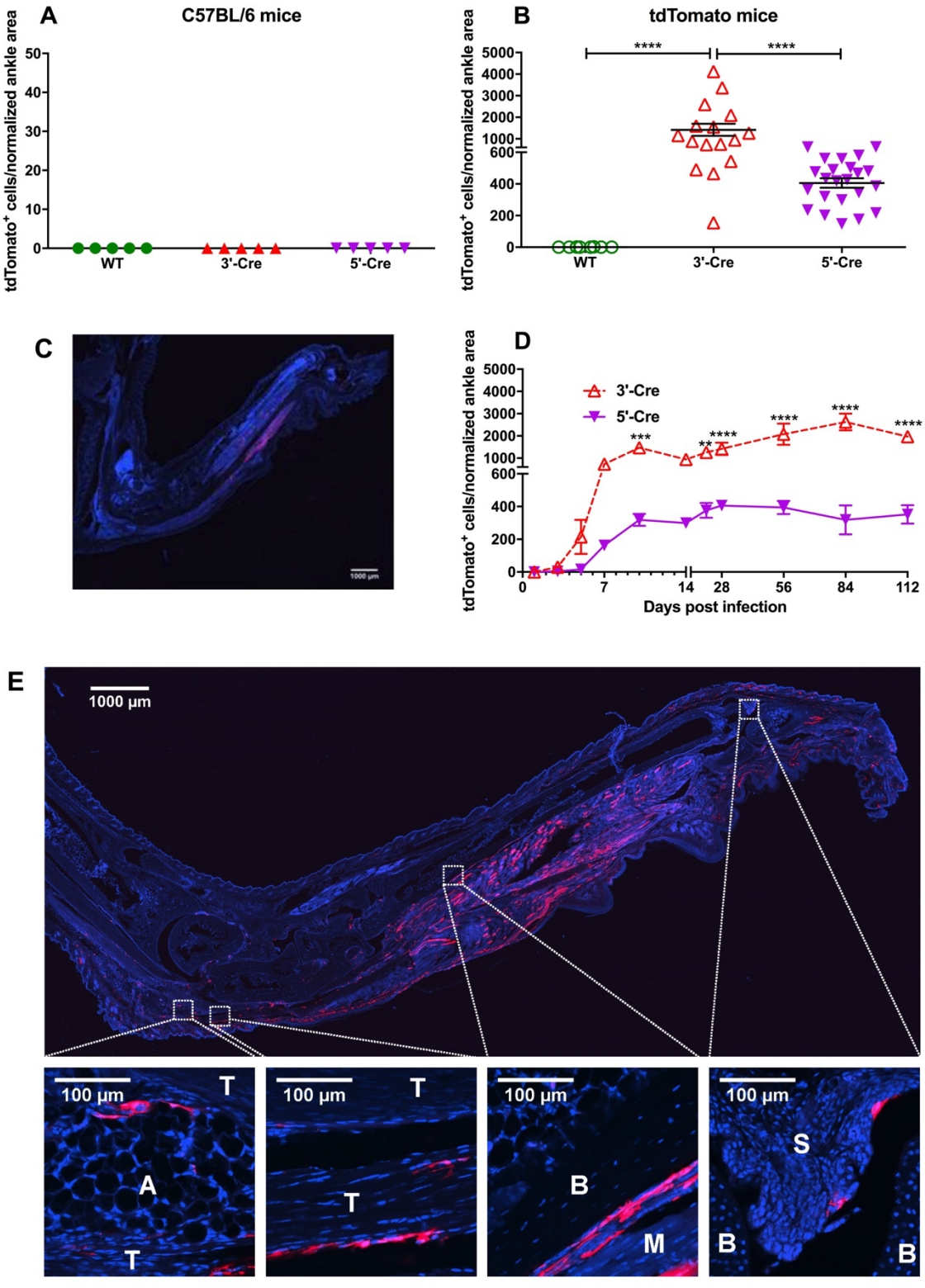

Figure S2.5: Cells are marked by CHIKV-5'-Cre or CHIKV-3'-Cre at chronic time points.

(A) C57BL/6 or **(B)** tdTomato mice were infected with 10^6 PFU CHIKV-WT (WT, green circles), CHIKV-5'-Cre (5'-Cre, purple inverted triangles), or 10^6 PFU CHIKV-3'-Cre (3'-Cre, red triangles). Ipsilateral ankles were taken for frozen sections at 28 dpi, and the total number of tdTomato$^+$ cells was quantified. Open green circles for WT and open red triangles for 3'-Cre indicate that these data are also shown in the corresponding Figure 2.4B graph. **(C)** Representative image of a whole foot/ankle from 5'-Cre at 28 dpi. Blue shows DAPI staining, and red is tdTomato; scale bar represents 1000 μm. **(D)** Time course of dtTomato mice infected with CHIKV-5'-Cre (purpled inverted triangles) or CHIKV-3'-Cre (open red triangles, also shown in Figure 2.4C) from 1 to 112 dpi. Each time point for each virus represents 6-20 mice. **(E)** Representative images of connective tissues in the ipsilateral ankle of a mouse infected with CHIKV-3'-Cre. Blue shows DAPI staining, and red is tdTomato; scale bar represents 1000 μm. In higher magnification inset images scale bars represent 100 μm; (A) is adipose tissue, (T) is tendon, (B) is bone, (M) is muscle, and (S) is synovium. Data from **A**, **B** and **D** were pooled from at least two independent experiments. Data in **A** and **B** were statistically analyzed with an ordinary one-way ANOVA using Tukey's post-test. Data in **D** were statistically analyzed with two-way ANOVA using Sidak's post-est. All error bars indicate SEM. Asterisks indicate statistical significance, with only relevant comparisons shown (*, $P < 0.05$; **, $P < 0.01$; ***, $P < 0.001$; ****, $P < 0.0001$).

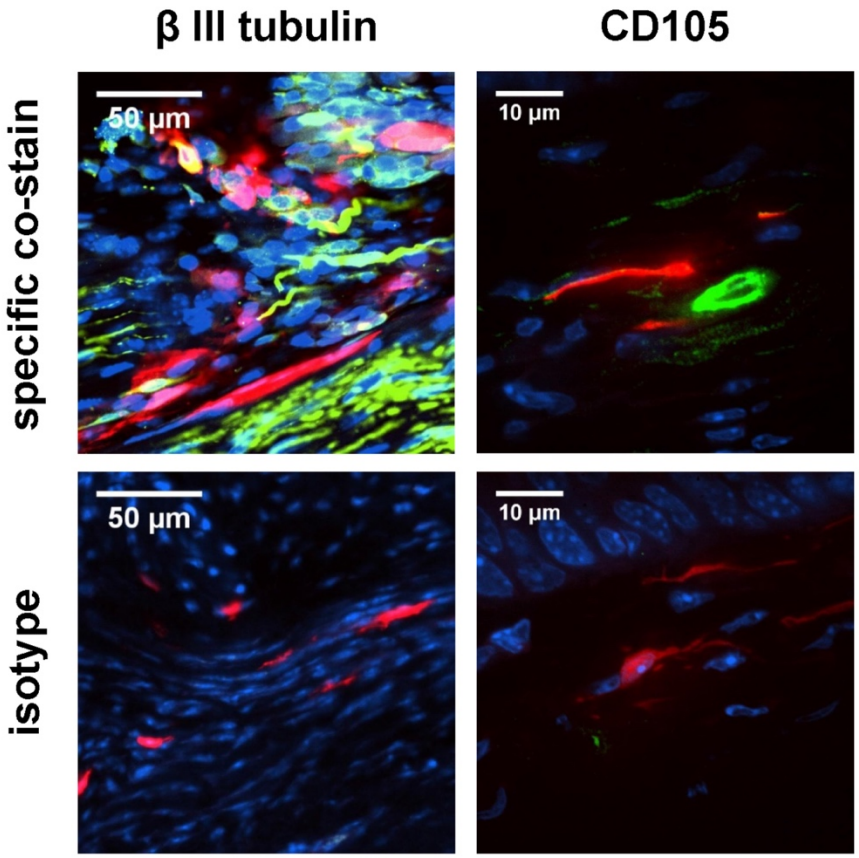

Figure S2.6: Immunofluorescence profiling of tdTomato$^+$ cells in the skin

tdTomato mice were infected with 10^6 PFU CHIKV-3'-Cre, and ipsilateral ankles were taken for frozen sections at 28 dpi. Frozen sections were stained for beta III tubulin (nerve fibers) and CD105 (fibroblasts and endothelial cells), with the corresponding isotype control shown below each co-stain. Blue shows DAPI staining, red is tdTomato, and green is the indicated co-staining marker; scale bars represent 10 or 50 μm as indicated.

Chapter 3:

Modulations of the CHIKV-Cre System

3.1 Introduction

CHIKV is an arthritogenic alphavirus that causes both acute and chronic musculoskeletal disease. In Chapter 2, we introduced a CHIKV-Cre reporter mouse system to study the chronic pathogenesis of CHIKV (**Figure 2.1A**). We engineered two versions of CHIKV that express Cre recombinase: CHIKV-5'-Cre and CHIKV-3'-Cre (**Figure S2.1A**). In the process of optimizing this reporter system, we experimented with varying the viral dose. We ultimately settled on a 10^6 PFU dose of CHIKV- 3'-Cre for our detailed analysis of chronic CHIKV pathogenesis, as it exhibited the highest number of tdTomato$^+$ cells in the ipsilateral foot. However, we observed noticeable effects on pathogenesis depending on dose.

Our experimentation with varying the dose of CHIKV-Cre was initially driven by published optimization experiments with other viruses that express Cre. Increasing the dose (ranging from 10^1 to 10^5 PFU) of WT Influenza A (IAV) or IAV-Cre correlated with accelerated weight loss and increased mortality in mice [139]. Similarly, in a paper including a Herpes Simplex Virus 1 (HSV-1) expressing Cre, increasing the dose of WT HSV-1 from 10^3 to 10^6 PFU corresponded with an increase in the number of animals infected [140].

Several studies have previously disclosed effects of modulating infection in various models of CHIKV infection. *In vitro* cell culture assays have consistently displayed that an increased CHIKV MOI is associated with increased viral titers in cells including fibroblasts, macrophages, and HeLa cells [42,58,59,66]. Our data from Chapter 2 with C2C12s or MEFs infected at a low (0.05) and high MOI (1.0) exhibit a similar trend (**Figures 2.1D-E, S2.1D-E**). We have also seen similar results with primary osteoblasts (data not shown).

Varying the CHIKV inoculation dose has also been explored *in vivo*. In a non-human primate CHIKV model, macaques were infected with 10^1 to 10^8 PFU CHIKV [56]. Increasing the CHIKV dosage corresponded with an earlier day of peak viremia and a higher maximum viral RNA load in the serum. Increased CHIKV doses also correlated with more and worsening

symptoms that closely mimicked human disease, including fever, rash, joint effusion, and edema, and at the highest dose meningoencephalitis and death [56].

Several published mouse CHIKV models have modulated infection variables with varying results. Immunocompromised ($IFNAR^{-/-}$ or $STAT1^{-/-}$) mice exhibited earlier mortality when inoculated with 10^6 PFU of CHIKV compared to 10^2 PFU [58]. In WT mice, it was reported that mice had to be infected with a dose higher than $1.5x10^7$ PFU of the CHIKV 181/25 vaccine strain in order to achieve dissemination to distal sites; however, a more detailed analysis of how dose affected pathogenesis was not disclosed [163]. While not explicitly testing dosage, in a neonatal mouse model of infection, increasing the age of infection from 6 to 9 to 12-day-old pups decreased mortality; this effect was associated with type I Interferon expression [124]. The effect of dosage on pathogenesis in the adult arthritis model of CHIKV infection does not appear to have been explicitly explored.

3.2 Results

3.2.1 Increasing the dose of CHIKV accelerates acute disease and clearance in the ipsilateral foot

We first examined the effect of CHIKV dose on swelling in the ipsilateral foot. C57BL/6 mice were inoculated with 10^2, 10^4, or 10^6 PFU of CHIKV-WT, CHIKV-5'-Cre, or CHIKV-3'-Cre and monitored for ipsilateral foot swelling. The 10^6 PFU dose of CHIKV-WT exhibited increased swelling at 1 and 2 dpi, but it exhibited the lowest swelling peaks at 3 and 7 dpi. Strikingly, the 10^2 PFU dose of CHIKV-WT exhibited the highest swelling peaks at 3 and 7 dpi and took the longest to resolve swelling (**Figure 3.1A**). Similar results were seen with varying doses of CHIKV-5'-Cre, although with lower overall swelling for the 10^2 PFU dose compared to CHIKV-WT (**Figure 3.1B**). With CHIKV-3'-Cre swelling, the first peak of swelling from 1 to 3 dpi was absent, as we have seen previously. For the second swelling peak for CHIKV-3'-Cre, the 10^6 PFU dose peaked at 5

and 6 dpi, the 10^4 PFU dose peaked at 7 dpi, and the 10^2 PFU dose peaked at 8 dpi (**Figure 3.1C**).

We next examined the effect of CHIKV dose on infectious viral titers in the ipsilateral ankle. C57BL/6 mice were inoculated with 10^2, 10^4, or 10^6 PFU of CHIKV-WT, CHIKV-5'-Cre, or CHIKV-3'-Cre, and the ipsilateral ankle was harvested at 1, 3, 5, and 7 dpi for viral quantification by plaque assay. For all three CHIKV viruses, increasing the viral dose corresponded with an increase in viral titers at 1 dpi (**Figure 3.2A-C**). At 3 and 5 dpi, the viral titers were not statistically different for CHIKV-WT or CHIKV-5'-Cre; however, the 10^6 PFU dose of CHIKV-3'-Cre was significantly decreased at 5 dpi compared to the other doses. Intriguingly, increasing the viral dose corresponded with a decrease in viral titers at 7 dpi for all three viruses.

These acute data thus suggest that increasing the viral dose initially increased swelling and infectious virus in the ipsilateral foot, but increasing the dose also corresponded with accelerated clearance of infectious virus.

3.2.2 Increasing the dose of CHIKV-WT increases dissemination and accelerates clearance at acute time points

We next sought to determine how viral dose affected dissemination outside of the ipsilateral foot and ankle. C57BL/6 mice were inoculated with 10^2, 10^4, or 10^6 PFU of CHIKV-WT, CHIKV-5'-Cre, or CHIKV-3'-Cre. Serum, the ipsilateral quadriceps muscle, the contralateral ankle, and the spleen were harvested at 1, 3, 5, and 7 dpi for viral quantification by plaque assay. At 1 dpi, increasing the viral dose corresponded with an increase in viremia for all three viruses (**Figures 3.3A-C**). A similar trend of higher doses correlating with higher viral titers was seen with infectious CHIKV-WT levels in the ipsilateral quad at 1 dpi (**Figure 3.3D**), the contralateral ankle at 1 and 3 dpi (**Figure 3.3G**), and the spleen at 1 dpi (**Figure 3.3J**). After 3 dpi, the reverse was true, and the 10^2 PFU dose of CHIKV-WT exhibited the highest levels of virus in the serum at 3

dpi (**Figure 3.3A**), in the ipsilateral quad at 3 dpi (**Figure 3.3D**), the contralateral ankle at 7 dpi (**Figure 3.3G**), and the spleen at 5 dpi (**Figure 3.3J**).

These trends were not as evident for disseminated tissues in mice infected with CHIKV-5'-Cre or CHIKV-3'-Cre (**Figures 3.3B-C, 3.3E-F, 3.3H-I, 3.3K-L**). Overall, dissemination of the CHIKV-Cre viruses was attenuated compared to CHIKV-WT (see **Figures S2.2C-F** for direct comparisons of disseminated viral titers for the 10^6 PFU dose of the three CHIKV viruses). Ultimately, increasing the dose of CHIKV-WT did increase early dissemination and clearance, but increasing the dose of the CHIKV-Cre viruses had less of a pronounced effect on dissemination.

3.2.3 Increasing the dose of CHIKV decreases chronic disease in the ipsilateral foot

We next sought to examine the effect of viral dose on chronic disease. C57BL/6 mice or tdTomato reporter mice were infected in the footpad with 10^2, 10^4, or 10^6 PFU of CHIKV-WT, CHIKV-5'-Cre, or CHIKV-3'-Cre. The ipsilateral ankles were harvested for viral RNA or histological analysis at 28 dpi. Increasing the dose of CHIKV-WT corresponded with a decrease in persistent viral RNA levels (**Figure 3.4A**), and a similar result was seen with CHIKV-5'-Cre (**Figure 3.4B**). However, increasing the dose of CHIKV-5'-Cre did not have a significant impact on the number of tdTomato$^+$ cells in the ipsilateral foot (**Figure 3.4C**). For CHIKV-3'-Cre, increasing the viral dose had no significant effect on persistent viral RNA levels (**Figure 3.4D**) or the number of tdTomato$^+$ cells in the ipsilateral foot (**Figure 3.4E**). While increasing the dose of CHIKV-WT or CHIKV-5'-Cre corresponded with a decrease in level of persistent viral RNA, these results did not extend to the number of tdTomato$^+$ cells.

3.2.4 Increasing the dose of CHIKV-Cre has no effect on the number of tdTomato$^+$ cells at dissemination sites

Since an increased dose of CHIKV-5'-Cre or CHIKV-3'-Cre was associated with increased early viremia and dissemination to the ipsilateral quad (**Figure 3.3B-C, 3.3E-F**), we next sought

to determine if increasing the CHIKV-Cre dose would increase the number of tdTomato$^+$ cells at sites of dissemination. tdTomato reporter mice were infected in the footpad with 10^2, 10^4, or 10^6 PFU of CHIKV-5'-Cre or CHIKV-3'-Cre, and the contralateral ankle and spleen were harvested for histological analysis at 28 dpi. Increasing the dose had no significant impact on the number of tdTomato$^+$ cells in the contralateral ankle or spleen for either virus (**Figure 3.5A-B**). The majority of samples had less than 10 tdTomato$^+$ cells per tissue section, which is much lower compared to the hundreds to thousands of tdTomato$^+$ cells observed in the ipsilateral ankle (**Figures 3.4C, 3.4E**). A handful of samples exhibited ~50-500 tdTomato$^+$ cells per section; however, this occurrence was rare and did not appear to exhibit any trends towards dose, virus, or tissue type.

3.3 Discussion

Overall, our preliminary data demonstrate that modulating the dosage of the CHIKV inoculum can have a significant impact on viral pathogenesis. Increasing the dose of CHIKV (WT, 5'-Cre, and 3'-Cre) was associated with an earlier peak of swelling and infectious titers in the ipsilateral ankle. Alterations in the swelling curves, especially the second swelling peak, could be due to alterations in the quantity or quality of cells infiltrating the tissue. Early dissemination was also increased at higher doses of CHIKV-WT. This initial early replication at higher doses was also associated with earlier resolution of swelling and faster clearance of infectious virus in the ipsilateral ankle and distal sites. This accelerated clearance phenotype could explain why levels of persistent viral RNA tended to be lower in the ipsilateral ankle with increasing initial inoculum.

These results do not necessarily contradict previous studies showing increased CHIKV dosage correlates with increased pathogenesis in macaques [56]. The mouse system exhibits fewer observable symptoms than macaques; rash, fever, and death does not occur in WT mice at the doses used in our studies. Acute and chronic histological damage was not analyzed by

H&E sections, so it is possible that higher doses exhibit increased acute and or chronic tissue damage to correlate with increased early swelling and infectious viral titers.

We hypothesize that this increased early replication and accelerated clearance phenotype at higher virus inoculum is associated with a more vigorous innate immune reaction. A higher initial dose leads to increased early replication, as has been demonstrated with *in vitro* cell culture. Furthermore, a higher MOI is also associated with higher expression of IFN-β, as shown in MEFs, human foreskin fibroblast (HFF), and lung fibroblast immortalized cell lines [58]. Our preliminary data *in vivo* also confirm that increasing the CHIKV inoculum corresponds with an increase in IFN-β RNA expression at 1 dpi (data not shown). Increased viremia has also been associated with increased levels of IFN-α in patient sera [58,125]. We predict that such increased expression of type I IFNs leads to an advanced immune response leading to accelerated clearance of virus at a higher initial inoculum. In order to further explore this hypothesis, a closer examination of the immune response is warranted in our system using varying viral doses. For instance, it would be critical to measure the expression of additional innate immune factors such as ISGs, cytokines, and chemokines as well as to analyze the numbers and types of immune cells that infiltrate into the ipsilateral ankle.

A similar hypothesis relating increased early replication, accelerated immune response, and advanced clearance has been proposed for other viruses, including adenovirus, infectious bronchitis virus, IAV, and human parainfluenza virus (HPIV) [164–166]. Optimization of the inoculum dose is of especial importance for vaccines. For instance, a higher initial vaccine inoculum generally leads to more robust stimulation of the immune system but might worsen side effects and permit for lower coverage of the population in the event of vaccine shortages.

This association between CHIKV inoculum and replication kinetics could have interesting implications for human CHIKV disease. Previous studies using human serum samples have demonstrated an association between increased likelihood of chronic CHIKV with elevated acute

viremia levels [54,89]. It has also been shown that feeding *A. albopictus* mosquitos with increasing amounts of CHIKV resulted in increased dissemination to the salivary glands [167]. Furthermore, the minimum infectious dose from a blood meal of a viremic individual was estimated to ranges from approximately 10^4 to 10^5 PFU/mL for chikungunya virus in *A. aegypti* and *A. albopictus* mosquitoes [168]. However, what remains unknown is how the initial inoculum dosage from a mosquito correlates with viremia and thus acute and chronic disease in humans.

Based on our results, it could be possible that mosquitos that inject a lower amount of virus in humans could correlate with prolonged viremia, delayed clearance, and more severe chronic disease. Such a trend if demonstrated could even be an evolutionary adaptation for arboviruses overall; perhaps mosquitos only need to transmit a low dose of virus in order to cause a high enough level of viremia in humans to enable transmission to a new vector. While still speculative, our results should at least caution researchers that increasing the dose of a virus such as CHIKV does not always correlate with increased chronic disease and highlights the complex interplay between host and virus.

Overall, these data highlight the significant impact that viral inoculum can have on the pathogenesis of CHIKV in mice. For Chapter 2, we decided that a high dose of CHIKV-3'-Cre was optimal for study of tdTomato$^+$ cells in the ipsilateral ankle. However, using a lower dose of CHIKV-WT could be optimal for other studies of chronic CHIKV pathogenesis where maximizing the levels of persistent viral RNA is desired. Whether such results also apply to humans remains to be seen, though in practice it would be difficult to determine without being able to measure the exact dose of mosquito bites.

3.4 Materials and Methods

3.4.1 Viruses

The following viruses were used in these studies: CHIKV-WT, CHIKV-5'-Cre, and CHIKV-3'-Cre. Viruses were cloned and produced as described in Section 2.5.1.

3.4.2 Mice

The following strains of mice were obtained from the Jackson Laboratory: C57BL/6 (JAX Stock No: 000664; C57BL/6J) and tdTomato reporter mice (JAX Stock No: 007914; B6.Cg-*Gt(ROSA)*$^{26Sortm14(CAG-tdTomato)Hze}$/J). Mice were maintained as described in Section 2.5.2.

3.4.3 Viral Burden Studies in Animals

Four-week old C57BL/6 mice were inoculated with 10^2, 10^4, or 10^6 PFU of virus. Virus dilutions were made using a two-step 1:100 dilution series. Viral burden studies were completed as described in Section 2.5.6.

3.4.4 Quantitative Real-Time PCR

RNA was isolated from tissues E1 and nsP1 levels quantified as described in Section 2.5.7.

3.4.5 Histology Studies

Four-week old tdTomato mice were infected and frozen section histology samples harvested as described in Section 2.5.8.

3.4.6 Statistical Analysis

All data were analyzed using the Prism software, version 7 (GraphPad), as detailed in the figure captions. The following statistical tests were used: ordinary one-way analysis of variance

(ANOVA), ordinary two-way ANOVA, and two-way repeated-measures ANOVA, all with Tukey's post-test as a multiple comparisons test. All error bars indicate standard error of the mean (SEM); if error bars are not visible, then they are shorter than the height of the symbol. Asterisks indicate statistical significance, with only relevant comparisons shown (*, $P < 0.05$; **, $P < 0.01$; ***, $P < 0.001$; ****, $P < 0.0001$).

3.5 Figures

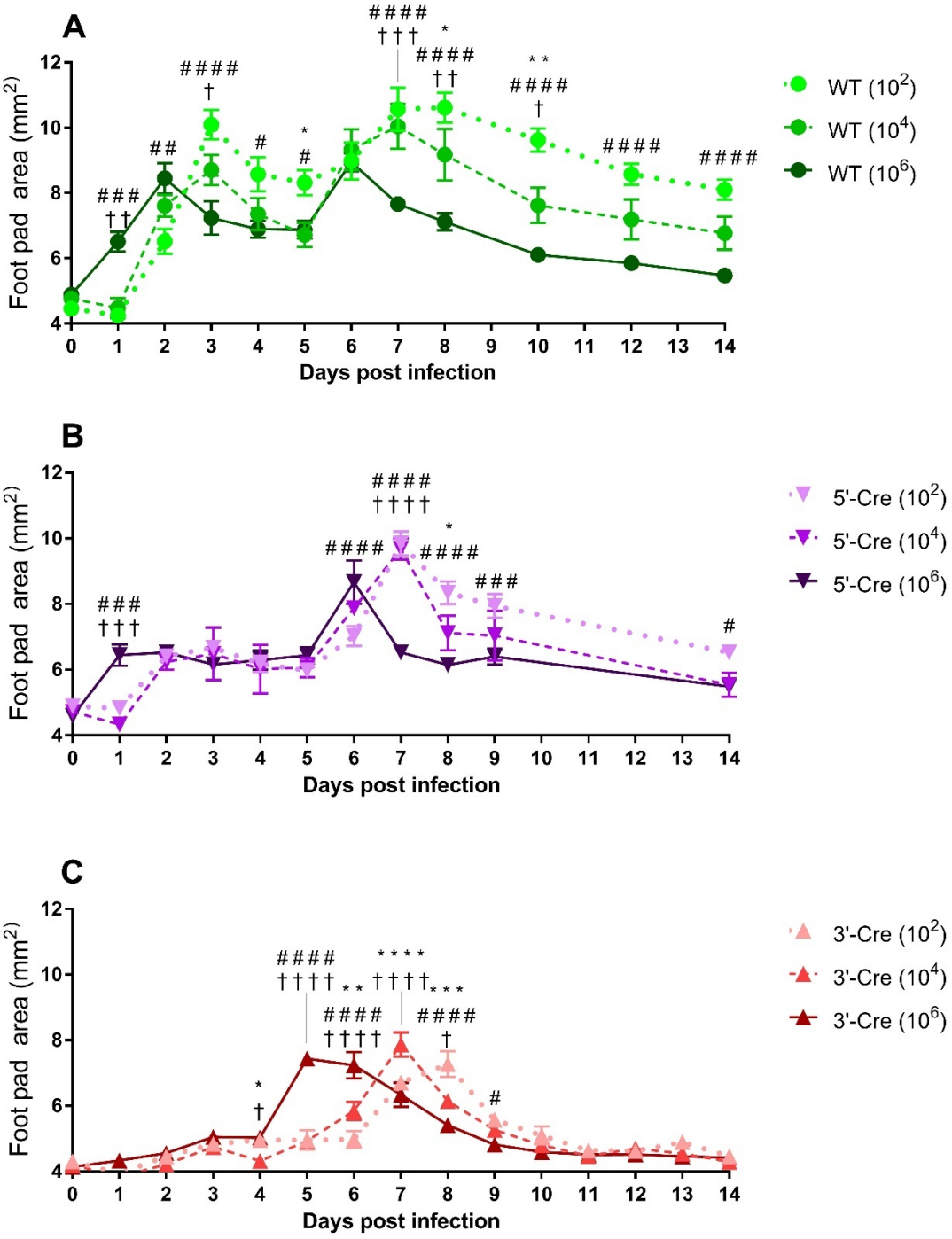

Figure 3.1: Ipsilateral foot swelling at varying CHIKV doses

C57BL/6 mice were infected in the footpad with 10^2, 10^4, or 10^6 PFU of **(A)** CHIKV-WT (WT, green circles), **(B)** CHIKV-5'-Cre (5'-Cre, purple inverted triangles), or **(C)** CHIKV-3'-Cre (3'-Cre, red triangles), and ipsilateral foot swelling was measured. Data are representative of two independent experiments and represent 3-8 mice per virus and dose. Data were analyzed with a two-way repeated measures ANOVA with Tukey's post-test. Error bars indicating SEM. If error bars are not visible, then they are shorter than the height of the data symbol. The following symbols indicate statistical significance, with asterisks (*) indicating 10^2 vs. 10^4, pound signs ($^{\#}$) indicating 10^2 vs. 10^6, and dagger signs (†) indicating 10^4 vs. 10^6 (*, $^{\#}$, †, $P < 0.05$; **, $^{\#\#}$, ††, $P < 0.01$; ***, $^{\#\#\#}$, †††, $P < 0.001$; ****, $^{\#\#\#\#}$, ††††, $P < 0.0001$).

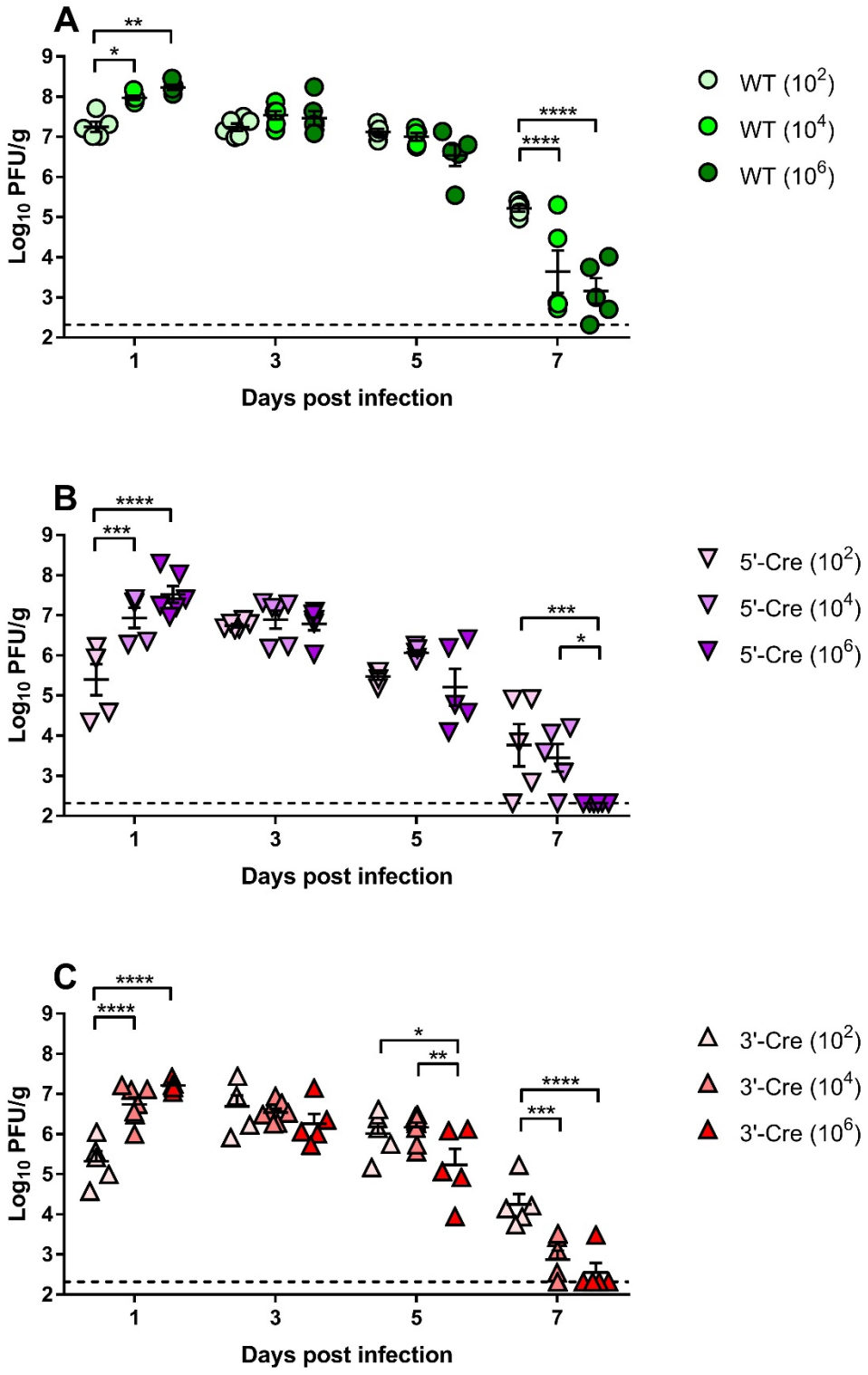

Figure 3.2: Viral titers in the ipsilateral ankle at varying CHIKV doses

C57BL/6 mice were infected in the footpad with 10^2, 10^4, or 10^6 PFU of **(A)** CHIKV-WT (WT, green circles), **(B)** CHIKV-5'-Cre (5'-Cre, purple inverted triangles), or **(C)** CHIKV-3'-Cre (3'-Cre, red

triangles). The level of infectious virus in the ipsilateral foot and ankle during acute infection were measured by plaque assay and normalized to gram of tissue. The data for the 10^6 PFU dose for each virus was also shown in the corresponding graph in Figure 2.2B and Figure S2.2B. Each time point for each virus represents 5-6 mice and were pooled from at least 2 independent experiments. The dashed line represents limit of detection, and data were log-transformed prior to analysis. Data were statistically analyzed with an ordinary two-way ANOVA with Tukey's post-test. All error bars indicate SEM. Asterisks indicate statistical significance (*, $P < 0.05$; **, $P < 0.01$; ***, $P < 0.001$; ****, $P < 0.0001$).

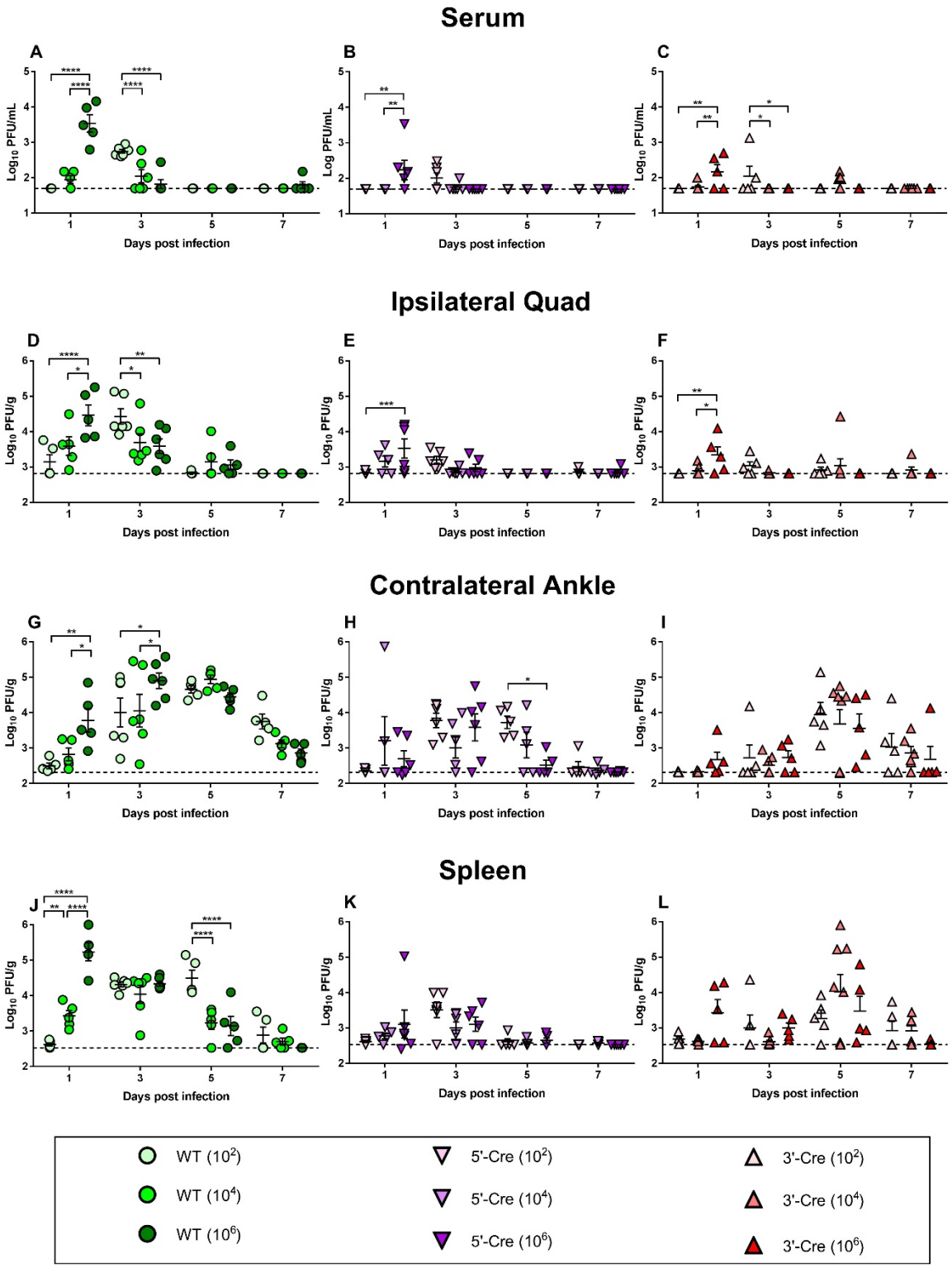

Figure 3.3: Viral titers in disseminated tissues at varying CHIKV doses

C57BL/6 mice were infected in the footpad with 10^2, 10^4, or 10^6 PFU of **(A, D, G, J)** CHIKV-WT (WT, green circles), **(B, E, H, K)** CHIKV-5'-Cre (5'-Cre, purple inverted triangles), or **(C, F, I, L)** CHIKV-3'-Cre (3'-Cre, red triangles). The level of infectious virus in the serum (A-C), ipsilateral quadriceps muscle (D-F), contralateral ankle (G-I), and spleen (J-L) during acute infection was measured by plaque assay and normalized to gram of tissue. Each time point for each virus represents 5-6 mice and were pooled from at least 2 independent experiments. The data for the 10^6 PFU dose for each virus and tissue was also shown in the corresponding graph in Figure S2.2C-F. The dashed line represents limit of detection, and data were log-transformed prior to analysis. Data were statistically analyzed with an ordinary two-way ANOVA with Tukey's post-test. All error bars indicate SEM. Asterisks indicate statistical significance (*, $P < 0.05$; **, $P < 0.01$; ***, $P < 0.001$; ****, $P < 0.0001$).

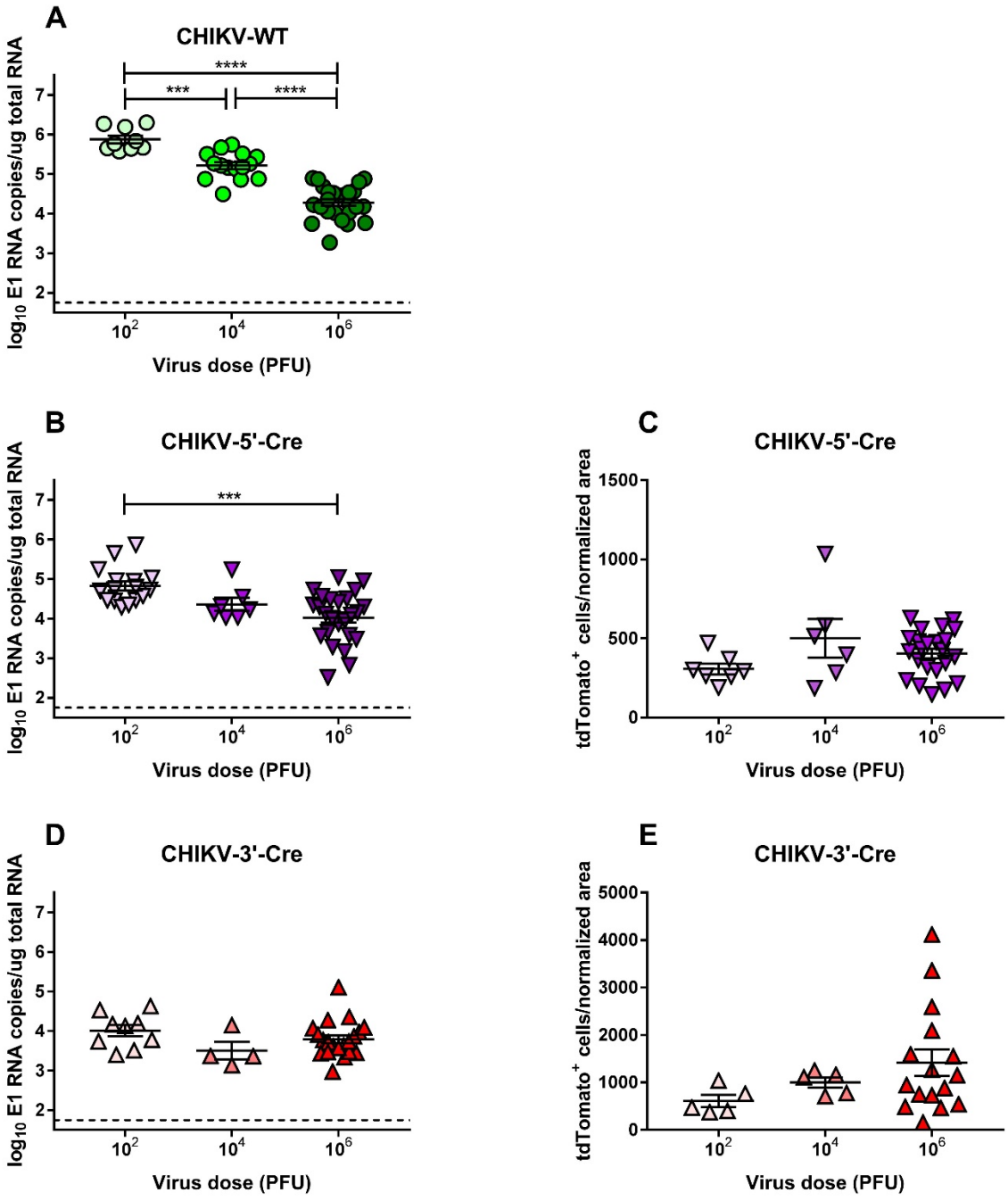

Figure 3.4: Viral RNA levels and tdTomato$^+$ cells in the ipsilateral ankle at varying CHIKV doses

C57BL/6 mice or tdTomato reporter mice were infected in the footpad with 10^2, 10^4, or 10^6 PFU of **(A)** CHIKV-WT (WT, green circles), **(B-C)** CHIKV-5'-Cre (5'-Cre, purple inverted triangles), or **(D-E)** CHIKV-3'-Cre (3'-Cre, red triangles). Ipsilateral feet and ankles were taken for CHIKV E1

RNA analysis **(A, B, D)** or for tdTomato frozen section histological analysis **(C, E)** at 28 dpi. The data for the 10^6 PFU dose for each virus was also shown in the corresponding graph in Figure 2.3C, Figure 2.4B, Figure S2.4C, and Figure S2.5B. The dashed line for **A**, **B**, and **D** represents limit of detection, and data in **A**, **B**, and **D** were log-transformed prior to analysis. Data were statistically analyzed with an ordinary one-way ANOVA using Tukey's post-test. All error bars indicate SEM. Asterisks indicate statistical significance (*, $P < 0.05$; **, $P < 0.01$; ***, $P < 0.001$; ****, $P < 0.0001$).

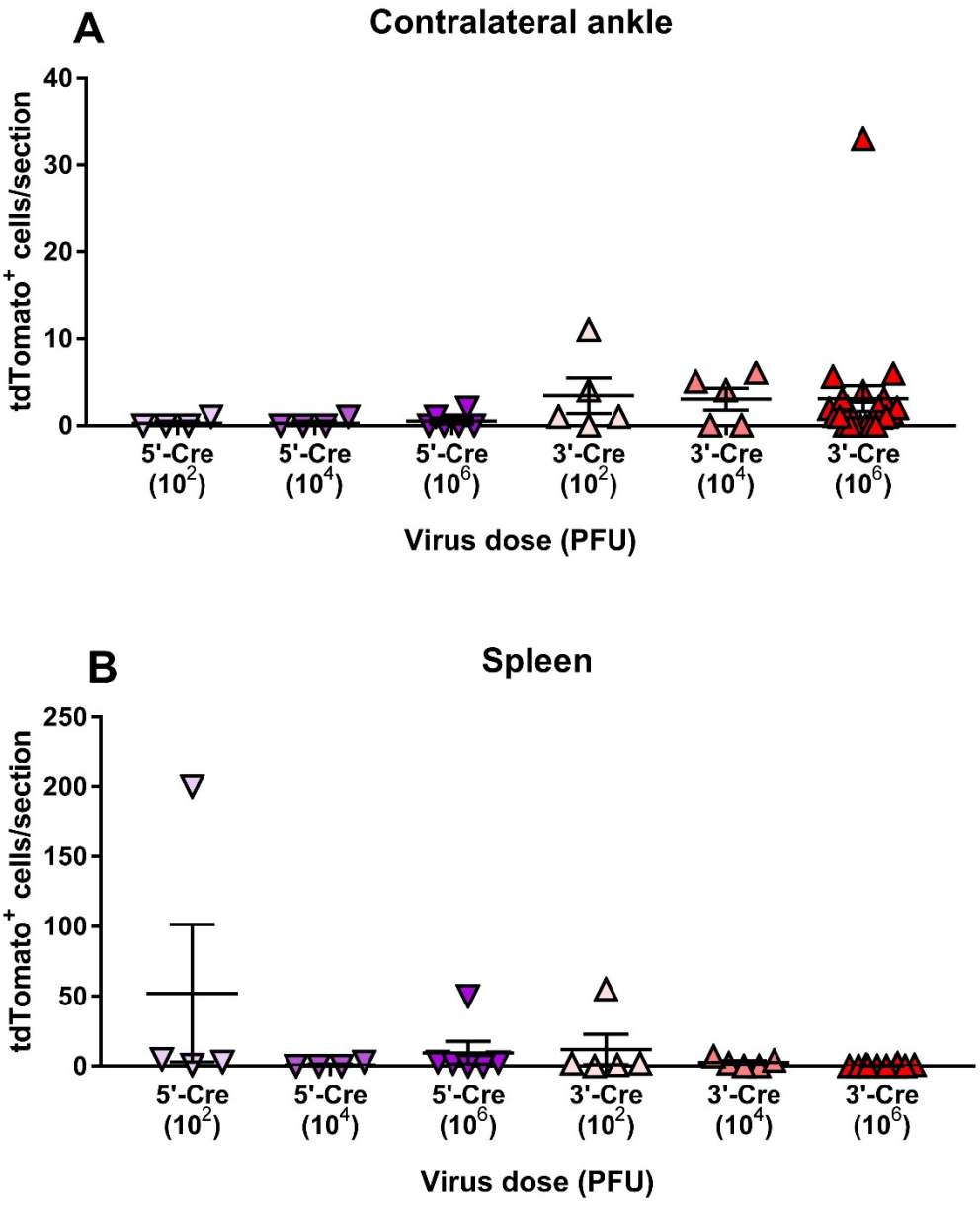

Figure 3.5: tdTomato$^+$ cells in disseminated tissues at varying CHIKV-Cre doses

tdTomato reporter mice were infected in the footpad with 10^2, 10^4, or 10^6 PFU of CHIKV-5'-Cre (5'-Cre, purple inverted triangles) or CHIKV-3'-Cre (3'-Cre, red triangles). **(A)** Contralateral feet/ankles and **(B)** spleens were taken for tdTomato frozen section histological analysis at 28 dpi. Data were statistically analyzed with an ordinary one-way ANOVA with Tukey's post-test. All error bars indicate SEM.

Chapter 4:

Summary and Future Directions

4.1 Summary

CHIKV is an arthritogenic alphavirus that causes chronic joint and muscle pain of unknown etiology in a significant subset of patients. In Chapter 2, we introduced a CHIKV-Cre reporter mouse system to study the chronic pathogenesis of CHIKV. We showed that these CHIKV-Cre viruses recapitulate many aspects of acute and chronic disease caused by CHIKV-WT. Using tdTomato reporter mice, we also showed that the majority of tdTomato$^+$ cells at chronic time points were myofibers and fibroblasts, and that anti-Mxra8 treatment preferentially reduced the fibroblast population. In Chapter 3, we experimented with varying doses for our CHIKV-Cre system. A higher dose of CHIKV was associated with increased early replication and dissemination, but it also correlated with earlier clearance of the virus and lower persistent RNA levels.

A more detailed analysis of the implications of these results can be found in the Discussion Sections for Chapters 2 and 3 (Sections 2.4 and 3.3). What follows are some additional, more speculative or preliminary interpretations of data from the CHIKV-Cre system. Also highlighted are various future experiments and uses of the CHIKV-Cre system, ranging from single-cell sequencing and electron microscopy to human studies and clinical applications.

4.1.1 Comparison of CHIKV-5'-Cre and CHIKV-3'-Cre

For our studies, we engineered two versions of CHIKV that express Cre recombinase: CHIKV-5'-Cre and CHIKV-3'-Cre (**Figure S2.1A**). For our more detailed studies, we used CHIKV-3'-Cre rather than CHIKV-5'-Cre, as certain aspects of CHIKV-3'-Cre infection more closely resembled CHIKV-WT infection than CHIKV-5'-Cre. For example, whereas the CHIKV-3'-Cre E1:nsP1 curve was very similar to CHIKV-WT (**Figure 2.3E**), the CHIKV-5'-Cre E1:nsP1 curve was dramatically different during the first seven days of infection (**Figure S2.4D**). This difference is likely due to the fact that in CHIKV-5'-Cre the E1 gene is under the replicative influence of two subgenomic promoters, while the internal genomic structure of CHIKV-3'-Cre is identical to

CHIKV-WT (**Figure S2.1A**). In CHIKV-3'-Cre, the Cre gene is downstream of two subgenomic promoters, which could explain why CHIKV-3'-Cre infection resulted in a higher Cre to nsP1 ratio compared to CHIKV-5'-Cre (**Figure S2.4E**). This increased Cre expression could also explain why CHIKV-3'-Cre infection produced significantly more tdTomato$^+$ cells than CHIKV-5'-Cre *in vitro* (**Figure S2.1B**) as well as *in vivo* (**Figure S2.5B-D**).

In addition to the CHIKV-5'-Cre and CHIKV-3'-Cre constructs, it could also be possible to introduce Cre recombinase into another locus in the CHIKV genome, such as the nsP3 gene as has been done for mCherry with minimal attenuation *in vitro* [137]. It is possible that a CHIKV-nsP3-Cre virus would produce even less Cre recombinase without the influence of the subgenomic promoter and be less sensitive in marking tdTomato cells. It is also possible that CHIKV-nsP3-Cre would be more stable in terms of its expression and mark more cells than CHIKV-3'-Cre.

4.1.2 Time course kinetics of tdTomato$^+$ cells

We conducted an extensive time course to examine the overall levels of tdTomato$^+$ cells in the ipsilateral foot from 1 to 112 dpi for both CHIKV-3'-Cre (**Figure 2.4C**) and CHIKV-5'-Cre (**Figure S2.5D**). Intriguingly, substantial numbers of tdTomato$^+$ cells are not apparent until 7-10 dpi; however, the peak of infectious titers in the ipsilateral ankle occurs at 1 dpi (**Figures 2.2B, S2.2B**). Our preliminary *in vitro* infections with tdTomato MEFs have shown that it takes at most 18 hours for detectable levels of tdTomato protein to be produced following infection (data not shown); however, we have not determined if this tdTomato expression time differs *in vivo* or in different cell types. It is thus possible that the majority of cells infected during the early acute stage of infection (1-5 dpi) lyse and do not persist as tdTomato$^+$ cells. There are much lower levels of infectious virus during the later stage of acute infection (5-10 dpi), but perhaps cells infected at

this stage of infection persist as tdTomato$^+$ cells. However, as discussed previously (Section 2.4), our system does not enable us to determine when a tdTomato$^+$ cell was infected.

After 7-10 dpi, the number of tdTomato$^+$ cells remains relatively constant up to 112 dpi. There are some variations in the mean number of tdTomato$^+$ cells at chronic timepoints, such as the gradual increase between 7 and 112 dpi. Indeed, some of the differences reached statistical significance (**Figure 4.1**). Such differences could be due to a low number of samples at some time points. However, such fluctuations could be due to the turnover of tdTomato$^+$ cells or potentially a low level of infectious virus.

4.1.3 CHIKV RNA copy number per tdTomato$^+$ cell

In addition to a tdTomato$^+$ cell time course, we also conducted a viral RNA time course using the same time points (**Figures 2.3D, S2.4C**). Combining such data enables us to preliminarily calculate the CHIKV RNA copy number per tdTomato$^+$ cell for both CHIKV-5'-Cre and CHIKV-3'-Cre (**Figure 4.2**). Interestingly, the RNA copy number per tdTomato$^+$ cell was higher for CHIKV-5'-Cre compared to CHIKV-3'-Cre; this trend is likely due to the fact that CHIKV-5'-Cre had slightly higher levels of viral RNA and significantly lower levels of tdTomato$^+$ cells at all time points.

From 1 to 10 dpi, both viruses exhibited a steep decrease in viral RNAs per tdTomato$^+$ cell. CHIKV-5'-Cre decreased from a high of 2.1 x 10^{11} RNAs/cell at 1 dpi to 8.9 x 10^3 RNAs/cell at 10 dpi, a ~7.3 $\log_{10}$ decrease. Similarly, CHIKV-3'-Cre decreased from a high of 1.4 x 10^{10} RNAs/cell at 1 dpi to 5.2 x 10^2 RNAs/cell at 10 dpi, a ~7.4 $\log_{10}$ decrease. This decrease could correlate with the majority of infected cells dying, much of the virus being contained by the immune response, and or a shift from active viral replication to little or no replication.

It is important to note that these calculations represent a mean of viral RNAs per tdTomato$^+$ cell. The viral RNA may not be evenly distributed between tdTomato$^+$ cells, and some

viral RNA may be present in tdTomato$^-$ cells. However, these results do highlight the possibility that at chronic time points tdTomato$^+$ cells likely harbor a low number of RNA copies, an average of ~300 copies per cell from 28 to 112 dpi for CHIKV-3'-Cre. Such a concentration is likely below the detection limit of RNA ISH for formalin-fixed tissue samples and could explain why detection of CHIKV RNA$^+$ cells is so rare during chronic time points.

4.1.4 Cell type distribution of chronic tdTomato$^+$ cell population

It is intriguing to consider why skeletal myofibers and fibroblasts are the predominant cell type to survive acute CHIKV infection when so many cell types are known to be permissive to CHIKV. Perhaps, myofibers and fibroblasts are the most permissive cell types to CHIKV infection, as suggested by *in vitro* growth curves and at the histological level by our ISH staining (**Figure S2.3A**); thus, even if similar percentages of all infected cell types die, many more myofibers and fibroblasts survive infection since a high number were initially infected. Another possibility is that these cells are somehow immune privileged and more resistant to programmed cell death pathways normally triggered during an infection. Related to this hypothesis is the idea that the virus or viral RNA may persist in a protected niche within these cells but is still able to induce chronic inflammatory pathways. As described in in the next section, single-cell RNA-seq and electron microscopy could help tease apart these possibilities.

4.2 Future Directions

Chapter 2 introduced our CHIKV-Cre reporter mouse system and its application to studying chronic pathogenesis and anti-Mxra8 treatment. Many questions remain about chronic CHIKV pathogenesis, such as the location and status of persistent viral RNA, and our system could provide valuable insight. For example, single cell or nucleus RNA-seq could help determine whether persistent viral RNA is concentrated in tdTomato$^+$ cells, the nature of this persistent viral RNA, and whether the host transcriptome of tdTomato$^+$ cells is altered. Electron microscopy could

help determine the subcellular location of persistent viral RNA within tdTomato$^+$ cells. CHIKV-Cre infection of Diphtheria toxin receptor (DTR) mice could allow for depletion of DTR$^+$ cells and exploration of how these cells contribute to chronic pathogenesis. Additional applications of our CHIKV-Cre system include chronic experiments using tdTomato MEFs, alternative routes of virus inoculation, applications to other genotypes and virus strains, and applications to clinical research.

4.2.1 Applications of the *In Vivo* Reporter System

Many questions remain about chronic CHIKV pathogenesis, such as the location and status of persistent viral RNA, and our system could provide valuable insight. For instance, is viral RNA in fact concentrated in tdTomato$^+$ cells? What is the state of this persistent viral RNA? Is it intact or mutated? Replicating or quiescent? Furthermore, is the transcriptome of tdTomato$^+$ cells altered, and how do these marked cells contribute to chronic CHIKV pathogenesis?

Is viral RNA present in tdTomato$^+$ cells?

Our work with anti-Mxra8 treatment showed a positive correlation between the levels of chronic viral RNA and the number of tdTomato$^+$ cells (**Figure 2.6**). However, further work is needed to determine the exact location of the persistent viral RNA. Currently IFA and ISH are not sensitive enough to consistently detect viral components in the tissues of WT mice at chronic time points. In the Influenza system, tdTomato$^+$ cells were sorted out of single cell lung homogenates, allowing for identification of the cell type that was marked by the IAV-Cre virus and transcriptional analysis of those cells [139]. A similar analysis in our system has proven to be more difficult, especially for myofibers and muscle fibroblasts. We have attempted isolation of tdTomato$^+$ cells through flow cytometry or laser capture microdissection, but we have thus far been unsuccessful.

Single cell RNA sequencing (RNA-seq) represents a powerful new tool that could help determine whether viral RNA is present in tdTomato RNA$^+$ cells, potentially acting as a dsRNA

trigger for chronic inflammation. tdTomato^{+} fibroblasts could be detected through either single-cell or single-nucleus RNA-seq, but analysis of tdTomato^{+} myofibers would be limited to single-nucleus RNA-seq due to their large size and fragility [169–171]. Single-nucleus RNA-seq is a less powerful tool in our system than single-cell RNA-seq as CHIKV RNA is likely present in the cytoplasm and not the nucleus; thus, single-nucleus RNA-seq would be unable to characterize CHIKV RNA outside the nucleus in tdTomato^{+} cells. Therefore, our analysis of single-cell RNA-seq may be restricted to the dermal and muscle fibroblasts. Importantly, a BSL3 10x Genomics machine will soon be available to use for single-cell or single-nucleus RNA-seq, thus avoiding the need to fix samples.

Is the transcriptome of tdTomato^{+} cells altered?

If single-cell or single-nucleus RNA-seq is successful, it could help answer many questions about chronic CHIKV pathogenesis, as was done previously for Influenza using IAV-Cre [138,139]. Such results could help decipher how CHIKV infection manipulates the transcriptome of individual infected cells. Previous studies have conducted whole tissue RNAseq or proteomic analysis on CHIKV-infected tissues or cells, demonstrating an overall upregulation of inflammatory markers [37,160,161]. Our system could demonstrate whether these inflammatory markers are specifically upregulated in tdTomato^{+} cells, and thus whether CHIKV infection results in a population of pathogenically altered cells. It is also possible that CHIKV infection induces cellular or viral programs that could abort productive replication, potentially allowing the viral RNA to persist long-term.

What is the state of the persistent viral RNA?

Sequencing of persistent CHIKV RNA has thus far only been reported in RAG1$^{-/-}$ mice, which lack an adaptive immune response and fail to clear infectious virus from the serum, joints, and other tissues. Two groups have deep sequenced viral RNA from RAG1$^{-/-}$ mouse serum, brain,

and kidney samples at 28, 42, and 100 dpi. Sequence analyses revealed a complete genome with relatively few and minor fixed mutations [117,151]; they did not indicate the presence of negative strand genomes or an increased ratio of structural to non-structural gene transcription, both of which would be indicative of active viral replication. Presumably, deep sequencing of persistent viral RNA has not yet been reported in WT mice as the level in whole tissue homogenates would be too low to detect. Assuming persistent viral RNA can be found in tdTomato$^+$ cells, single cell RNA-seq could offer increased sensitivity compared to whole tissue sequencing and allow for characterization of the viral RNA in immunocompetent mice. Such data could help reveal the replication status of the viral RNA through the presence of negative strands or subgenomes, whether the entire viral genome persists, or the presence of any dominant mutations.

In addition to single cell RNA-seq, our CHIKV-Cre system could also be applied to sensitive microscopy techniques. In Chapter 2, we imaged tdTomato$^+$ cells in ankle tissues using high-power fluorescence microscopy (**Figure 2.5**). Attempts to co-stain for CHIKV antigen at chronic time points were unsuccessful (data not shown), and we have not yet attempted to co-stain with antibody against dsRNA, which has proven useful for detecting other RNA viruses [172]. Higher magnification studies of tdTomato$^+$ cells could be performed using transmission electron microscopy (TEM). TEM has previously been used to detect CHIKV at acute time points [42], but detection of viral particles at chronic time points has not been reported. Fluorescence of the tdTomato protein would not be visible during TEM, but the protein could be labeled using anti-tdTomato immunogold antibodies. tdTomato$^+$ cells from *in vitro* or *in vivo* samples could be examined for the presence of viral particles or potentially co-stained with anti-CHIKV or anti-dsRNA antibodies with an alternatively-sized immunogold label. Using TEM, we could potentially identify the specific subcellular localizations of the virus or viral RNA during chronic stages of the infection, potentially explaining how it can persist for so long after infection.

Do cells marked by CHIKV-Cre play a role in chronic pathogenesis?

In order to probe further into chronic CHIKV pathogenesis, we could use our CHIKV-Cre viruses in Cre-responsive mice other than tdTomato reporter mice. For example, mice that express the chimpanzee diphtheria toxin receptor (DTR, also called heparin binding EGF like growth factor, HBEGF) upon Cre-induced removal of a stop cassette (JAX Stock No:007900 C57BL/6-Gt(ROSA) 26Sor$^{tm1(HBEGG)Awai}$/J) can be used to deplete DTR^{+} cells with diphtheria toxin (DT) at a desired time point [173]. For example, DT could be administered after infectious virus is cleared (10-14 dpi), and we could examine whether this depletion has an effect on a chronic time point (28 dpi). For instance, depletion of DTR^{+} cells could result in a decrease in the level of persistent viral RNA, a decrease in chronic myositis and synovitis, and an improvement in the whole-tissue host transcriptome. Such results would indicate that cells marked by CHIKV-Cre play a critical role in chronic CHIKV pathogenesis.

We have performed a variety of preliminary experiments involving DTR mice injected with CHIKV-WT, CHIKV-3'-Cre, or CHIKV-5'-Cre and treated with DT. However, we were unable to determine a virus dose or DT dosing schedule that resulted in a decrease in persistent viral RNA levels (data not shown). We were unable to determine if CHIKV-3'-Cre or CHIKV-5'-Cre infection caused an increase in DTR^{+} cells compared to CHIKV-WT, as we see in tdTomato reporter mice. We unsuccessfully attempted IFA to co-stain for DTR protein and RT-qPCR to detect DTR RNA (data not shown). It is possible that DTR^{+} cells were produced and that DT injection did deplete them, but the persistent viral RNA levels did not correspondingly decrease. In this case, it is possible that the DTR^{+} cells do not contain viral RNA. It is also possible that viral RNA is released from the depleted DTR^{+} cells but then persists in the tissue or is taken up by other cells. Another issue is that the chronic model currently in use is not robust histologically (chronic inflammation is mild and not seen in every mouse), so it remains difficult to assess the impact of DTR^{+} cells depletion on histopathology.

Additional studies could also be performed with tdTomato reporter or DTR depletion mice that express tdTomato or DTR under a tissue-specific promoter, as opposed to the constitutive Rosa locus. For example, mesenchyme-specific or myofiber-specific promoters could be used to determine the specific contribution of these cell types to chronic pathogenesis.

4.2.2 Applications of the *In Vitro* Reporter System

In Chapter 2, we showed that tdTomato$^+$ MEFs can be detected 48 hpi with CHIKV-3'-Cre or CHIKV-5'-Cre (**Figures 2.1B-C, S2.1B-C**). Of note, in preliminary experiments, tdTomato$^+$ MEFs could be detected at 28 dpi after infection with CHIKV-5'-Cre, a chronic time point (data not shown). Fibroblasts represented a large subset of the tdTomato$^+$ cell population, thus tdTomato MEFs could be a viable *in vitro* system to begin to test our hypotheses about chronic pathogenesis. A major question would be to determine if viral components (antigen or RNA) are specifically enriched in tdTomato$^+$ MEFs compared to tdTomato$^-$ MEFs. Assays such as IHC, IFA, ISH, and RNA-seq could be more sensitive in an *in vitro* setting, without the high background that is often found in animal tissue samples. Additional primary cells from tdTomato mice could also be used such as synovial fibroblasts or myoblasts; however, some of these primary cells may be unable to survive in culture for several weeks.

4.2.3 Alternative inoculation techniques

Our CHIKV-Cre viruses exhibited low levels of dissemination, as demonstrated by attenuated viral titers and chronic tdTomato$^+$ cells in the contralateral ankle and spleen (**Figure 3.3, 3.5**). We sought to determine whether using alternative sites for inoculation could increase the number of tdTomato$^+$ cells in disseminated tissues.

In a preliminary experiment, tdTomato reporter mice were inoculated normally (subcutaneously in the footpad) or via intraperitoneal (IP), intravenous (IV), flank, or retro orbital (RO) routes with 10^6 PFU of CHIKV-5'-Cre (see Section 4.3.4 of the Methods for more details).

The feet/ankles and spleen were harvested for histological analysis at 7 and 14 dpi. These alternative inoculation sites did not increase dissemination to the joints, as few tdTomato$^+$ cells were observed in either ankle (data not shown). However, RO injection did correspond with an increased number of tdTomato$^+$ cells in the spleen, especially at 14 dpi (**Figure 4.3A**). It is unclear why IV tail vein injections did not produce similar levels of tdTomato$^+$ cells in the spleen to RO injections since both involve direct injection of virus into the blood.

Such results with the RO route of infection are somewhat surprising. In a macaque model of CHIKV infection, intravenous (IV) or intradermal (ID) infection did not appear to have a significant effect on viremia, fever, or blood cell counts [56]; however, viral titers in disseminated tissues were not explored. RO injection may be a better model of viremia than IV injection. It would be interesting to see if acute viral titers and persistent viral RNA were correspondingly increased in the spleen using RO inoculation. While RO injections could be helpful for study of chronic pathogenesis in the spleen, it is likely not as applicable a model of infection to humans as subcutaneous inoculation that mimics a mosquito bite.

In addition to the above mentioned alternative inoculation sites, we also experimented with calf injections of virus. When tdTomato reporter mice were inoculated normally (subcutaneously in the footpad), the tdTomato$^+$ cells were concentrated in the foot and do not extend past the ankle into the calf muscle (**Figure 2.4A**). However, the foot muscles can be difficult to micro-dissect, so we sought to determine if tdTomato$^+$ cells could be found in the calf muscles using an alternative inoculation site. In a preliminary experiment, tdTomato reporter mice were inoculated subcutaneously above the gastrocnemius muscle with 10^6 PFU of CHIKV-3'-Cre, and the calf muscles were dissected for histological analysis at 28 dpi. A plethora of tdTomato$^+$ cells were observed in the calf muscle (**Figure 4.3B**). It appears by morphological appearance that the majority of tdTomato$^+$ cells in the calf muscle were myofibers and few cells were fibroblasts; however, this observation has not yet been confirmed by immunofluorescence analysis.

Calf injections could be helpful for applications of the CHIKV-Cre system, such as RNA-seq, that necessitate taking larger muscle samples than is possible with footpad infections or that are sensitive to decalcification. However, the muscle population of tdTomato$^+$ cells could be different between subcutaneous footpad and calf injections, so future experimentation is warranted.

4.2.4 Applications to Other Genotypes and Virus Strains

In Chapter 2, we used our CHIKV-3'-Cre and tdTomato system to test how treatment with anti-Mxra8 mAbs affected the number and type of tdTomato$^+$ cells at a chronic time point (**Figure 2.6**). We have also conducted preliminary studies with other mAb treatments. In one preliminary study we tested how CHIKV neutralizing antibodies (CHK-152, CHK-166) affected the abundance of tdTomato$^+$ cells [72,75]. When administered at 3 dpi, treatment with CHK-152 and CHK-166 did decrease the swelling in the ipsilateral foot at 6 dpi (**Figure 4.3A**). However, there was no difference in the number of tdTomato$^+$ cells in the ipsilateral or contralateral ankles at 28 dpi between CHIKV-neutralizing antibody and the isotype control (**Figure 4.3B**). Such a result is not entirely surprising as a similar treatment with CHK-152 and CHK-166 at 3 dpi using CHIKV-WT and C57BL/6 mice did not affect the levels of persistent viral RNA in the ipsilateral ankle (data not shown). It is possible that treatment with CHIKV neutralizing antibodies prior to infection would both reduce the number of tdTomato$^+$ cells and the level of persistent viral RNA at 28 dpi.

We have also conducted tests using mAbs against IFN-α or IFN-β [174,175]. Treatment with a pan anti-IFN-α mAb increased both the number of tdTomato$^+$ cells and the level of persistent viral RNA in the contralateral ankle at 28 dpi compared to an anti-IFN-β mAb or isotype control (data not shown). Efforts are underway with IFA co-staining to explore whether the tdTomato$^+$ cells in the contralateral ankles of anti-IFN-α treated mice show a different cellular tropism than the tdTomato$^+$ cells in the ipsilateral ankle. Taken together with the results of the

anti-Mxra8 treatment, these results demonstrate a correlative relationship between the number of tdTomato$^+$ cells in a tissue and the level of persistent RNA, suggesting that some viral RNA is indeed found within the tdTomato$^+$ cells. Our system could be thus applied to other host genotypes through mAb treatment. In the event that a mAb is not available against a specific target, tdTomato reporter mice could be bred to a knockout mouse or other mouse genotype of interest (assuming that the gene of interest is not on murine chromosome 6, the location of the tdTomato reporter).

In addition to studying different host genotypes, our system could also be applied to other viral genotypes. CHIKV-Cre viruses could be constructed from other CHIKV strains or mutant viruses to further dissect how the viral genetics contribute to tropism and chronic pathogenesis [66]. For example, one study demonstrated that a virulent IOL CHIKV strain isolated in 2006 from the La Réunion Island outbreak (LR2006-OPY1) can infiltrate and grow within skeletal muscle fibers while a pre-epidemic strain cannot [57]. It would be intriguing to generate a Cre virus of the pre-epidemic CHIKV strain to further explore the tropism differences between these two strains.

4.2.5 Implications for Clinical Studies

The detection of CHIKV antigen or RNA in patient samples from chronic time points has previously been rare. One study reported detection of CHIKV RNA and antigen in the synovial macrophages of one patient 18 months after infection [54]. Another study reported detection of CHIKV antigen in a human quadriceps muscle specimen at least three months after acute infection [61]. However, another study did not detect chronic CHIKV RNA in patient synovial fluid [118]. Results from our CHIKV-Cre infections demonstrate that the majority of tdTomato$^+$ cells are not concentrated in the synovial tissues, but rather in the skeletal muscle and skin (**Figure 2.4A**). Previous clinical studies may have thus been looking at suboptimal tissues, and our results could provide strong enough evidence to collect more invasive tissue samples from chronic CHIKV

patients, such as skin and muscle biopsies from areas near the chronic joint or muscle pain in addition to synovial tissue samples.

4.3 Materials and Methods

4.3.1 Viruses

The following viruses were used in these studies: CHIKV-WT, CHIKV-5'-Cre, and CHIKV-3'-Cre. Viruses were cloned and produced as described in Section 2.5.1.

4.3.2 Mice

The following strains of mice were obtained from the Jackson Laboratory: C57BL/6 (JAX Stock No: 000664; C57BL/6J) and tdTomato reporter mice (JAX Stock No: 007914; B6.Cg-*Gt(ROSA)*$^{26Sortm14(CAG-tdTomato)Hze}$/J). Mice were maintained as described in Section 2.5.2.

For CHK neutralizing mAb studies, tdTomato reporter mice were infected with CHIKV-3'-Cre as described in Section 2.5.2. The mice were injected intraperitoneally with 500 ug of human isotype control (WNV E16) or human anti-CHIKV E2 mAbs diluted in PBS [72,75] (250 ug each of CHK-152 and CHK-166) at 3 dpi. Samples were harvested for histology and frozen section slide processing and quantification was performed as described in Section 2.5.8.

4.3.3 Quantitative Real-Time PCR

RNA was isolated from tissues and RT-qPCR for CHIKV E1 was performed as described in Section 2.5.7.

4.3.4 Histology Studies

Four-week old tdTomato mice were infected and histology samples harvested and processed as described in Section 2.5.8. Alternative inoculation techniques were also used. Foot pad injection refers to injecting virus subcutaneously into the left (ipsilateral) footpad, between the

second and third digits. Intraperitoneal (IP) injection refers to injecting virus into the abdomen. Intravenous (IV) injection refers to injecting virus into the tail vein. Flank injection refers to injecting virus subcutaneously into skin on the dorsal left side of the mouse, near the relative position of the spleen. Retroorbital injection refers to injecting virus into the retroorbital sinus, which is superior and posterior to the eyeball, through the medial canthus. Calf injection refers to injecting virus subcutaneously above the gastrocnemius muscle.

4.3.5 Calculation of CHIKV E1 copy number per tdTomato$^+$ cell

The total amount of E1 RNA copies for each RT-qPCR sample was calculated by multiplying each E1/µg (E1 RNA copies per µg of total RNA) value by the total µg of RNA (ng/µL multiplied by the total µL for each sample divided by 1000). The total amount of tdTomato$^+$ cells for each histology sample was calculated by estimating the percentage that one 30 µm foot section represents of the entire foot. A mouse foot is on average 2.8 mm wide horizontally (averaged from swelling data), and sagittal sections are taken from the foot. Thus one 30 µm section represents approximately 1/93.33 fraction of the foot, assuming that the foot is closer to a rectangular prism than a cylinder. The number of tdTomato$^+$ cells per normalized tissue section was thus multiplied by 93.33 to roughly calculate the total number of tdTomato$^+$ cells per foot. The total number of E1 copies was then averaged for each time point and virus and then divided by the average number of tdTomato$^+$ cells for the corresponding time point and virus. Data were then log-transformed prior to graphing.

4.3.6 Statistical analysis

All data were analyzed using the Prism software, version 7 (GraphPad), as detailed in the figure captions. The following statistical tests were used: unpaired t test, ordinary one-way analysis of variance (ANOVA), ordinary two-way ANOVA. The following post-tests for multiple comparisons were also used: Tukey's post-test and Sidak's post-test. All error bars indicate

standard error of the mean (SEM); if error bars are not visible, then they are shorter than the height of the symbol. Asterisks indicate statistical significance, with only relevant comparisons shown (*, $P < 0.05$; **, $P < 0.01$; ***, $P < 0.001$; ****, $P < 0.0001$).

4.4 Figures

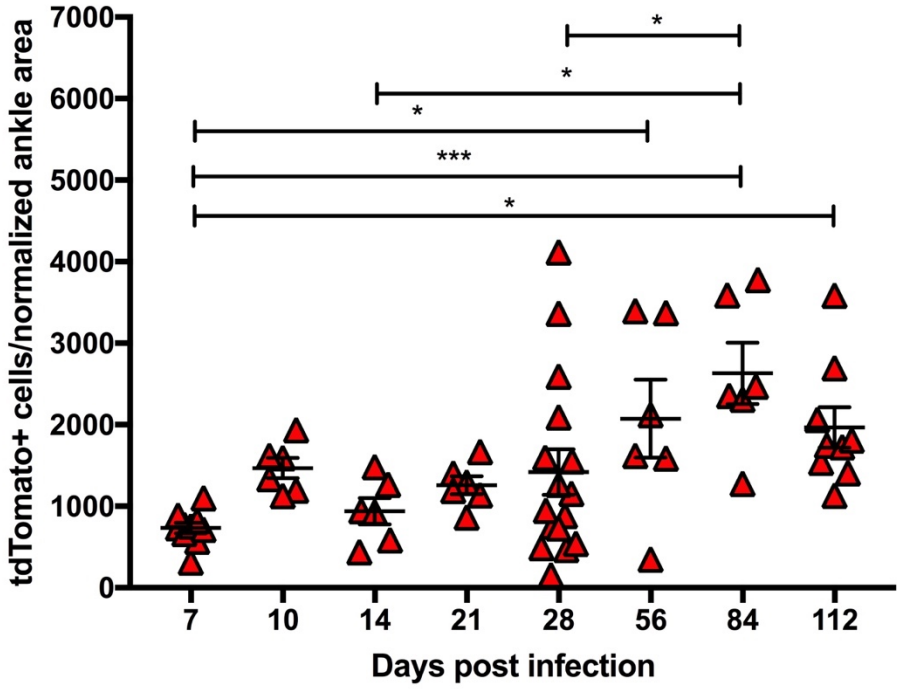

Figure 4.1: **tdTomato$^+$ cells in the ipsilateral foot during chronic timepoints**

tdTomato mice were infected with 10^6 PFU CHIKV-3'-Cre (red triangles), and ipsilateral feet were taken for frozen sections at 7-112 dpi. These data are also shown in Figures 2.4C and S2.5C. The total number of tdTomato$^+$ cells from was quantified for each section and normalized to ankle area as described in the Methods Section 2.5.8. Data were pooled from at least two independent experiments, and data were statistically analyzed with an ordinary one-way ANOVA using Tukey's post-test. All error bars indicate SEM. Asterisks indicate statistical significance (*, $P < 0.05$; **, $P < 0.01$; ***, $P < 0.001$; ****, $P < 0.0001$).

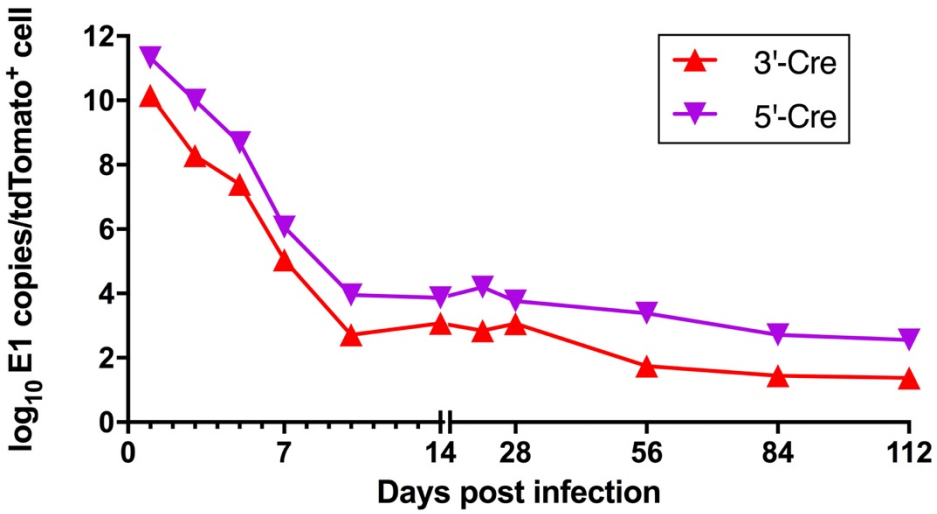

Figure 5.2: CHIKV E1 RNA copies per tdTomato$^+$ cells

Preliminary calculation of the number of CHIKV RNA copies per tdTomato$^+$ cell, for 10^6 PFU CHIKV-5'-Cre (purple inverted triangles) or 10^6 PFU CHIKV-3'-Cre (red triangles). C57/BL6 mice were infected with 10^6 PFU CHIKV-5'-Cre or 10^6 PFU CHIKV-3'-Cre, and the ipsilateral ankles were taken for RNA analysis at 1 to 112 dpi. The level of CHIKV E1 RNA was measured using RT-qPCR (these data are also shown in Figures 2.3D, S2.4C). The total amount of RNA copies per ankle was calculated (see the Methods Section 4.3.5). tdTomato mice were also infected with 10^6 PFU CHIKV-5'-Cre or 10^6 PFU CHIKV-3'-Cre, and the ipsilateral feet/ankles were taken for frozen sections at 1-112 dpi (these data are also shown in Figures 2.4C and S2.5C). The total number of tdTomato$^+$ cells in each sample was calculated (see the Methods Section 4.3.5). The mean total E1 copy number at each timepoint and virus was then divided by the mean total tdTomato$^+$ cells at each corresponding timepoint and virus to arrive at a preliminary calculation of viral copies per tdTomato$^+$ cell. Data were pooled from at least two independent experiments.

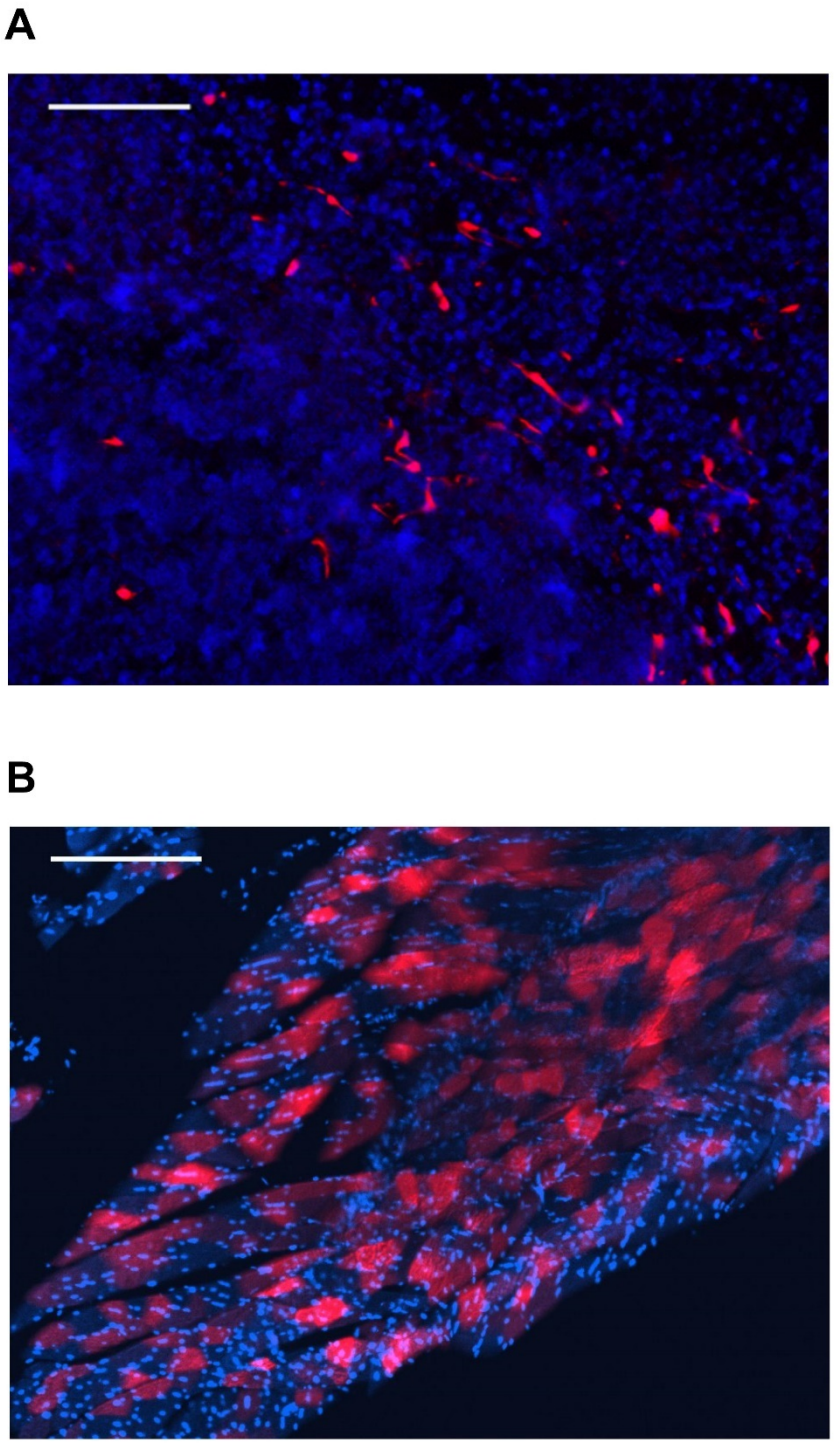

Figure 6.3: Alternative inoculation sites for CHIKV-Cre

(A) tdTomato reporter mice were inoculated retro-orbitally with 10^6 PFU of CHIKV-5'-Cre, and spleens were taken for histological analysis at 14 dpi. A representative image from two

independent experiments is shown, with blue showing DAPI staining and red showing tdTomato; scale bar represents 100 μm. **(B)** tdTomato reporter mice were inoculated subcutaneously above the calf muscle with 10^6 PFU of CHIKV-3'-Cre, and the ipsilateral calf muscle was taken for histological analysis at 28 dpi. A representative image from two independent experiments is shown, with blue showing DAPI staining and red showing tdTomato; scale bar represents 250 μm.

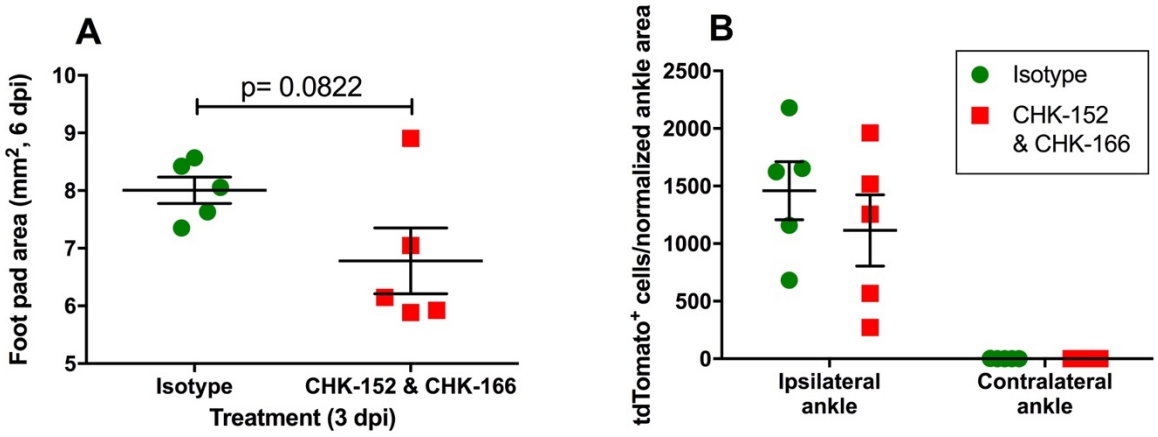

Figure 7.4: CHIKV neutralizing antibodies given at 3 dpi do not affect the number of tdTomato$^+$ cells

tdTomato mice were infected with 10^6 PFU CHIKV-3'-Cre and treated with CHIKV neutralizing mAbs (CHK-152 & CHK-166; red squares) or an isotype control (isotype; green circles) at 3 dpi. **(A)** Ipsilateral foot swelling was measured at 6 dpi. **(B)** At 28 dpi, the ipsilateral and contralateral ankles/feet were harvested for histological analysis, the total number of tdTomato$^+$ cells in each sample was quantified. Data in **A** were statistically analyzed with an un-paired t test. Data in **B** were statistically analyzed with a two-way ANOVA using Sidak's post-test. All error bars indicate SEM.

References

1. Robinson MC. An Epidemic of Virus Disease in Southern Province, Tanganyika Territory, in 1952-53, I. Clinical Features. Trans R Soc Trop Med Hyg. 1955;49(1):28–32.

2. Lumsden WHR. An Epidemic of Virus Disease in Southern Province, Tanganyika Territory, in 1952-53, II. General Description and Epidemiology. Trans R Soc Trop Med Hyg. 1955;49(1):33–57.

3. Ross RW. The Newala Epidemic, III. The Virus: Isolation, Pathogenic Properties and Relationship to the Epidemic. J Hyg. 1955;54(2):177–91.

4. Schwartz O, Albert ML. Biology and pathogenesis of chikungunya virus. Nat Rev Microbiol [Internet]. 2010 Jul [cited 2014 Jul 18];8(7):491–500. Available from: http://www.ncbi.nlm.nih.gov/pubmed/20551973

5. Powers AM, Brault AC, Tesh RB, Weaver SC. Re-emergence of chikungunya and o'nyong-nyong viruses : evidence for distinct geographical lineages and distant evolutionary relationships. J Gen Virol. 2000;81:471–9.

6. Volk SM, Chen R, Tsetsarkin KA, Adams P, Garcia TI, Sall AA, et al. Genome-Scale Phylogenetic Analyses of Chikungunya Virus Reveal Independent Emergences of Recent Epidemics and Various Evolutionary Rates Genome-Scale Phylogenetic Analyses of Chikungunya Virus Reveal Independent Emergences of Recent Epidemics and Various. J Virol. 2010;84(13):6497–504.

7. Voss A, Ahmedabad I. Chikungunya epidemic in India: a major public-health disaster. Lancet Infect Dis. 2007;7(May):306–7.

8. Outbreak and Spread of Chikungunya. Wkly Epidemiol Rec. 2007;82(47):409–16.

9. Pardigon N. The biology of chikungunya: a brief review of what we still do not know. Pathol Biol (Paris) [Internet]. 2009 Mar [cited 2014 Nov 19];57(2):127–32. Available from: http://www.ncbi.nlm.nih.gov/pubmed/18456435

10. Sergon K, Njuguna C, Kalani R, Ofula V, Onyango C, Konongoi LS, et al. Seroprevalence of Chikungunya Virus (CHIKV) Infection on Lamu Island, Kenya, October 2004. Am J Trop Med Hyg. 2008;78(October 2004):333–7.

11. Staples JE, Breiman RF, Powers AM. Chikungunya fever: an epidemiological review of a re-emerging infectious disease. Clin Infect Dis [Internet]. 2009 Sep 15 [cited 2014 Nov 10];49(6):942–8. Available from: http://www.ncbi.nlm.nih.gov/pubmed/19663604

12. Lemant J, Boisson V, Winer A, Thibault L, André H, Tixier F, et al. Serious acute chikungunya virus infection requiring intensive care during the Reunion Island outbreak in 2005-2006. Crit Care Med [Internet]. 2008 Sep [cited 2014 Nov 19];36(9):2536–41. Available from: http://www.ncbi.nlm.nih.gov/pubmed/18679124

13. Ramful D, Carbonnier M, Pasquet M, Bouhmani B, Ghazouani J, Noormahomed T, et al. Mother-to-child transmission of Chikungunya virus infection. Pediatr Infect Dis J [Internet]. 2007 Sep [cited 2014 Nov 20];26(9):811–5. Available from: http://www.ncbi.nlm.nih.gov/pubmed/17721376

14. Bodenmann P, Genton B. Chikungunya: an epidemic in real time. Lancet. 2006;368:2006.

15. Aedes albopictus as an epidemic vector of chikungunya virus: another emerging problem ? Lancet

Infect Dis. 2006;6:463–4.

16. Townson H, Nathan MB. Resurgence of chikungunya. Trans R Soc Trop Med Hyg [Internet]. 2008 Apr [cited 2014 Nov 18];102(4):308–9. Available from: http://www.ncbi.nlm.nih.gov/pubmed/18178232

17. Tsetsarkin K a, Vanlandingham DL, McGee CE, Higgs S. A single mutation in chikungunya virus affects vector specificity and epidemic potential. PLoS Pathog [Internet]. 2007 Dec [cited 2014 Jul 10];3(12):e201. Available from: http://www.pubmedcentral.nih.gov/articlerender.fcgi?artid=2134949&tool=pmcentrez&rendertype=abstract

18. Weaver SC. Arrival of chikungunya virus in the new world: prospects for spread and impact on public health. PLoS Negl Trop Dis [Internet]. 2014 Jun [cited 2014 Jul 11];8(6):e2921. Available from: http://www.pubmedcentral.nih.gov/articlerender.fcgi?artid=4072586&tool=pmcentrez&rendertype=abstract

19. Mavalankar D, Shastri P, Bandyopadhyay T, Parmar J, Ramani K V. Increased Mortality Rate Associated with Chikungunya Epidemic, Ahmedabad, India. Emerg Infect Dis. 2008;14(3):412–5.

20. Bortel W Van, Dorleans F, Rosine J, Blateau A, Rousset D, Matheus S. Chikungunya outbreak in the Caribbean region, December 2013 to March 2014, and the significance for Europe. Euro Surveill. 2014;19(13).

21. Chikungunya in the Americas [Internet]. CDC. Available from: http://www.cdc.gov/chikungunya/geo/americas.html

22. Nasci RS. Movement of chikungunya virus into the Western hemisphere. Emerg Infect Dis [Internet]. 2014 Aug;20(8):1394–5. Available from: http://www.pubmedcentral.nih.gov/articlerender.fcgi?artid=4111178&tool=pmcentrez&rendertype=abstract

23. Halstead S. Chikungunya reappearance, formerly called dengue. Emerg Infect Dis. 2015;21(4):557–61.

24. Miner JJ, Yeang HXA, Fox JM, Taffner S, Malkova ON, Oh ST, et al. Brief report: Chikungunya viral arthritis in the United States: A mimic of seronegative rheumatoid arthritis. Arthritis Rheumatol. 2015;67(5):1214–20.

25. Centers for Disease Control and Prevention (CDC). Chikungunya virus in the United States [Internet]. 2018. p. 1–4. Available from: https://www.cdc.gov/chikungunya/geo/united-states.html

26. Siberia W, Onishi T. Transcontinental Movement of Asian Genotype Chikungunya Virus. Emerg Infect Dis. 2014;20(8):1400–2.

27. Lanciotti RS, Lambert AJ. Phylogenetic analysis of Chikungunya virus strains circulating in the Western Hemisphere. Am J Trop Med Hyg. 2016;94(4):800–3.

28. Solignat M, Gay B, Higgs S, Briant L, Devaux C. Replication cycle of chikungunya: a re-emerging arbovirus. Virology [Internet]. 2009 Oct 25 [cited 2014 Nov 11];393(2):183–97. Available from: http://www.pubmedcentral.nih.gov/articlerender.fcgi?artid=2915564&tool=pmcentrez&rendertype=abstract

29. Assunção-Miranda I, Cruz-Oliveira C, Da Poian AT. Molecular mechanisms involved in the pathogenesis of alphavirus-induced arthritis. Biomed Res Int [Internet]. 2013 Jan;2013:973516.

Available from:
http://www.pubmedcentral.nih.gov/articlerender.fcgi?artid=3771267&tool=pmcentrez&rendertype=abstract

30. Hyde JL, Chen R, Trobaugh DW, Diamond MS, Weaver SC, Klimstra WB, et al. The 5' and 3' ends of alphavirus RNAs – non-coding is not non- functional. Virus Res. 2015;206:99–107.

31. Chen R, Wang E, Tsetsarkin KA, Weaver SC. Chikungunya Virus 3′ Untranslated Region: Adaptation to Mosquitoes and a Population Bottleneck as Major Evolutionary Forces. PLoS Pathog. 2013;9(8).

32. Morley VJ, Noval MG, Chen R, Weaver SC, Vignuzzi M, Stapleford KA, et al. Chikungunya virus evolution following a large 3′UTR deletion results in host-specific molecular changes in protein-coding regions. Virus Evol [Internet]. 2018;4(1):1–12. Available from: https://academic.oup.com/ve/article/doi/10.1093/ve/vey012/5032629

33. Sreejith R, Rana J, Dudha N, Kumar K, Gabrani R, Sharma SK, et al. Mapping interactions of Chikungunya virus nonstructural proteins. Virus Res [Internet]. 2012 Oct [cited 2014 Dec 2];169(1):231–6. Available from: http://www.ncbi.nlm.nih.gov/pubmed/22951312

34. Kumar S, Kumar A, Mamidi P, Tiwari A, Kumar S, Mayavannan A, et al. Chikungunya virus nsP1 interacts directly with nsP2 and modulates its ATPase activity. Sci Rep. 2018;8(1):1–14.

35. Sharma R, Kesari P, Kumar P, Tomar S. Structure-function insights into chikungunya virus capsid protein: Small molecules targeting capsid hydrophobic pocket. Virology [Internet]. 2018;515(January):223–34. Available from: https://doi.org/10.1016/j.virol.2017.12.020

36. Kuo S-C, Chen Y-J, Wang Y-M, Tsui P-Y, Kuo M-D, Wu T-Y, et al. Cell-based analysis of Chikungunya virus E1 protein in membrane fusion. J Biomed Sci [Internet]. 2012 Jan [cited 2014 Aug 26];19(1):44. Available from:
http://www.pubmedcentral.nih.gov/articlerender.fcgi?artid=3384457&tool=pmcentrez&rendertype=abstract

37. Wikan N, Khongwichit S, Phuklia W, Ubol S, Thonsakulprasert T, Thannagith M, et al. Comprehensive proteomic analysis of white blood cells from chikungunya fever patients of different severities. J Transl Med [Internet]. 2014 Jan [cited 2014 Sep 4];12(1):96. Available from:
http://www.pubmedcentral.nih.gov/articlerender.fcgi?artid=4022080&tool=pmcentrez&rendertype=abstract

38. Zhang R, Kim AS, Fox JM, Nair S, Basore K, Klimstra WB, et al. Mxra8 is a receptor for multiple arthritogenic alphaviruses. Nature [Internet]. 2018;1. Available from:
http://www.nature.com/articles/s41586-018-0121-3

39. Metz SW, Geertsema C, Martina BE, Andrade P, Heldens JG, Van Oers MM, et al. Functional processing and secretion of Chikungunya virus E1 and E2 glycoproteins in insect cells. Virol J [Internet]. 2011;8(1):353. Available from: http://www.virologyj.com/content/8/1/353

40. Silva LA, Dermody TS. Chikungunya virus: Epidemiology, replication, disease mechanisms, and prospective intervention strategies. J Clin Invest. 2017;127(3):737–49.

41. Melton J V., Ewart GD, Weir RC, Board PG, Lee E, Gage PW. Alphavirus 6K proteins form ion channels. J Biol Chem. 2002;277(49):46923–31.

42. Sourisseau M, Schilte C, Casartelli N, Trouillet C, Guivel-Benhassine F, Rudnicka D, et al. Characterization of reemerging chikungunya virus. PLoS Pathog [Internet]. 2007 Jun [cited 2014 May 25];3(6):e89. Available from:

http://www.pubmedcentral.nih.gov/articlerender.fcgi?artid=1904475&tool=pmcentrez&rendertype=abstract

43. Gay B, Bernard E, Solignat M, Chazal N, Devaux C, Briant L. pH-dependent entry of chikungunya virus into Aedes albopictus cells. Infect Genet Evol [Internet]. 2012 Aug [cited 2014 Dec 2];12(6):1275–81. Available from: http://www.ncbi.nlm.nih.gov/pubmed/22386853

44. Bernard E, Solignat M, Gay B, Chazal N, Higgs S, Devaux C, et al. Endocytosis of chikungunya virus into mammalian cells: role of clathrin and early endosomal compartments. PLoS One [Internet]. 2010 Jan [cited 2014 Dec 2];5(7):e11479. Available from: http://www.pubmedcentral.nih.gov/articlerender.fcgi?artid=2900206&tool=pmcentrez&rendertype=abstract

45. Hoornweg TE, van Duijl-Richter MKS, Ayala Nuñez N V., Albulescu IC, van Hemert MJ, Smit JM. Dynamics of Chikungunya Virus Cell Entry Unraveled by Single-Virus Tracking in Living Cells. J Virol [Internet]. 2016;90(9):4745–56. Available from: http://jvi.asm.org/lookup/doi/10.1128/JVI.03184-15

46. Rupp JC, Sokoloski KJ, Gebhart NN, Hardy RW. Alphavirus RNA synthesis and non-structural protein functions. J Gen Virol. 2015;96(9):2483–500.

47. Firth AE, Chung BYW, Fleeton MN, Atkins JF. Discovery of frameshifting in Alphavirus 6K resolves a 20-year enigma. Virol J. 2008;5:1–19.

48. Snyder JE, Kulcsar KA, Schultz KLW, Riley CP, Neary JT, Marr S, et al. Functional Characterization of the Alphavirus TF Protein. J Virol [Internet]. 2013;87(15):8511–23. Available from: http://jvi.asm.org/cgi/doi/10.1128/JVI.00449-13

49. Frolova EI, Gorchakov R, Pereboeva L, Atasheva S, Frolov I. Functional Sindbis Virus Replicative Complexes Are Formed at the Plasma Membrane. J Virol [Internet]. 2010;84(22):11679–95. Available from: http://jvi.asm.org/cgi/doi/10.1128/JVI.01441-10

50. Soonsawad P, Xing L, Milla E, Espinoza JM, Kawano M, Marko M, et al. Structural Evidence of Glycoprotein Assembly in Cellular Membrane Compartments prior to Alphavirus Budding. J Virol [Internet]. 2010;84(21):11145–51. Available from: http://jvi.asm.org/cgi/doi/10.1128/JVI.00036-10

51. Alphavirus: Virion [Internet]. Viral Zone. 2010. Available from: http://viralzone.expasy.org/all_by_species/625.html

52. Dhanwani R, Khan M, Bhaskar a SB, Singh R, Patro IK, Rao PVL, et al. Characterization of Chikungunya virus infection in human neuroblastoma SH-SY5Y cells: role of apoptosis in neuronal cell death. Virus Res [Internet]. 2012 Feb [cited 2014 May 25];163(2):563–72. Available from: http://www.ncbi.nlm.nih.gov/pubmed/22210004

53. Schmid MA, Glasner DR, Shah S, Michlmayr D, Kramer LD, Harris E, et al. Mosquito Saliva Increases Endothelial Permeability in the Skin, Immune Cell Migration, and Dengue Pathogenesis during Antibody-Dependent Enhancement. PLOS Pathog [Internet]. 2016;12(6):e1005676. Available from: http://dx.plos.org/10.1371/journal.ppat.1005676

54. Hoarau J-J, Jaffar Bandjee M-C, Krejbich Trotot P, Das T, Li-Pat-Yuen G, Dassa B, et al. Persistent chronic inflammation and infection by Chikungunya arthritogenic alphavirus in spite of a robust host immune response. J Immunol [Internet]. 2010 May 15 [cited 2014 May 25];184(10):5914–27. Available from: http://www.ncbi.nlm.nih.gov/pubmed/20404278

55. Couderc T, Chrétien F, Schilte C, Disson O, Michault A, Albert ML, et al. Cell and tissue tropisms of Chikungunya virus and its dissemination to the central nervous system. BMC Proc.

2008;2(Suppl 1):S7.

56. Labadie K, Larcher T, Joubert C, Mannioui A, Delache B, Brochard P, et al. Chikungunya disease in nonhuman primates involves long-term viral persistence in macrophages. J Clin Invest. 2010;120(3):894–906.

57. Rohatgi A, Corbo JC, Monte K, Higgs S, Vanlandingham DL, Kardon G, et al. Infection of Myofibers Contributes to Increased Pathogenicity during Infection with an Epidemic Strain of Chikungunya Virus. J Virol [Internet]. 2014 Mar [cited 2014 Mar 19];88(5):2414–25. Available from: http://www.ncbi.nlm.nih.gov/pubmed/24335291

58. Schilte C, Couderc T, Chretien F, Sourisseau M, Gangneux N, Guivel-Benhassine F, et al. Type I IFN controls chikungunya virus via its action on nonhematopoietic cells. J Exp Med [Internet]. 2010 Feb 15 [cited 2014 May 25];207(2):429–42. Available from: http://www.pubmedcentral.nih.gov/articlerender.fcgi?artid=2822618&tool=pmcentrez&rendertype=abstract

59. Her Z, Malleret B, Chan M, Ong EKS, Wong S-C, Kwek DJC, et al. Active infection of human blood monocytes by Chikungunya virus triggers an innate immune response. J Immunol [Internet]. 2010 May 15 [cited 2014 May 25];184(10):5903–13. Available from: http://www.ncbi.nlm.nih.gov/pubmed/20404274

60. Kumar S, Jaffar-Bandjee M-C, Giry C, Connen de Kerillis L, Merits A, Gasque P, et al. Mouse macrophage innate immune response to Chikungunya virus infection. Virol J [Internet]. 2012 Jan [cited 2014 May 29];9(1):313. Available from: http://www.pubmedcentral.nih.gov/articlerender.fcgi?artid=3577478&tool=pmcentrez&rendertype=abstract

61. Ozden S, Huerre M, Riviere J-P, Coffey LL, Afonso P V, Mouly V, et al. Human muscle satellite cells as targets of Chikungunya virus infection. PLoS One [Internet]. 2007 Jan [cited 2014 May 25];2(6):e527. Available from: http://www.pubmedcentral.nih.gov/articlerender.fcgi?artid=1885285&tool=pmcentrez&rendertype=abstract

62. Ng LFP, Chow A, Sun Y-J, Kwek DJC, Lim P-L, Dimatatac F, et al. IL-1beta, IL-6, and RANTES as biomarkers of Chikungunya severity. PLoS One [Internet]. 2009 Jan [cited 2014 Aug 28];4(1):e4261. Available from: http://www.pubmedcentral.nih.gov/articlerender.fcgi?artid=2625438&tool=pmcentrez&rendertype=abstract

63. Wauquier N, Becquart P, Nkoghe D, Padilla C, Ndjoyi-Mbiguino A, Leroy EM. The acute phase of Chikungunya virus infection in humans is associated with strong innate immunity and T CD8 cell activation. J Infect Dis [Internet]. 2011 Jul 1 [cited 2014 Nov 11];204(1):115–23. Available from: http://www.pubmedcentral.nih.gov/articlerender.fcgi?artid=3307152&tool=pmcentrez&rendertype=abstract

64. Morrison TE, Oko L, Montgomery S a, Whitmore AC, Lotstein AR, Gunn BM, et al. A mouse model of chikungunya virus-induced musculoskeletal inflammatory disease: evidence of arthritis, tenosynovitis, myositis, and persistence. Am J Pathol [Internet]. 2011 Jan [cited 2014 May 29];178(1):32–40. Available from: http://www.pubmedcentral.nih.gov/articlerender.fcgi?artid=3069999&tool=pmcentrez&rendertype=abstract

65. Priya R, Patro IK, Parida MM. TLR3 mediated innate immune response in mice brain following infection with Chikungunya virus. Virus Res [Internet]. 2014 Jun 4 [cited 2014 Aug 11];189C:194–205. Available from: http://www.ncbi.nlm.nih.gov/pubmed/24905288

66. Gardner J, Anraku I, Le TT, Larcher T, Major L, Roques P, et al. Chikungunya virus arthritis in adult wild-type mice. J Virol [Internet]. 2010 Aug [cited 2014 Dec 2];84(16):8021–32. Available from: http://www.pubmedcentral.nih.gov/articlerender.fcgi?artid=2916516&tool=pmcentrez&rendertype=abstract

67. Tharmarajah K, Mahalingam S, Zaid A. Chikungunya: vaccines and therapeutics. F1000Research [Internet]. 2017;6(0):2114. Available from: https://f1000research.com/articles/6-2114/v1

68. Delogu I, Pastorino B, Baronti C, Nougairède A, Bonnet E, de Lamballerie X. In vitro antiviral activity of arbidol against Chikungunya virus and characteristics of a selected resistant mutant. Antiviral Res [Internet]. 2011;90(3):99–107. Available from: http://dx.doi.org/10.1016/j.antiviral.2011.03.182

69. Briolant S, Garin D, Scaramozzino N, Jouan A, Crance JM. In vitro inhibition of Chikungunya and Semliki Forest viruses replication by antiviral compounds: Synergistic effect of interferon-α and ribavirin combination. Antiviral Res. 2004;61(2):111–7.

70. Delang L, Guerrero NS, Tas A, Quérat G, Pastorino B, Froeyen M, et al. Mutations in the chikungunya virus non-structural proteins cause resistance to favipiravir (T-705), a broad-spectrum antiviral. J Antimicrob Chemother. 2014;69(10):2770–84.

71. Karlas A, Berre S, Couderc T, Varjak M, Braun P, Meyer M, et al. A human genome-wide loss-of-function screen identifies effective chikungunya antiviral drugs. Nat Commun. 2016;7(May).

72. Scott A. Smith1, 5, 6, Laurie A. Silva2, 4, 6, Julie M. Fox7, Andrew Flyak3, Nurgun Kose5, Gopal Sapparapu5, Solomiia Khomadiak2, 4, Alison W. Ashbrook2, 3, 4, Kristen M. Kahle5, Rachel H. Fong5, Sherri Swayne5, Benjamin J. Doranz5, Charles E. McGee6, Mar A, Jr. JEC. Isolation and characterization of broad and ultrapotent human monoclonal antibodies with therapeutic activity against chikungunya virus. Cell Host Microbe. 2016;23(10):1780–9.

73. Miner JJ, Cook LE, Hong JP, Smith AM, Richner JM, Shimak RM, et al. Therapy with CTLA4-Ig and an antiviral monoclonal antibody controls chikungunya virus arthritis. Sci Transl Med. 2017;9(375):1–10.

74. Broeckel R, Fox JM, Haese N, Kreklywich CN, Sukulpovi-petty S, Legasse A, et al. Therapeutic administration of a recombinant human monoclonal antibody reduces the severity of chikungunya virus disease in rhesus macaques. PLoS Negl Trop Dis [Internet]. 2017; Available from: http://dx.doi.org/10.1371/journal.pntd.0005637

75. Pal P, Dowd K a., Brien JD, Edeling M a., Gorlatov S, Johnson S, et al. Development of a Highly Protective Combination Monoclonal Antibody Therapy against Chikungunya Virus. PLoS Pathog. 2013;9(4).

76. Weaver SC, Osorio JE, Livengood JA, Chen R, Stinchcomb DT. Chikungunya virus and prospects for a vaccine. Expert Rev Vaccines. 2013;11(9):1087–101.

77. Gorchakov R, Wang E, Leal G, Forrester NL, Plante K, Rossi SL, et al. Attenuation of Chikungunya virus vaccine strain 181/clone 25 is determined by two amino acid substitutions in the E2 envelope glycoprotein. J Virol [Internet]. 2012 Jun [cited 2014 Dec 4];86(11):6084–96. Available from: http://www.pubmedcentral.nih.gov/articlerender.fcgi?artid=3372191&tool=pmcentrez&rendertype=abstract

78. Brandler S, Ruffié C, Combredet C, Brault JB, Najburg V, Prevost MC, et al. A recombinant measles vaccine expressing chikungunya virus-like particles is strongly immunogenic and protects

mice from lethal challenge with chikungunya virus. Vaccine [Internet]. 2013;31(36):3718–25. Available from: http://dx.doi.org/10.1016/j.vaccine.2013.05.086

79. Reisinger EC, Tschismarov R, Beubler E, Wiedermann U, Firbas C, Loebermann M, et al. Immunogenicity, safety, and tolerability of the measles-vectored chikungunya virus vaccine MV-CHIK: a double-blind, randomised, placebo-controlled and active-controlled phase 2 trial. Lancet [Internet]. 2018;6736(18):1–10. Available from: https://linkinghub.elsevier.com/retrieve/pii/S0140673618324887

80. Chang LJ, Dowd KA, Mendoza FH, Saunders JG, Sitar S, Plummer SH, et al. Safety and tolerability of chikungunya virus-like particle vaccine in healthy adults: A phase 1 dose-escalation trial. Lancet [Internet]. 2014;384(9959):2046–52. Available from: http://dx.doi.org/10.1016/S0140-6736(14)61185-5

81. Erasmus JH, Auguste AJ, Kaelber JT, Luo H, Shannan L, Fenton K, et al. A Chikungunya Fever Vaccine Utilizing an Insect-Specific Virus Platform. Nat Med. 2017;23(2):192–9.

82. Taylor A, Liu X, Zaid A, H Goh LY, Hobson-Peters J, Hall RA, et al. Mutation of the N-Terminal Region of Chikungunya Virus Capsid Protein: Implications for Vaccine Design. 2017;8(1):1970–86. Available from: http://mbio.asm.org/

83. Mehta R, Gerardin P, de Brito CAA, Soares CN, Ferreira MLB, Solomon T. The neurological complications of chikungunya virus: A systematic review. Rev Med Virol. 2018;28(3).

84. Johnson BW, Russell BJ, Goodman CH. Laboratory Diagnosis of Chikungunya Virus Infections and Commercial Sources for Diagnostic Assays. J Infect Dis. 2017;214(July 2015).

85. Moro ML, Grilli E, Corvetta A, Silvi G, Angelini R, Mascella F, et al. Long-term chikungunya infection clinical manifestations after an outbreak in Italy: A prognostic cohort study. J Infect [Internet]. 2012;65(2):165–72. Available from: http://dx.doi.org/10.1016/j.jinf.2012.04.005

86. Mathew AJ, Goyal V, George E, Thekkemuriyil D V., Jayakumar B, Chopra A. Rheumatic-musculoskeletal pain and disorders in a naïve group of individuals 15 months following a Chikungunya viral epidemic in south India: A population based observational study. Int J Clin Pract. 2011;65(12):1306–12.

87. Rahim AA, Thekkekara RJ, Bina T, Paul BJ. Disability with persistent pain following an epidemic of chikungunya in rural south India. J Rheumatol. 2016;43(2):440–4.

88. Taubitz W, Cramer JP, Kapaun A, Pfeffer M, Drosten C, Dobler G, et al. Chikungunya Fever in Travelers: Clinical Presentation and Course. Clin Infect Dis [Internet]. 2007;45(1):e1–4. Available from: https://academic.oup.com/cid/article-lookup/doi/10.1086/518701

89. Chow A, Her Z, Ong EKS, Chen J, Dimatatac F, Kwek DJC, et al. Persistent arthralgia induced by Chikungunya virus infection is associated with interleukin-6 and granulocyte macrophage colony-stimulating factor. J Infect Dis. 2011;203(2):149–57.

90. Ramachandran V, Kaur P, Kanagasabai K, Vadivoo S, Murhekar M. Persistent arthralgia among Chikungunya patients and associated risk factors in Chennai, South India. J Postgrad Med. 2014;60(1):3–6.

91. Rodríguez-Morales AJ, Calvache-Benavides CE, Giraldo-Gómez J, Hurtado-Hurtado N, Yepes-Echeverri MC, García-Loaiza CJ, et al. Post-chikungunya chronic arthralgia: Results from a retrospective follow-up study of 131 cases in Tolima, Colombia. Travel Med Infect Dis. 2016;14(1):58–9.

92. Yaseen HM, Simon F, Deparis X, Marimoutou C. Identification of initial severity determinants to predict arthritis after chikungunya infection in a cohort of French gendarmes. BMC Musculoskelet Disord. 2014;15(1):1–8.

93. Borgherini G, Poubeau P, Jossaume A, Gouix A, Cotte L, Michault A, et al. Persistent Arthralgia Associated with Chikungunya Virus: A Study of 88 Adult Patients on Reunion Island. Clin Infect Dis [Internet]. 2008;47(4):469–75. Available from: https://academic.oup.com/cid/article-lookup/doi/10.1086/590003

94. Gérardin P, Fianu A, Malvy D, Mussard C, Boussaïd K, Rollot O, et al. Perceived morbidity and community burden after a Chikungunya outbreak: the TELECHIK survey, a population-based cohort study. BMC Med [Internet]. 2011;9(5). Available from: http://www.biomedcentral.com/1741-7015/9/5

95. Gérardin P, Fianu A, Michault A, Mussard C, Boussaïd K, Rollot O, et al. Predictors of Chikungunya rheumatism: A prognostic survey ancillary to the TELECHIK cohort study. Arthritis Res Ther [Internet]. 2013;15(1):R9. Available from: http://arthritis-research.com/content/15/1/R9

96. Paixão ES, Rodrigues LC, Costa M da CN, Itaparica M, Barreto F, Gérardin P, et al. Chikungunya chronic disease: a systematic review and meta-analysis. Trans R Soc Trop Med Hyg [Internet]. 2018;(July):1–16. Available from: https://academic.oup.com/trstmh/advance-article/doi/10.1093/trstmh/try063/5051873

97. van Aalst M, Nelen CM, Goorhuis A, Stijnis C, Grobusch MP. Long-term sequelae of chikungunya virus disease: A systematic review. Travel Med Infect Dis. 2017;15:8–22.

98. Marimoutou C, Vivier E, Oliver M, Boutin JP, Simon F. Morbidity and impaired quality of life 30 months after chikungunya infection: Comparative cohort of infected and uninfected french military policemen in reunion island. Med (United States). 2012;91(4):212–9.

99. Bouquillard É, Combe B. A report of 21 cases of rheumatoid arthritis following Chikungunya fever. A mean follow-up of two years. Jt Bone Spine. 2009;76(6):654–7.

100. Javelle E, Ribera A, Degasne I, Gaüzère BA, Marimoutou C, Simon F. Specific Management of Post-Chikungunya Rheumatic Disorders: A Retrospective Study of 159 Cases in Reunion Island from 2006-2012. PLoS Negl Trop Dis. 2015;9(3):1–18.

101. Soumahoro MK, Gérardin P, Boëlle PY, Perrau J, Fianu A, Pouchot J, et al. Impact of Chikungunya virus infection on health status and quality of life: A retrospective cohort study. PLoS One. 2009;4(11):1–6.

102. Schilte C, Staikowsky F, Couderc T, Madec Y, Carpentier F, Kassab S, et al. Chikungunya Virus-associated Long-term Arthralgia: A 36-month Prospective Longitudinal Study. PLoS Negl Trop Dis. 2013;7(3).

103. Marimoutou C, Ferraro J, Javelle E, Deparis X, Simon F. Chikungunya infection: Self-reported rheumatic morbidity and impaired quality of life persist 6 years later. Clin Microbiol Infect [Internet]. 2015;21(7):688–93. Available from: http://dx.doi.org/10.1016/j.cmi.2015.02.024

104. Simon F, Parola P, Grandadam M, Fourcade S, Oliver M, Brouqui P, et al. Chikungunya Infection: An Emerging Rheumatism Among Travelers Returned From Indian Ocean Islands. Report of 47 Cases. Medicine (Baltimore) [Internet]. 2007;86(3):123–37. Available from: http://content.wkhealth.com/linkback/openurl?sid=WKPTLP:landingpage&an=00005792-200705000-00001

105. Ramachandran V, Malaisamy M, Ponnaiah M, Kaliaperuaml K, Vadivoo S, Gupte MD. Impact of

Chikungunya on Health Related Quality of Life Chennai, South India. PLoS One. 2012;7(12).

106. Win MK, Chow A, Dimatatac F, Go CJ, Leo YS. Chikungunya fever in Singapore: Acute clinical and laboratory features, and factors associated with persistent arthralgia. J Clin Virol. 2010;49(2):111–4.

107. Huits R, De Kort J, Van Den Berg R, Chong L, Tsoumanis A, Eggermont K, et al. Chikungunya virus infection in Aruba: Diagnosis, clinical features and predictors of post-chikungunya chronic polyarthralgia. PLoS One. 2018;13(4):1–21.

108. Gerardin P, Barau G, Michault A, Bintner M, Randrianaivo H, Choker G, et al. Multidisciplinary Prospective Study of Mother-to-Child Chikungunya Virus Infections on the Island of La Reunion. PLoS Med. 2008;5(3):413–23.

109. Gérardin P, Sampériz S, Ramful D, Boumahni B, Bintner M, Alessandri JL, et al. Neurocognitive Outcome of Children Exposed to Perinatal Mother-to-Child Chikungunya Virus Infection: The CHIMERE Cohort Study on Reunion Island. PLoS Negl Trop Dis. 2014;8(7).

110. Laoprasopwattana K, Suntharasaj T, Petmanee P, Suddeaugrai O, Geater A. Chikungunya and dengue virus infections during pregnancy: Seroprevalence, seroincidence and maternal-fetal transmission, southern Thailand, 2009-2010. Epidemiol Infect. 2016;144(2):381–8.

111. Maek-a-nantawat W, Silachamroon U. Presence of Autoimmune Antibody in Chikungunya Infection. Case Rep Med [Internet]. 2009;2009:1–4. Available from: http://www.hindawi.com/journals/crim/2009/840183/

112. Reddy V, Desai A, Krishna SS, Vasanthapuram R. Molecular Mimicry between Chikungunya Virus and Host Components: A Possible Mechanism for the Arthritic Manifestations. PLoS Negl Trop Dis. 2017;11(1):1–20.

113. Goh LYH, Hobson-Peters J, Prow N a, Gardner J, Bielefeldt-Ohmann H, Suhrbier A, et al. Monoclonal antibodies specific for the capsid protein of chikungunya virus suitable for multiple applications. J Gen Virol [Internet]. 2014;(May):507–12. Available from: http://www.ncbi.nlm.nih.gov/pubmed/25480927

114. Her Z, Teng T, Tan JJL, Teo T, Kam Y, Lum F, et al. Loss of TLR3 aggravates CHIKV replication and pathology due to an altered virus-specific neutralizing antibody response. EMBO Mol Med. 2015;7(1):24–41.

115. Teo T-H, Lum F-M, Claser C, Lulla V, Lulla A, Merits A, et al. A pathogenic role for CD4+ T cells during Chikungunya virus infection in mice. J Immunol [Internet]. 2013;190(1):259–69. Available from: http://www.ncbi.nlm.nih.gov/pubmed/23209328

116. Teo TH, Lum FM, Ghaffar K, Chan YH, Amrun SN, Tan JJL, et al. Plasmodium co-infection protects against chikungunya virus-induced pathologies. Nat Commun [Internet]. 2018;9(1). Available from: http://dx.doi.org/10.1038/s41467-018-06227-9

117. Poo YS, Rudd P a., Gardner J, Wilson J a C, Larcher T, Colle MA, et al. Multiple Immune Factors Are Involved in Controlling Acute and Chronic Chikungunya Virus Infection. PLoS Negl Trop Dis. 2014;8(12).

118. Chang AY, Martins KAO, Encinales L, Reid SP, Acuña M, Encinales C, et al. Chikungunya Arthritis Mechanisms in the Americas: A Cross-Sectional Analysis of Chikungunya Arthritis Patients Twenty-Two Months After Infection Demonstrating No Detectable Viral Persistence in Synovial Fluid. Arthritis Rheumatol. 2018;70(4):585–93.

119. Mccarthy MK, Morrison TE. Persistent RNA virus infections: Do PAMPS drive chronic disease ? Curr Opin Virol [Internet]. 2017;23:8–15. Available from: http://dx.doi.org/10.1016/j.coviro.2017.01.003

120. Hawman DW, Stoermer K a., Montgomery S a., Pal P, Oko L, Diamond MS, et al. Chronic Joint Disease Caused by Persistent Chikungunya Virus Infection Is Controlled by the Adaptive Immune Response. J Virol [Internet]. 2013;87(24):13878–88. Available from: http://jvi.asm.org/cgi/doi/10.1128/JVI.02666-13

121. Zare F, Bokarewa M, Nenonen N, Bergstrom T, Alexopoulou L, Flavell RA, et al. Arthritogenic Properties of Double-Stranded (Viral) RNA. J Immunol [Internet]. 2004;172(9):5656–63. Available from: http://www.jimmunol.org/cgi/doi/10.4049/jimmunol.172.9.5656

122. Magnusson M, Zare F, Tarkowski A. Requirement of type I interferon signaling for arthritis triggered by double-stranded RNA. Arthritis Rheum. 2006;54(1):148–57.

123. Haese NN, Broeckel RM, Hawman DW, Heise MT, Morrison TE, Streblow DN. Animal models of chikungunya virus infection and disease. J Infect Dis. 2016;214(Suppl 5):S482–7.

124. Couderc T, Chrétien F, Schilte C, Disson O, Brigitte M, Guivel-Benhassine F, et al. A mouse model for Chikungunya: Young age and inefficient type-I interferon signaling are risk factors for severe disease. PLoS Pathog. 2008;4(2).

125. Werneke SW, Schilte C, Rohatgi A, Monte KJ, Michault A, Arenzana-Seisdedos F, et al. ISG15 is critical in the control of Chikungunya virus infection independent of UbE1L mediated conjugation. PLoS Pathog [Internet]. 2011 Oct [cited 2014 Sep 2];7(10):e1002322. Available from: http://www.pubmedcentral.nih.gov/articlerender.fcgi?artid=3197620&tool=pmcentrez&rendertype=abstract

126. Schilte C, Buckwalter MR, Laird ME, Diamond MS, Schwartz O, Albert ML. Cutting edge: independent roles for IRF-3 and IRF-7 in hematopoietic and nonhematopoietic cells during host response to Chikungunya infection. J Immunol [Internet]. 2012 Apr 1 [cited 2014 Oct 17];188(7):2967–71. Available from: http://www.ncbi.nlm.nih.gov/pubmed/22371392

127. Rudd PA, Wilson J, Gardner J, Larcher T, Babarit C, Le TT, et al. Interferon Response Factors 3 and 7 Protect against Chikungunya Virus Hemorrhagic Fever and Shock. J Virol [Internet]. 2012;86(18):9888–98. Available from: http://jvi.asm.org/cgi/doi/10.1128/JVI.00956-12

128. Fox JM, Diamond MS. Immune-Mediated Protection and Pathogenesis of Chikungunya Virus. J Immunol [Internet]. 2016;197(11):4210–8. Available from: http://www.jimmunol.org/lookup/doi/10.4049/jimmunol.1601426

129. Chan Y-H, Lum F-M, Ng L. Limitations of Current in Vivo Mouse Models for the Study of Chikungunya Virus Pathogenesis. Med Sci [Internet]. 2015;3(3):64–77. Available from: http://www.mdpi.com/2076-3271/3/3/64/

130. Binn LN, Harrison VR, Randall R. Patterns of viremia and antibody observed in rhesus monkeys inoculated with chikungunya and other serologically related group A arboviruses. Am J Trop Med Hyg. 1967;16(6):782–5.

131. Messaoudi I, Vomaske J, Totonchy T, Kreklywich CN, Haberthur K, Springgay L, et al. Chikungunya Virus Infection Results in Higher and Persistent Viral Replication in Aged Rhesus Macaques Due to Defects in Anti-Viral Immunity. PLoS Negl Trop Dis. 2013;7(7).

132. Akahata W, Yang1 Z, Andersen H, Sun S, Holdaway HA, Kong W-P, et al. A VLP vaccine for epidemic Chikungunya virus protects non-human primates against infection. Nat Med [Internet].

2010;16(3):334–8. Available from: http://www.sciencemag.org/content/306/5703/1895.short

133. Chen CI, Clark DC, Pesavento P, Lerche NW, Luciw P a., Reisen WK, et al. Comparative pathogenesis of epidemic and enzootic Chikungunya viruses in a pregnant Rhesus macaque model. Am J Trop Med Hyg. 2010;83(6):1249–58.

134. Pal P, Fox JM, Hawman DW, Huang Y-JS, Messaoudi I, Kreklywich C, et al. Chikungunya Viruses That Escape Monoclonal Antibody Therapy Are Clinically Attenuated, Stable, and Not Purified in Mosquitoes. J Virol [Internet]. 2014;88(15):8213–26. Available from: http://jvi.asm.org/cgi/doi/10.1128/JVI.01032-14

135. Tsetsarkin K, Higgs S, McGee CE, De Lamballerie X, Charrel RN, Vanlandingham DL. Infectious Clones of Chikungunya Virus (La Reunion Isolate) for Vector Competence Studies. Vector-Borne Zoonotic Dis. 2006;6(4).

136. Vanlandingham DL, Tsetsarkin K, Hong C, Klingler K, McElroy KL, Lehane MJ, et al. Development and characterization of a double subgenomic chikungunya virus infectious clone to express heterologous genes in Aedes aegypti mosqutioes. Insect Biochem Mol Biol. 2005;35(10):1162–70.

137. Kümmerer BM, Grywna K, Gläsker S, Wieseler J, Drosten C. Construction of an infectious Chikungunya virus cDNA clone and stable insertion of mCherry reporter genes at two different sites. J Gen Virol [Internet]. 2012 Sep [cited 2014 Dec 8];93(Pt 9):1991–5. Available from: http://www.ncbi.nlm.nih.gov/pubmed/22673932

138. Hamilton JR, Sachs D, Lim JK, Langlois RA, Palese P, Heaton NS. Club cells surviving influenza A virus infection induce temporary nonspecific antiviral immunity. Proc Natl Acad Sci U S A [Internet]. 2016;(13):2–7. Available from: http://dx.doi.org/10.1073/pnas.1522376113 VN - readcube.com

139. Heaton NS, Langlois R a., Sachs D, Lim JK, Palese P, TenOever BR. Long-term survival of influenza virus infected club cells drives immunopathology. J Exp Med [Internet]. 2014;211(9):jem.20140488-. Available from: http://jem.rupress.org/content/early/2014/08/12/jem.20140488.abstract

140. Shivkumar M, Milho R, May JS, Nicoll MP, Efstathiou S, Stevenson PG. Herpes simplex virus 1 targets the murine olfactory neuroepithelium for host entry. J Virol [Internet]. 2013;87(19):10477–88. Available from: http://www.ncbi.nlm.nih.gov/pubmed/23903843

141. Ma JZ, Russell TA, Spelman T, Carbone FR, Tscharke DC. Lytic Gene Expression Is Frequent in HSV-1 Latent Infection and Correlates with the Engagement of a Cell-Intrinsic Transcriptional Response. PLoS Pathog. 2014;10(7).

142. Schuffenecker I, Iteman I, Michault A, Murri S, Frangeul L, Vaney M-C, et al. Genome microevolution of chikungunya viruses causing the Indian Ocean outbreak. PLoS Med [Internet]. 2006 Jul [cited 2014 Aug 8];3(7):e263. Available from: http://www.pubmedcentral.nih.gov/articlerender.fcgi?artid=1463904&tool=pmcentrez&rendertype=abstract

143. Centers for Disease Control and Prevention (CDC). Countries and territories where chikungunya cases have been reported (as of May 29, 2018) [Internet]. Cdc. 2018. p. 1. Available from: http://www.cdc.gov/chikungunya/geo/index.html

144. Alphavirus [Internet]. Viral Zone. 2018. Available from: https://viralzone.expasy.org/625?outline=all_by_species

145. Yaseen HM, Simon F, Deparis X, Marimoutou C. Estimation of Lasting Impact of a Chikungunya

Outbreak in Reunion Island. Epidemiology [Internet]. 2012;S2(003):1–6. Available from: accessed on Dec.2015

146. Javelle E, Gautret P, Ribéra A, Gaüzère BA, Cabié A, Corail PR, et al. The challenge of chronic chikungunya. Travel Med Infect Dis. 2017;15:3–4.

147. Chaaitanya IK, Muruganandam N, Sundaram SG, Kawalekar O, Sugunan AP, Manimunda SP, et al. Role of Proinflammatory Cytokines and Chemokines in Chronic Arthropathy in CHIKV Infection. Viral Immunol. 2011;24(4):265–71.

148. Kelvin A a, Banner D, Silvi G, Moro ML, Spataro N, Gaibani P, et al. Inflammatory cytokine expression is associated with chikungunya virus resolution and symptom severity. PLoS Negl Trop Dis [Internet]. 2011 Aug [cited 2014 Sep 2];5(8):e1279. Available from: http://www.pubmedcentral.nih.gov/articlerender.fcgi?artid=3156690&tool=pmcentrez&rendertype=abstract

149. Chirathaworn C, Rianthavorn P, Wuttirattanakowit N, Poovorawan Y. Serum IL-18 and IL-18BP levels in patients with Chikungunya virus infection. Viral Immunol [Internet]. 2010 Feb;23(1):113–7. Available from: http://www.ncbi.nlm.nih.gov/pubmed/20121409

150. Hawman DW, Fox JM, Ashbrook AW, May NA, Schroeder KMS, Torres RM, et al. Pathogenic Chikungunya Virus Evades B cell Responses to Establish Persistence. Cell Rep. 2016;16(5):1326–38.

151. Seymour RL, Adams AP, Leal G, Alcorn MDH, Weaver SC. A Rodent Model of Chikungunya Virus Infection in RAG1 -/- Mice, with Features of Persistence, for Vaccine Safety Evaluation. PLoS Negl Trop Dis [Internet]. 2015;9(6):e0003800. Available from: http://www.pubmedcentral.nih.gov/articlerender.fcgi?artid=4482609&tool=pmcentrez&rendertype=abstract

152. Heath CJ, Lowther J, Noël TP, Mark-George I, Boothroyd DB, Mitchell G, et al. The identification of risk factors for chronic chikungunya arthralgia in Grenada, West Indies: A cross-sectional cohort study. Open Forum Infect Dis. 2018;5(1).

153. Hoffman PN, Lopata MA, Watson DF, Luduenafl RF. Axonal Transport of Class II and III Beta-tubulin: Evidence that the Slow Component Wave Represents the Movements of Only a Small Fraction of the Tubulin in Mature Motor Axons. J Cell Biol. 1992;119(3):595–604.

154. Rieske P, Krynska B, Azizi SA. Human fibroblast-derived cell lines have characteristics of embryonic stem cells and cells of neuro-ectodermal origin. Differentiation [Internet]. 2005;73(9–10):474–83. Available from: http://dx.doi.org/10.1111/j.1432-0436.2005.00050.x

155. Yusuf B, Gopurappilly R, Dadheech N, Gupta S, Bhonde R, Pal R. Embryonic fibroblasts represent a connecting link between mesenchymal and embryonic stem cells. Dev Growth Differ. 2013;55(3):330–40.

156. Couderc T, Lecuit M. Focus on Chikungunya pathophysiology in human and animal models. Microbes Infect. 2009;11(14–15):1197–205.

157. Noret M, Herrero L, Rulli N, Rolph M, Smith PN, Li RW, et al. Interleukin 6, RANKL, and Osteoprotegerin Expression by Chikungunya Virus - Infected Human Osteoblasts. J Infect Dis. 2012;206(3):455–459.

158. Chen W, Foo S-S, Taylor A, Lulla A, Merits A, Hueston L, et al. Bindarit, an Inhibitor of Monocyte Chemotactic Protein Synthesis, Protects against Bone Loss Induced by Chikungunya Virus Infection. J Virol [Internet]. 2015 Jan 1 [cited 2015 Jan 12];89(1):581–93. Available from:

http://www.ncbi.nlm.nih.gov/pubmed/25339772

159. Miner JJ, Cook LE, Hong JP, Smith AM, Richner JM, Shimak RM, et al. Therapy with CTLA4-Ig and an antiviral monoclonal antibody controls chikungunya virus arthritis. Sci Transl Med. 2017;9(375):1–10.

160. Wilson JAC, Prow NA, Schroder WA, Ellis JJ, Cumming HE, Gearing LJ, et al. RNA-Seq analysis of chikungunya virus infection and identification of granzyme A as a major promoter of arthritic inflammation. Vol. 13, PLoS Pathogens. 2017. 1-32 p.

161. Nakaya HI, Gardner J, Poo YS, Major L, Pulendran B, Suhrbier A. Gene profiling of chikungunya virus arthritis in a mouse model reveals significant overlap with rheumatoid arthritis. Arthritis Rheum. 2012;64(11):3553–63.

162. National Research Council. Guide for the care and use of laboratory animals [Internet]. Vol. 8th Ed. Washington, DC: National Academies Press, Washington, DC; 2011. Available from: http://www.ncbi.nlm.nih.gov/pubmed/21595115

163. Mahauad-Fernandez WD, Jones PH, Okeoma CM. Critical role for BST-2 in acute Chikungunya virus infection. J Gen Virol [Internet]. 2014 Jul 22 [cited 2014 Aug 26];319–35. Available from: http://www.ncbi.nlm.nih.gov/pubmed/25053563

164. Li Y, Handel A. Modeling inoculum dose dependent patterns of acute virus infections. J Theor Biol [Internet]. 2014;347(1):63–73. Available from: http://dx.doi.org/10.1016/j.jtbi.2014.01.008

165. Society R, Only FR. Exploring the impact of inoculum dose on host immunity and morbidity to inform model-based vaccine design. 2017;1–18.

166. Marois I, Cloutier A, Garneau E, Richter M V. Initial infectious dose dictates the innate, adaptive, and memory responses to influenza in the respiratory tract. J Leukoc Biol [Internet]. 2012;92(1):107–21. Available from: http://www.jleukbio.org/cgi/doi/10.1189/jlb.1011490

167. Vazeille M, Moutailler S, Coudrier D, Rousseaux C, Khun H, Huerre M, et al. Two Chikungunya isolates from the outbreak of La Reunion (Indian Ocean) exhibit different patterns of infection in the mosquito, Aedes albopictus. PLoS One. 2007;2(11).

168. Ledermann JP, Borland EM, Powers AM. Minimum infectious dose for chikungunya virus in Aedes aegypti and Ae. albopictus mosquitoes. Rev Panam Salud Publica [Internet]. 2017;41:e65. Available from: http://www.scielosp.org/scielo.php?script=sci_arttext&pid=S1020-49892017000100410&lng=en&nrm=iso&tlng=en%0Ahttp://www.ncbi.nlm.nih.gov/pubmed/28902278

169. Habib N, Avraham-Davidi I, Basu A, Burks T, Shekhar K, Hofree M, et al. Massively parallel single-nucleus RNA-seq with DroNc-seq. Nat Methods. 2017;14(10):955–8.

170. Zeng W, Jiang S, Kong X, El-Ali N, Ball AR, Ma CIH, et al. Single-nucleus RNA-seq of differentiating human myoblasts reveals the extent of fate heterogeneity. Nucleic Acids Res. 2016;44(21):1–13.

171. Bergmann O, Jovinge S. Isolation of Cardiomyocyte Nuclei from Post-mortem Tissue. J Vis Exp [Internet]. 2012;(65):1–6. Available from: http://www.jove.com/video/4205/

172. Son K-N, Liang Z, Lipton HL. Double-Stranded RNA Is Detected by Immunofluorescence Analysis in RNA and DNA Virus Infections, Including Those by Negative-Stranded RNA Viruses. J Virol [Internet]. 2015;89(18):9383–92. Available from: http://jvi.asm.org/lookup/doi/10.1128/JVI.01299-15

173. Buch T, Heppner FL, Tertilt C, Heinen TJ a J, Kremer M, Wunderlich FT, et al. A Cre-inducible diphtheria toxin receptor mediates cell lineage ablation after toxin administration. Nat Methods. 2005;2(6):419–26.

174. Sheehan KCF, Lazear HM, Diamond MS, Schreiber RD. Selective blockade of Interferon-α and -β reveals their non-redundant functions in a mouse model of West Nile virus infection. PLoS One. 2015;10(5):1–19.

175. Ng CT, Sullivan BM, Teijaro JR, Lee AM, Welch M, Rice S, et al. Blockade of Interferon Beta, but Not Interferon Alpha, Signaling Controls Persistent Viral Infection. Cell Host Microbe [Internet]. 2015;17(5):653–61. Available from: http://www.sciencedirect.com/science/article/pii/S1931312815001638